WESTINGHOUSE CLASS 3 (Non-Proprietary)

Westinghouse Energy Systems

WESTINGHOUSE CLASS 3 (Non-Proprietary)

Westinghouse Energy Systems

WCAP-13975

SCALING LOGIC FOR THE CORE MAKEUP TANK TEST

D. Aumiller
L. E. Hochreiter

Westinghouse Electric Corporation
Energy Systems
P. O. Box 355
Pittsburgh, Pennsylvania 15230

t:\0614.wpf:1d/021094

AP600 DOCUMENT COVER SHEET

Form 58202F(9/93) [WP xxxx]
0058.FRM

AP600 CENTRAL FILE USE ONLY: _____ RFS #: _____ RFS ITEM #: _____

AP600 DOCUMENT NO.	REVISION NO.	PAGES ATTACHED	ASSIGNED TO
MT01-T6R-001	0		

ALTERNATE DOCUMENT NUMBER: WCAP-13963
DESIGN AGENT ORGANIZATION: Westinghouse Electric
PROJECT: AP600
WORK BREAKDOWN #: 2.6.10.8
TITLE: SCALING LOGIC FOR THE CORE MAKEUP TANK TEST

WCAP-13963 (class 2)
WCAP-13975 (class 3)

ATTACHMENTS

CALCULATION/ANALYSIS REFERENCE:

DCP #/REV. INCORPORATED:

ELECTRONIC FILENAME:	APPLICATION:
WPF1877D: 1d/020794	WORDPERFECT

☒ WESTINGHOUSE PROPRIETARY CLASS 2
This document contains information proprietary to Westinghouse Electric Corporation; it is submitted in confidence and is to be used solely for the purpose for which it is furnished and returned upon request. This document and such information is not to be reproduced, transmitted, disclosed or used otherwise in whole or in part without prior written authorization of Westinghouse Electric Corporation, Energy Systems Business Unit, subject to the legends contained hereof.

☐ WESTINGHOUSE CLASS 3 (NON PROPRIETARY)

☐ **DOE DESIGN CERTIFICATION PROGRAM** GOVERNMENT LIMITED RIGHTS STATEMENT [See reverse side of this form]

☒ (C) WESTINGHOUSE ELECTRIC CORPORATION 19 94
A license is reserved to the U.S. Government under contract DE-AC03-90SF18495.

☐ DOE CONTRACT DELIVERABLES (DELIVERED DATA)
Subject to specified exceptions, disclosure of this data is restricted until September 30, 1995 or Design Certification under DOE contract DE-AC03-90SF18495, whichever is later.

EPRI CONFIDENTIAL/OBLIGATION NOTICES: NOTICE: 1 ☒ 2 ☐ 3 ☐ 4 ☐ 5 ☐
CATEGORY: A ☒ B ☐ C ☐ D ☐ E ☐ F ☐

☐ **ARC FOAKE PROGRAM** ARC LIMITED RIGHTS STATEMENT [See reverse side of this form]

☐ (C) WESTINGHOUSE ELECTRIC CORPORATION 19__
A license is reserved to the U.S. Government under contract DE-FC02-NE34267 and subcontract ARC-93-3-SC-001.

☐ ARC CONTRACT DELIVERABLES (DELIVERED DATA)
Subject to specified exceptions, disclosure of this data is restricted under ARC Subcontract ARC-93-3-SC-001.

ORIGINATOR	SIGNATURE/DATE	
L. E. HOCHREITER	L E Hochreiter 1/31/94	
AP600 RESPONSIBLE MANAGER	SIGNATURE*	APPROVAL DATE
E. J. PIPLICA	E J Piplica	2/4/94

*Approval of the responsible manager signifies that document is complete, all required reviews are complete, electronic file is attached and document is released for use.

Form 58202F(9/93)

LIMITED RIGHTS STATEMENTS

DOE GOVERNMENT LIMITED RIGHTS STATEMENT

(A) These data are submitted with limited rights under government contract No. DE-AC03-90SF18495. These data may be reproduced and used by the government with the express limitation that they will not, without written permission of the contractor, be used for purposes of manufacture nor disclosed outside the government; except that the government may disclose these data outside the government for the following purposes, if any, provided that the government makes such disclosure subject to prohibition against further use and disclosure:
   (I) This "Proprietary Data" may be disclosed for evaluation purposes under the restrictions above.
   (II) The "Proprietary Data" may be disclosed to the Electric Power Research Institute (EPRI), electric utility representatives and their direct consultants, excluding direct commercial competitors, and the DOE National Laboratories under the prohibitions and restrictions above.

(B) This notice shall be marked on any reproduction of these data, in whole or in part.

ARC LIMITED RIGHTS STATEMENT:

This proprietary data, furnished under Subcontract Number ARC-93-3-SC-001 with ARC may be duplicated and used by the government and ARC, subject to the limitations of Article H-17.F. of that subcontract, with the express limitations that the proprietary data may not be disclosed outside the government or ARC, or ARC's Class 1 & 3 members or EPRI or be used for purposes of manufacture without prior permission of the Subcontractor, except that further disclosure or use may be made solely for the following purposes:

This proprietary data may be disclosed to other than commercial competitors of Subcontractor for evaluation purposes of this subcontract under the restriction that the proprietary data be retained in confidence and not be further disclosed, and subject to the terms of a non-disclosure agreement between the Subcontractor and that organization, excluding DOE and its contractors.

DEFINITIONS

DELIVERED DATA — Consists of documents (e.g. specifications, drawings, reports) which are generated under the DOE or ARC contracts.

EPRI CONFIDENTIALITY / OBLIGATION NOTICES

NOTICE 1: The data in this document is subject to no confidentiality obligations.

NOTICE 2: The data in this document is proprietary and confidential to Westinghouse Electric Corporation and/or its Contractors. It is forwarded to recipient under an obligation of Confidence and Trust for limited purposes only. Any use, disclosure to unauthorized persons, or copying of this document or parts thereof is prohibited except as agreed to in advance by the Electric Power Research Institute (EPRI) and Westinghouse Electric Corporation. Recipient of this data has a duty to inquire of EPRI and/or Westinghouse as to the uses of the information contained herein that are permitted.

NOTICE 3: The data in this document is proprietary and confidential to Westinghouse Electric Corporation and/or its Contractors. It is forwarded to recipient under an obligation of Confidence and Trust for use only in evaluation tasks specifically authorized by the Electric Power Research Institute (EPRI). Any use, disclosure to unauthorized persons, or copying this document or parts thereof is prohibited except as agreed to in advance by EPRI and Westinghouse Electric Corporation. Recipient of this data has a duty to inquire of EPRI and/or Westinghouse as to the uses of the information contained herein that are permitted. This document and any copies or excerpts thereof that may have been generated are to be returned to Westinghouse, directly or through EPRI, when requested to do so.

NOTICE 4: The data in this document is proprietary and confidential to Westinghouse Electric Corporation and/or its Contractors. It is being revealed in confidence and trust only to Employees of EPRI and to certain contractors of EPRI for limited evaluation tasks authorized by EPRI. Any use, disclosure to unauthorized persons, or copying of this document or parts thereof is prohibited. This Document and any copies or excerpts thereof that may have been generated are to be returned to Westinghouse, directly or through EPRI, when requested to do so.

NOTICE 5: The data in this document is proprietary and confidential to Westinghouse Electric Corporation and/or its Contractors. Access to this data is given in Confidence and Trust only at Westinghouse facilities for limited evaluation tasks assigned by EPRI. Any use, disclosure to unauthorized persons, or copying of this document or parts thereof is prohibited. Neither this document nor any excerpts therefrom are to be removed from Westinghouse facilities.

EPRI CONFIDENTIALITY / OBLIGATION CATEGORIES

CATEGORY "A" — (See Delivered Data) Consists of CONTRACTOR Foreground Data that is contained in an issued reported.

CATEGORY "B" — (See Delivered Data) Consists of CONTRACTOR Foreground Data that is not contained in an issued report, except for computer programs.

CATEGORY "C" — Consists of CONTRACTOR Background Data except for computer programs.

CATEGORY "D" — Consists of computer programs developed in the course of performing the Work.

CATEGORY "E" — Consists of computer programs developed prior to the Effective Date or after the Effective Date but outside the scope of the Work.

CATEGORY "F" — Consists of administrative plans and administrative reports.

ACKNOWLEDGEMENTS

The authors would like to acknowledge the excellent work performed by Dr. Jośe Reyes of Oregon State University in establishing clear guidelines and scaling criteria for complex two-phase flow system behavior. His scaling report on the AP600 Low Pressure Integral Systems Effects Tests was used as a guide in this report. The authors also acknowledge the help and support given by E. J. Piplica, L. E. Conway, J. P. Cunningham, J. C. Butler and D. Ruff in preparing and reviewing this report.

TABLE OF CONTENTS

LIST OF FIGURES

LIST OF FIGURES (Continued)

LIST OF FIGURES (Continued)

LIST OF FIGURES (Continued)

LIST OF TABLES

ACRONYMS

ADS	Automatic Depressurization System
CL	Cold Leg
CMT	Core Makeup Tank
DAS	Data Acquisition System
DVI	Discharge/Direct Vessel Injection
IRWST	In-Containment Refueling Water Storage Tank
LBLOCA	Large Break Loss of Coolant Accident
LOCA	Loss of Coolant Accident
MSLB	Main Steamline Break
NRHRS	Nonsafety Residual Heat Removal System
PBL	Pressure Balance Line
PCT	Peak Cladding Temperature
PIRT	Phenomena Identification and Ranking Table
PRHR	Passive Residual Heat Removal System
RCS	Reactor Coolant System
RTD	Resistance Temperature Detector
S	Safety
SBLOCA	Small Break Loss of Coolant Accident
SGTR	Steam Generator Tube Rupture
SSAR	Standard Safety Analysis Report
SW	Steam Water
SWR	Steam Water Reservoir
TC	Thermocouple

SUMMARY

The design and scaling logic of the Westinghouse Core Makeup Tank (CMT) test has been assessed to insure that the test facility has the capability of representing the important thermal-hydraulic phenomena for CMT operation. The expected CMT phenomena have been identified in a Phenomena Identification and Ranking Table (PIRT) for the thermal-hydraulic processes that are expected to be of importance for the CMT. Estimates of the different expected phenomena are made and are compared between the experiment and the prototype CMT. Scaling distortions of the CMT test are also described and assessed relative to the expected behavior of the AP600.

1.0 INTRODUCTION

1.1 PURPOSE

The purpose of this report is to establish that the Core Makeup Tank (CMT) test will produce the necessary data to develop and verify the computer code models for the CMT performance for the AP600 design. The CMT test is a scaled, separate effects test in which the boundary conditions can be controlled over a wide range to produce thermal-hydraulic conditions of interest for computer code verification.

Since the test is not full scale, there are compromises that can exist with the test data and its application. The purposes of this document are to develop the scaling logic that supports the application of the data for code assessment, show that the key thermal-hydraulic phenomena of interest are reproduced in the test facility, and show that the test facility can be operated and controlled over a sufficiently broad range that captures all CMT modes of operation.

1.2 CMT DESIGN AND OPERATION

The AP600 design utilizes passive methods to perform core and containment cooling functions for a postulated loss of coolant. The CMT shown in Figure 1-1 is an important feature of the AP600 passive safety system. Each tank stores 2000 ft^3 of cold borated water at Reactor Coolant System (RCS) pressure that can be gravity injected into the RCS to provide reactivity control and core cooling. The CMTs provide the same function as the high pressure safety injection system in existing pressurized water reactors (PWRs), with the difference being that current plants require the availability of AC power to perform their safety function, whereas the CMTs perform this function using only gravity-driven flows.

The CMTs are connected to the RCS, as shown in Figure 1-1, by isolation valves on the cold leg balance line and the CMT discharge line. The cold leg balance line and CMT discharge valves open on an S- (Safety) signal, and remain open. The tanks are maintained at full system pressure by the pressurizer balance line. The condensation that may occur in the pressurizer balance line is drained through a condensate drain and is removed upstream of the cold leg balance line isolation valve.

During normal operation, the CMTs are completely filled and the steam/water interface will reside in the top nozzle of the CMT.

In addition to adding coolant and boron to the reactor systems, the CMTs have an additional safety function. As the tanks continue to drain, they indicate that an unrecoverable loss of coolant accident (LOCA) has occurred. When approximately 25 percent of the tank liquid has drained, the CMT level sensing device activates the first stage of the Automatic Depressurization System (ADS) and the plant begins a controlled blowdown through the ADS valves into the in-containment refueling water storage tank (IRWST). The second stage ADS valves open when the CMT volume reaches approximately 60 percent. The third stage ADS valves open when the CMT volume reaches approximately 50 percent. If the CMTs would continue to drain, and the volume reaches 20 percent, the fourth stage ADS valves, which are located on the hot legs, open, providing a large vent path directly to containment to depressurize the RCS to containment pressure. As the RCS depressurizes by opening the ADS valves on the pressurizer and hot legs, the CMTs continue to add coolant to the RCS to maintain continued core cooling during the depressurization.

Each AP600 CMT, shown in Figure 1-2, is a 2000 ft^3 tank using hemispherical heads and a cylindrical shell. The hemispherical heads are stainless steel clad carbon steel [ ]^{a,c} with a total thickness of [ ]^{a,c} inches. The cylindrical portion of the tank is also stainless steel clad and is a total of [ ]^{a,c} thick. The top of the tank is located [ ]^{a,c} above the RCS cold legs providing a gravity head to drive the flow into the reactor vessel downcomer. There are two balance lines attached to the top of the CMT and a drain line at the bottom. The drain line is connected through an isolation valve and two check valves to the direct vessel injection line. The cold leg balance line is an [ ]^{a,c} There is an isolation valve near the top of this balance line. The pressurizer balance line is a [ ]^{a,c} There are also check valves in this line to prevent back flow from the CMT to the pressurizer in the event of a pressurizer break. The AP600 piping schematic for the CMT and its balance lines is shown in Figure 1-3.

There are two modes of operation for the CMTs: recirculation and draining. During the initial phase of a small break LOCA, steamline break, or steam generator tube rupture event, the RCS inventory is still at or near its steady-state value. When an S-signal occurs (typically low pressurizer pressure), the

reactor coolant pumps trip and the CMT isolation valves open. The elevation head in the pressurizer is sufficient to force fluid into the top of the cold leg balance line, condensing any steam there such that a complete flow path is formed between the reactor cold leg, cold leg balance line, CMT, and direct vessel injection line. With the liquid circuit formed, there will be a gravity-driven flow from the CMT to the reactor vessel and a return flow from the cold leg to the top of the CMT. This is the recirculation phase of operation for the CMTs. The colder, denser CMT water drives flow into the reactor vessel because of the density difference between the CMT water and the cold leg balance line (approximately 20 percent with T_{cold} at 550°F, and CMT water at 120°F). Figure 1-4, from the AP600 Standard Safety Analysis Report (SSAR) calculations, shows the calculated CMT draining flow during the recirculation period for a 2-inch diameter cold leg break. This flow will continue and steadily decrease as the colder CMT water is replaced by hotter water from the balance line; thereby decreasing the gravity draining head. As the break continues to drain the RCS, the cold leg balance line begins to void, as seen in Figure 1-5; the recirculation flow path is broken, and the CMT drains as the water volume is replaced by steam from the cold leg and pressurizer. This begins the draining mode of the CMT. The CMT injection flow rate is larger in this mode because of the greater density difference between the colder CMT water and the steam or two-phase mixture in the balance line.

Depending on how long the CMT is in the recirculation mode, there will be the potential for a thick, hot, liquid layer to exist at the top of the CMT. This will reduce the steam condensation when the CMT transitions into the draining mode: the hot liquid layer can flash as the RCS depressurizes, causing mixing and reducing the effects of condensation in the CMT.

If the break is larger, the recirculation period is reduced because the cold leg balance line will void sooner, breaking natural circulation. In these cases, the hot liquid layer in the CMT will be thinner or may not exist. For large break LOCAs there is no recirculation period since the entire RCS voids quickly. The accumulators begin injecting very early in a large break LOCA transient and have sufficient gas pressure such that they close the check valves in the CMT discharge line until the accumulators have finished injecting. The CMTs will begin injection after the accumulators are empty. By this time, the reactor vessel is refilled, the core peak cladding temperature (PCT) has been reached, and most, if not all, of the core has quenched.

1.3 DESCRIPTION OF THE CMT TEST FACILITY

The Westinghouse CMT test facility consists of an instrumented test vessel that simulates the CMT and a liquid/steam reservoir that simulates the remainder of the RCS. Connecting lines to supply steam and/or liquid to the top of the CMT are provided, as well as a drain line to allow flow out of the bottom of the CMT. A source of saturated steam from a boiler is attached to a steam reservoir and is connected to the liquid/steam reservoir. The test apparatus is shown schematically in Figure 1-6. A data acquisition system (DAS) is provided to record signals from thermocouples, pressure sensors, and flow meters.

The CMT test vessel is a vertically-mounted, uninsulated, carbon steel pressure vessel with an inside height of [ ]^{a,c} inches. The cylindrical portion of the vessel is constructed of [ ]^{a,c} pipe with an inside diameter of [ ]^{a,c} inches and a wall thickness of [ ]^{a,c} inches. The pipe is capped on either end with [ ]^{a,c} with a wall thicknesses of [ ]^{a,c} inches. The height of the heads represents only about [ ]^{a,c} percent of the total tank height. The vessel is elevated above the liquid/steam reservoir water level so that the gravity draining head is equivalent to that for the AP600 CMTs.

The steam/water reservoir is a vertically-mounted, insulated, carbon steel pressure vessel. The reservoir acts as the source of steam and/or liquid flow to the CMT, and accommodates the CMT liquid discharge. The location of the reservoir permits simple gravity drain of the CMT test vessel through the discharge line, under all pressure conditions. The reservoir supplies saturated liquid, or steam, to the top of the CMT test vessel through two steam lines. The reservoir is connected to a saturated steam source that has the capability to supply sufficient steam to accommodate the requirements of the test program. The steam source consists of a steam boiler and accumulators in which the steam can be stored at pressure until required. A pressure control valve between the steam accumulators and the steam/water reservoir allows the reservoir pressure to be maintained at any desired pressure over the range of 20 to 2250 psia.

The two steam supply lines connecting the reservoir to the CMT test vessel are constructed of 1.5-inch Schedule 160 piping. Steam supply line number 1 represents the pressurizer to CMT pressure balance line (PBL) which connects the top of the pressurizer to the header at the top of the CMT in AP600. It

consists of a continuously upward sloping section between the top of the reservoir and a high point above the CMT test vessel so that no water traps form due to the condensation. From the high point, the line slopes slightly downward to the CMT test vessel inlet header, joining the header and steam supply line number 2 at a T. The inlet header itself is a 2-foot section of 1.5-inch pipe, slightly sloped toward the vessel inlet elbow flange connection. Steam supply line number 2 represents the cold leg to CMT PBL, which runs between the cold leg and the header at the top of the CMT in AP600. This line extends into the liquid/steam reservoir so that its end is below a "HI" reservoir liquid level setpoint and above a "LO" setpoint. Adjusting the reservoir liquid level allows either liquid or steam to flow in the line. Steam supply line number 2 is heat traced and has thermocouples at 10-foot intervals. The heat tracing is used to heat and maintain fluid in the line at a desired temperature up to the saturation temperature corresponding to the pressure of the test run. Both steam supply lines number 1 and number 2 are insulated. Vent/vacuum lines are connected to the high point of line number 1 and to the CMT inlet elbow. These lines (and associated valves) provide for simulation of ADS depressurization, and can be used, along with a supplied vacuum system, to remove noncondensible gas prior to testing. The CMT test vessel water discharge line is also constructed of 1.5-inch Schedule 160 piping, and replaces the CMT discharge/direct vessel injection (DVI) line in AP600. This line is also insulated.

Level control systems and valves are included for both the CMT test vessel and the liquid/steam reservoir. For the CMT test vessel, the level control system will be used to maintain a fixed CMT liquid level during some of the tests. Measurement of the liquid drained out of the vessel to maintain level is a direct indication of the amount of steam condensation occurring on the vessel walls and liquid surface. For the steam/water reservoir, the level control system maintains a fixed liquid level. A secondary function of the level control system is to drain cold CMT discharge liquid so it does not enter the reservoir and change the liquid temperature, a situation that might lead to condensation at the steam/liquid interface.

The CMT vessel is highly instrumented with five inner surface and five outer surface wall thermocouples, 39 fluid thermocouples, and six differential pressure cells for level measurements. The wall thermocouples are brazed in the CMT wall in grooves to provide excellent thermal response. There are four radial locations where wall thermocouples are located. They are $^1/_8$ inch, $^1/_2$ inch, and $1^1/_2$ inches from the inner surface. All of these thermocouples are located at the same axial position

of the inner and outer wall thermocouples, such that a radial temperature profile can be measured through the CMT wall, and can be fitted numerically to calculate the inner wall heat flux. The fluid thermocouples are arranged in groups to detect thermal stratification and the presence of a hot liquid layer. There are thermocouples located at different radial positions at selected elevations within the tank. The differential pressure cells are arranged in levels to obtain the collapsed liquid level within the tank such that the transient tank inventory can be measured.

There are also liquid flow measurements on the CMT discharge, absolute pressure cells on the tank and piping, as well as pressure drop measurements on the steam lines that have been calibrated to obtain steam flow. Pressure measurements and controls also exist on the steam supply system.

The measurements will permit a transient mass and energy balance to be calculated for the facility.

1.4 PHENOMENA IDENTIFICATION AND RANKING TABLE FOR THE CMT

This section identifies and discusses the thermal-hydraulic phenomena that the CMT test will capture and provides the ranking of those phenomena. These phenomena are grouped into two modes of operation for the CMT: recirculation and draining.

1.4.1 CMT Recirculation Thermal-Hydraulic Phenomena

The CMT recirculation is driven by the density difference between the cold CMT water and the hotter cold leg balance line water. The result of the recirculation is to provide colder, denser water to the reactor vessel from the CMT, which is replaced by hotter, less dense cold leg water from the balance line. There is a net mass transfer from the CMT to the RCS due to the density difference, as well as a net energy transfer from the RCS back to the CMT. The rates of energy and mass transfer will depend on the buoyant differences and the hydraulic resistances in the flow path. The recirculating flow continuously diminishes with time as the CMT heats up and the resulting buoyant head decreases. As the cold leg piping and cold leg balance line void, the buoyant head increases, which increases the discharge flow as the tank begins to drain. Both single-phase and two-phase recirculation will occur for small break LOCAs, while single- and perhaps two-phase recirculation may occur for steamline breaks and steam generator tube ruptures.

There is CMT wall heat transfer during recirculation where the hot fluid from the cold leg balance line will transfer heat to the initially cold CMT walls. The heat transfer from the hot recirculating fluid to the colder CMT walls will heat them, while at the same time cool the recirculating fluid. There will be circulation patterns within the hot liquid layer in which the cooler water at the walls flows downward and mixes within the layer. As the flow recirculates, the CMT walls heat up, and the potential for large condensation to occur is reduced at a later time, when the CMT drains. Also, if the CMT walls become fully heated when the RCS depressurizes there can be reverse heat transfer from the CMT walls, back to the fluid in the tank. Because the walls are thick, the amount of heat transfer to the walls will be scenario dependent. This was observed in the ROSA-V experiment by Yonomoto et. al. (1993).

Fluid mixing can also occur at the top of the CMT during the recirculational phase of the transient. The hot liquid from the cold leg PBL will be injected into the CMT through the nozzle and will mix with the initially colder water in the CMT. The analysis of the ROSA-V experiment by Yonomoto et. al. (1993) indicates that the mixing behavior is one dimensional in nature and that conduction effects between fluid layers are negligible, while the convection effects appear to dominate.

As recirculation continues, the PBLs begin to void and a two-phase mixture is swept into the CMTs. Depending on how long recirculation has occurred, the CMT walls and the mixed liquid layer could be hotter or colder. If the liquid layer and the CMT walls are hot, there will be limited condensation, and the vapor will collect at the top of the CMT, break the natural circulation flow path, and draining will begin. If the walls and liquid are cold, condensation will occur that can draw more two-phase mixture up the balance line to the CMT, water recirculation can be re-established, and an intermittent recirculation can occur.

1.4.2 CMT Draining Phenomena

CMT draining is the flow of liquid from the bottom of the CMT with a decrease in the water volume in the CMT. As the CMT begins to drain, it can uncover CMT metal surfaces, which may be cold or warm depending upon the reciruclation. Depending upon the wall temperature, various amounts of steam will be condensed. The thick CMT walls will soon become conduction limited such that the

condensation rate is determined by the CMT wall temperature distribution, surface area, thickness, and degree of preheating due to the recirculation.

Condensation can also occur on the CMT water interface as the tank drains. The amount of surface condensation will be a function of the water temperature, the velocity of the steam as it impacts the surface, and the rate of condensate that flows from the walls to the liquid interface. The thickness of a hot liquid layer will also influence the interfacial condensation since it will tend to insulate the colder CMT water from the steam flow. The location of the liquid level, relative to the CMT inlet nozzle, also influences the amount of condensation since the steam jet from the nozzle may not be able to expand sufficiently and will penetrate into the liquid layer, increasing the amount of mixing and generating surface waves. If the liquid is sub-cooled, the surface waves will increase the interfacial heat transfer and condensation, which will draw more steam flow into the CMT. As the CMTs continue to drain, all of the above effects, which enhance interfacial heat transfer, should diminish and a thicker, warm liquid layer should form both from the direct interfacial heat transfer and from the tank wall condensate. This layer of hot condensate can later flash during RCS depressurization, when the later stages of the ADS valves open and the CMT depressurizes. The flashing will further enhance the mixing in this hot layer and can pressurize the top of the CMT such that the delivery is increased. Once additional cold CMT wall area is exposed, the additional steam generated from the flashing will condense and be recycled back to the liquid layer.

As the CMT drains there will be some liquid-to-liquid mixing, however, this effect is believed to be small since the system is in a thermally stable operating mode with the hot layer on the top. The axial temperature gradients in the ROSA-V test, given by Yonomoto et. al. (1993) and Yonomoto and Kukita (1993), indicate a relatively sharp interface between the heated layer and the cold CMT liquid.

As the CMT drains, there will also be heat transfer from the hotter liquid layer to the CMT walls by convection. The amount of heat transfer that occurs depends upon the thickness of the hotter layer, its temperature, the draining rate, and the CMT wall initial temperature. If the convection from the hot liquid layer heats the CMT walls, the condensation heat transfer from the steam will be reduced once the walls uncover.

1.4.3 CMT Phenomena Identification and Ranking Table of Key Thermal-Hydraulic Phenomena

From the above discussion, a Phenomena Identification and Ranking Table (PIRT) can be generated for the CMT. This is similar to the CMT phenomena table developed by Cozznol, Fisher, and Boucher (1993), and the PIRT developed J. Reyes (1993) for the AP600 low pressure integral test at Oregon State University. The relative ranking is given for different accident scenarios in which the CMTs play an important role. The PIRT for the CMT phenomena is given in Table 1-1. As seen from the table, different scenarios are dominated by different CMT operating modes. The large break LOCA CMT behavior is dominated by the CMT draining behavior, since recirculation does not have an opportunity to occur. Conversely, the CMT behavior for the main steamline break (MSLB) and steam generator tube rupture (SGTR) events are dominated by the recirculation phase of CMT operation since only a small amount, if any, CMT draindown occurs.

Depending upon the break size, the small break LOCA spans both modes of operation of the CMT. For small breaks, two inches or less, there is ample recirculation in the CMT such that a thick, heated liquid layer should be formed. For larger small breaks (two to ten inches) such as the double-ended guillotine of the DVI line, the RCS will quickly depressurize such that the recirculation time period is significantly reduced. For breaks of this size and larger, the recirculation will be very limited and condensation can occur as the CMT drains. Thus, while the large break model may ignore or be less precise for the recirculation period, and a MSLB and STGR model could be less precise for the draindown; the small break LOCA code must be able to model both operational modes with precision.

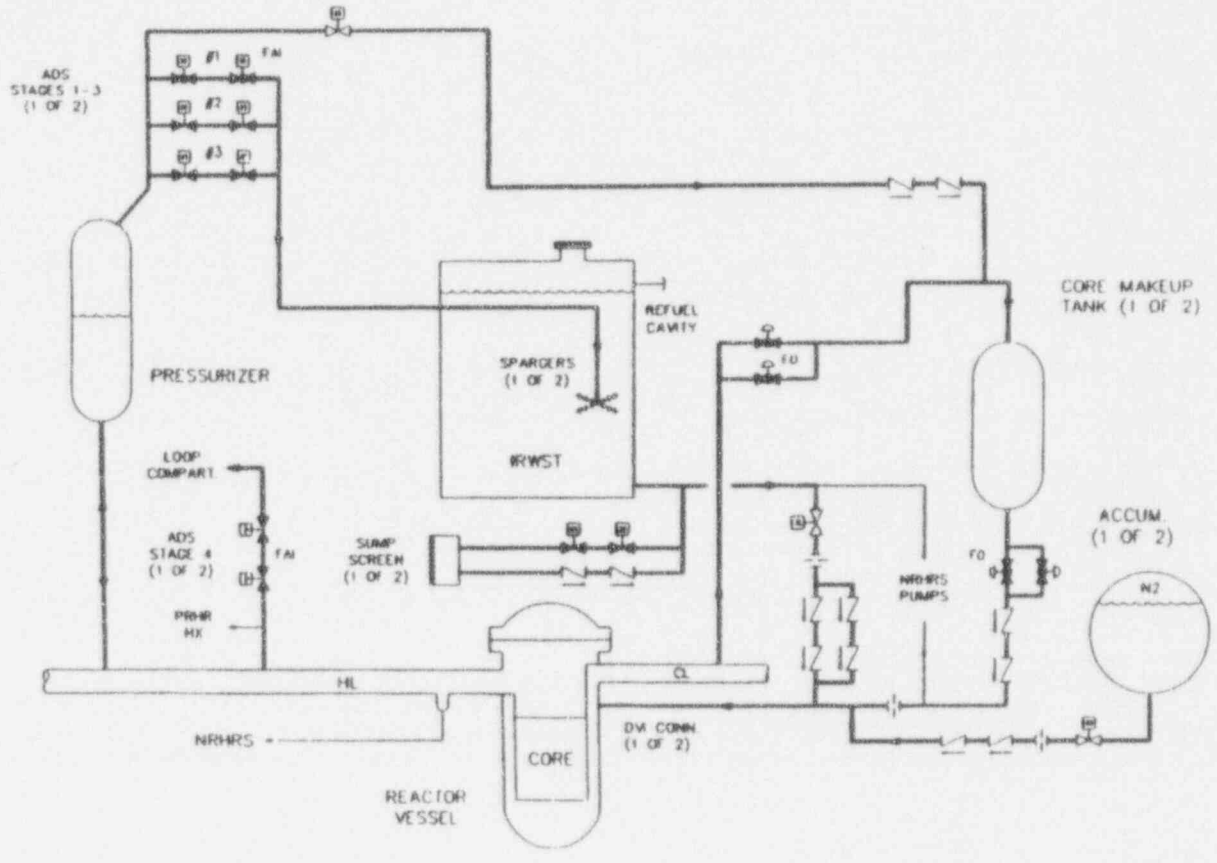

Figure 1-1 AP600 Passive Safety System Design

a,c

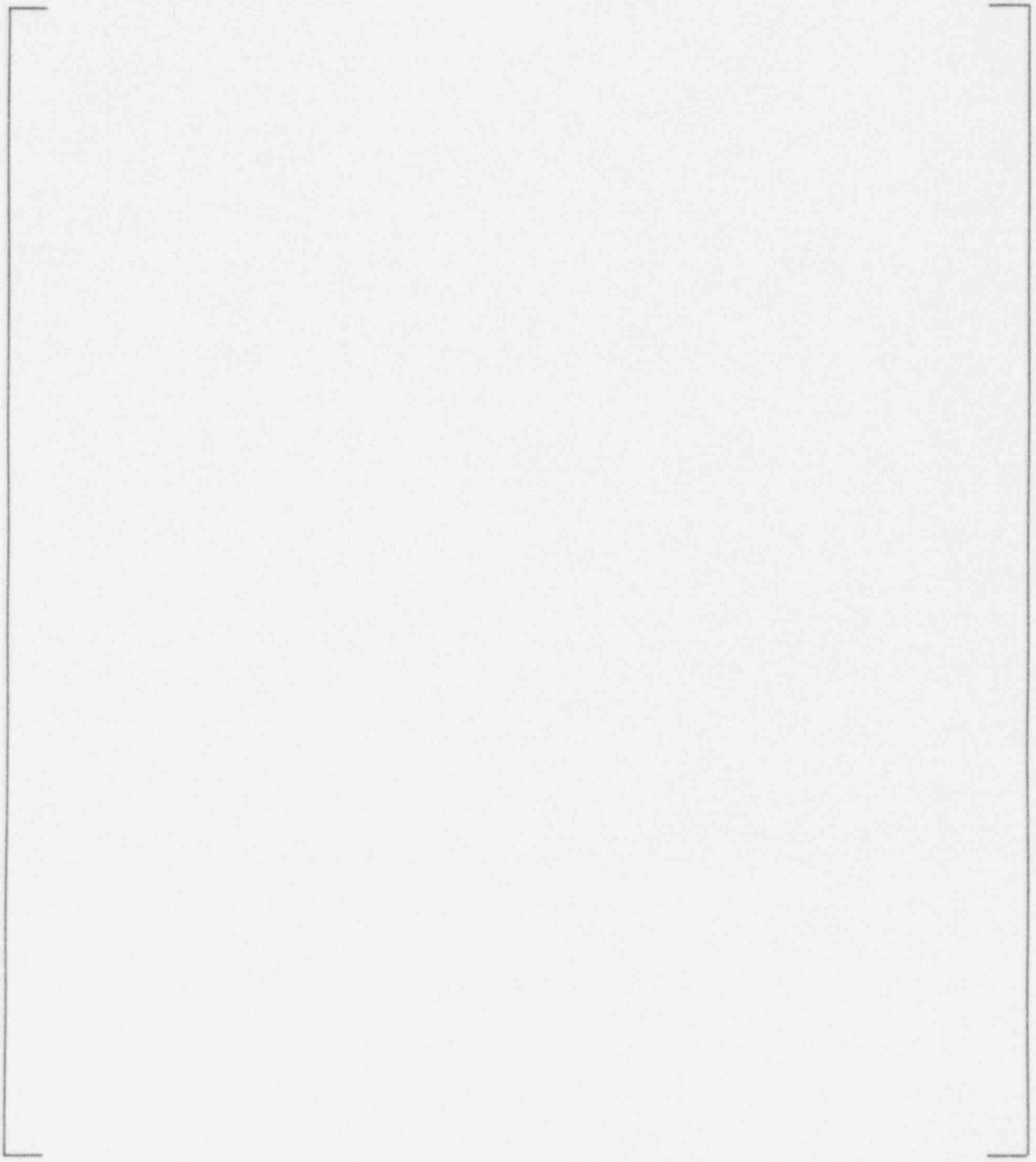

Figure 1-2 AP600 Core Makeup Tank

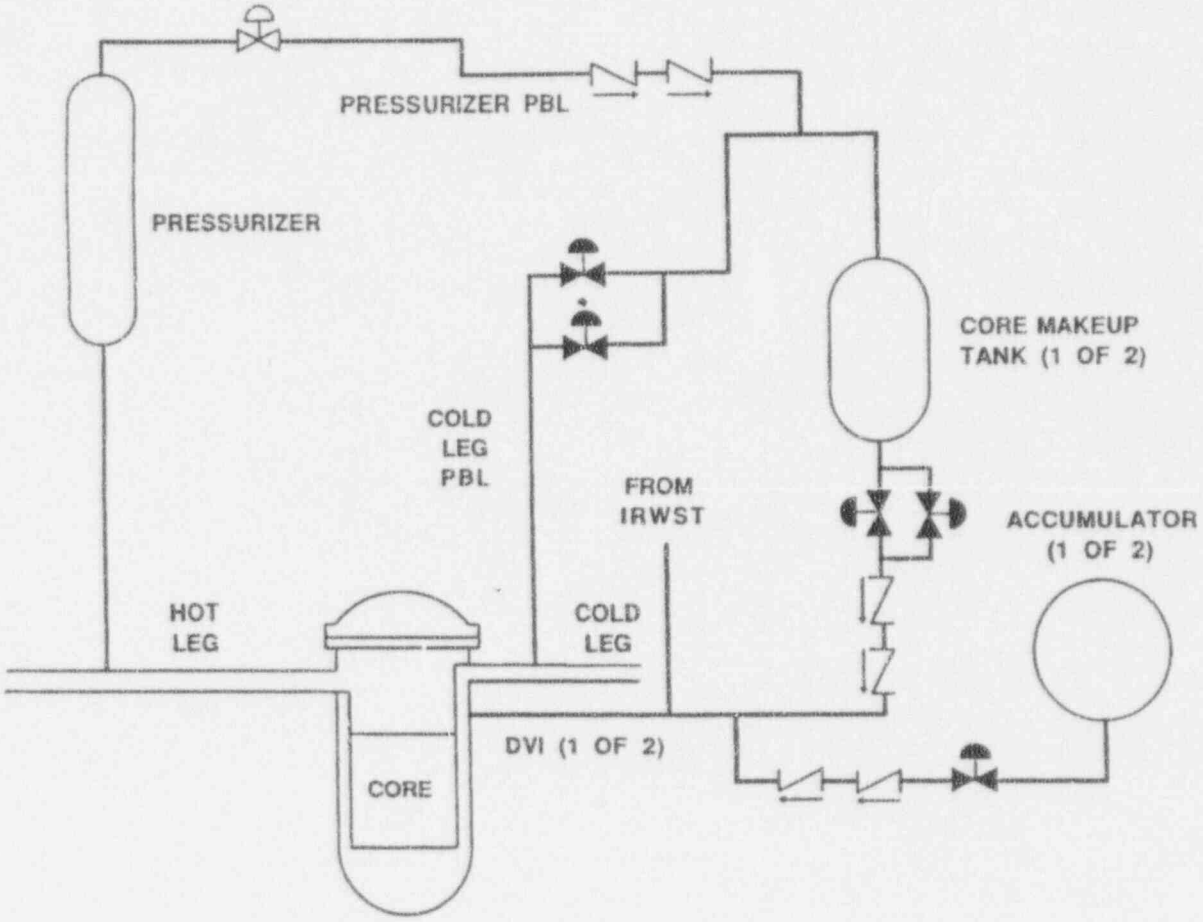

Figure 1-3 AP600 CMT Piping Layout

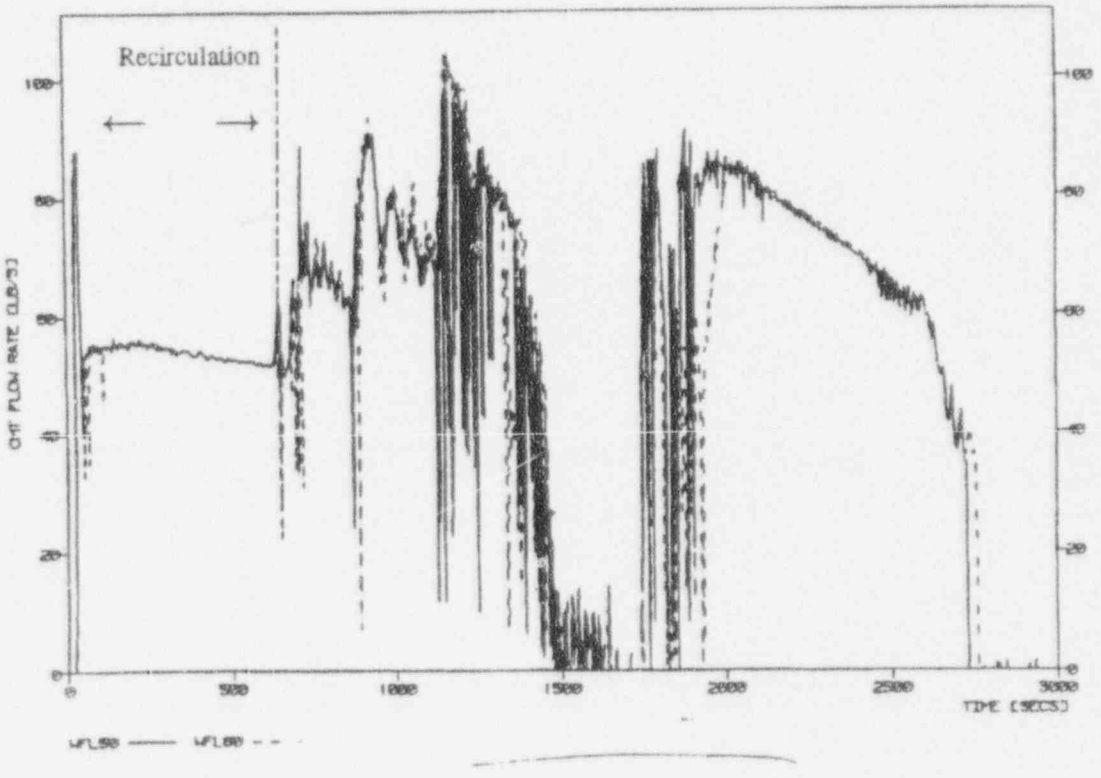

Figure 1-4 AP600 SSAR Calculation of CMT Draining Flow for 2-Inch Cold Leg Break

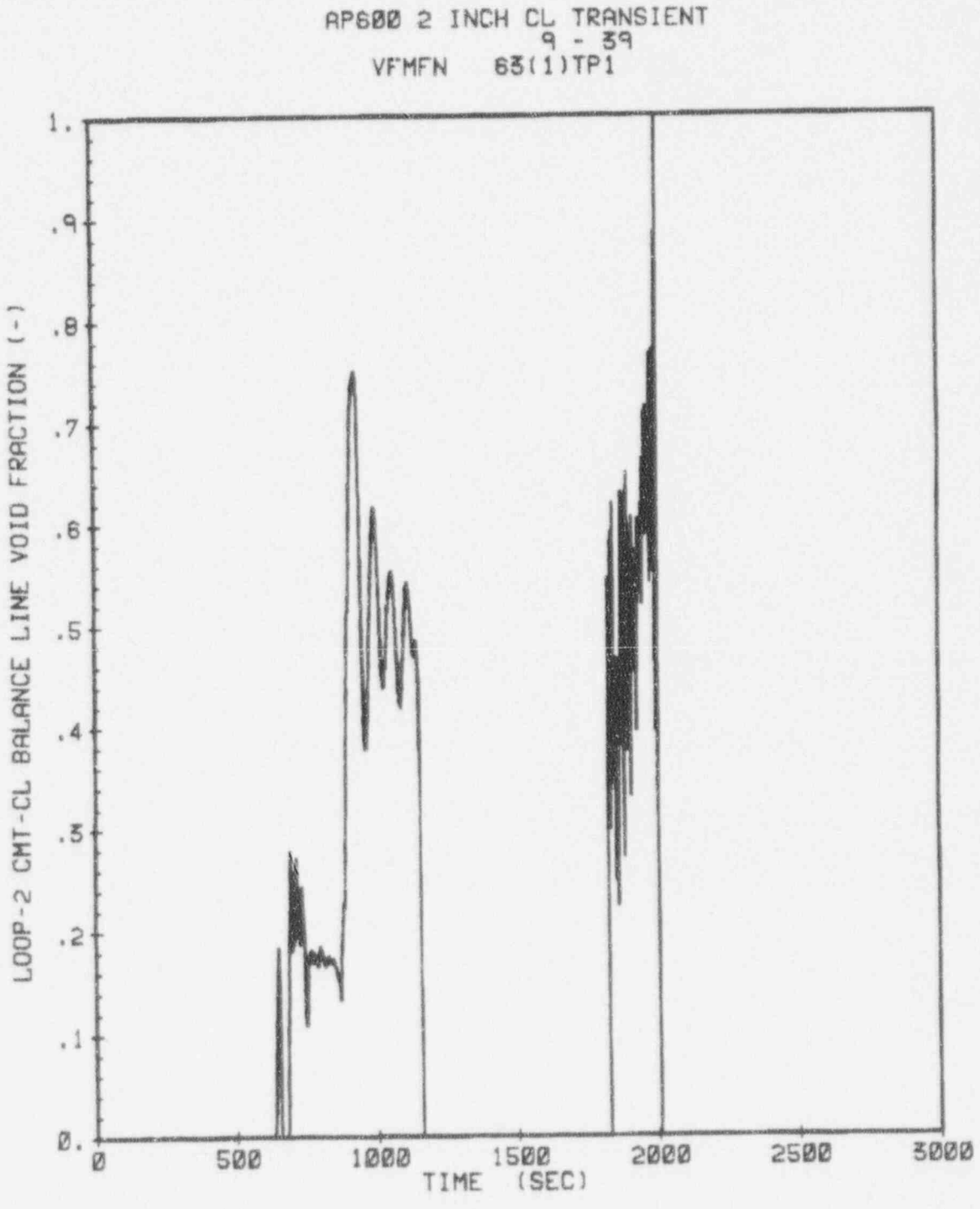

Figure 1-5 Cold Leg Balance Line Void Fraction for 2-Inch Cold Leg Break

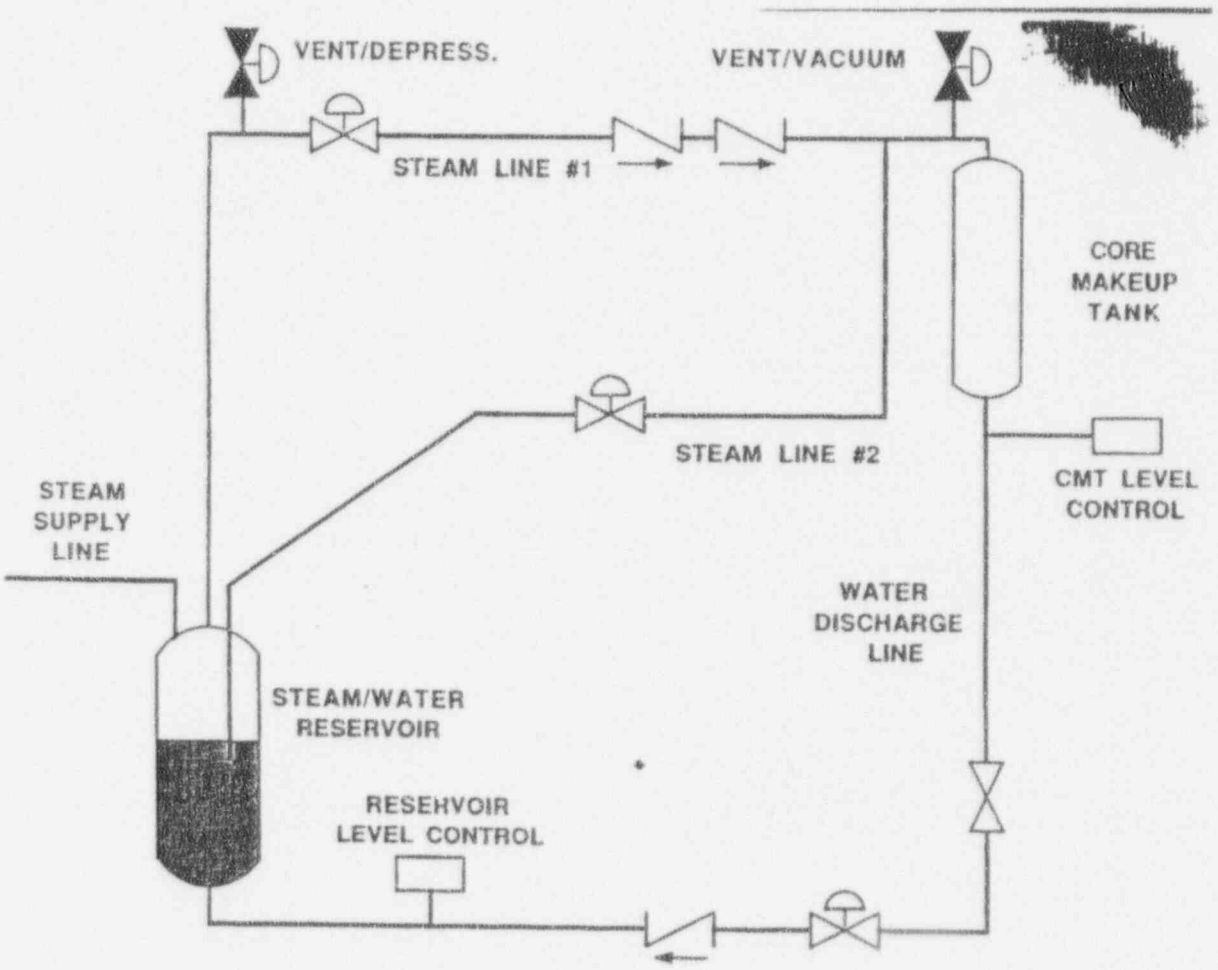

Figure 1-6 AP600 CMT Test Facility

[

a,c

]

2.0 CMT RECIRCULATION BEHAVIOR SCALING ASSESSMENT

In the recirculation mode of operation, there is volume replacement of the cold borated CMT water with hot water that flows up the cold leg balance line to the top of the CMT. The CMT remains full during this time period. This process continues until the CMT is fully heated and the natural circulation driving head for flow decreases to zero.

2.1 CMT RECIRCULATION BEHAVIOR

The ability of the CMT test facility to examine the recirculation performance of the plant CMT is examined. Both top-down and bottom-up scaling analyses are performed to assess the capability of the test CMT to provide the key thermal-hydraulic data for the recirculation period. This section will develop the governing equations and examine the scaling differences between the AP600 Plant CMT and the CMT test facility to insure that the key thermal-hydraulic phenomena presented in the PIRT are captured in the CMT test.

2.1.1 CMT Recirculation Behavior — Top-Down Analysis

Natural circulation behavior has been examined by Reyes (1993) for the Oregon State University AP600 Low Pressure Integral System Effects Tests. The general governing equations derived for the top-down scaling for single-phase recirculation are applicable for the single-phase recirculation of the CMT. The generalized system of equations that describe the natural circulation behavior are given in Equations 2-1 to 2-5.

Mass:

$$\frac{d}{dt}\left(\rho_\ell V_\ell\right) = \Delta\left[\rho_\ell Q_\ell\right] \tag{2-1}$$

Momentum:

$$\frac{d}{dt}\left(\rho_\ell U_\ell V_\ell\right) = \Delta\left[\rho_\ell U_\ell Q_\ell\right] + \beta_T g \rho_\ell \Delta T_\ell a_c - \frac{\rho_\ell U_\ell Q_\ell}{2}\left(\frac{fL_f}{D_h} + K\right) \tag{2-2}$$

Energy:

$$\frac{d}{dt}\left(\rho_\ell C_{v\ell} T_\ell V_\ell\right) = \Delta\left[\rho_\ell C_{P\ell} T_\ell Q_\ell\right] + H_s A_s\left(T_s - T_\ell\right)\big|_{Boundary} \tag{2-3}$$

Solid Energy Equation:

$$-k_s A_s\left(\frac{dT_s}{dx}\right)_{Boundary} = H_s A_s\left(T_s - T_\ell\right)\big|_{Boundary} \tag{2-4}$$

Boundary Condition:

$$\frac{d}{dt}\left(\rho_s C_{vs} T_s V_s\right) = H_s A_s\left(T_s - T_\ell\right)\big|_{Boundary} + q_s \tag{2-5}$$

The nomenclature for these equations is provided in Section 7.1.

If we consider the CMT recirculation process and assume:

1. quasi-steady state such that $\frac{d}{dt} \equiv 0$
2. no momentum effects
3. no heat transfer since we are investigating volume displacement
4. no mixing within the CMT

The system of equations reduces to

$$\Delta\left(\rho_\ell Q_\ell\right) = 0 \tag{2-6}$$

and

$$\beta_T g \rho_\ell \Delta T_\ell a_c = \frac{\rho_\ell U_\ell Q_\ell}{2}\left(\frac{fL_f}{D_H} + K\right) \tag{2-7}$$

If these equations are normalized on their initial conditions and any boundary conditions, the normalized equations become

a,c

[and

a,c]

Since we are preserving the fluid properties and the height of the test CMT relative to the plant, and the friction and form losses are also preserved, [ ]^{a,c} Therefore, the test should give recirculation performance similar to the plant. The bottom-up scaling analysis and calculations will verify the test CMT recirculation performance relative to the plant CMT.

2.1.2 CMT Recirculation Behavior — Bottom-Up Scaling Analysis

The bottom-up scaling analysis will calculate the recirculation performance of both the plant CMT and the test CMT to verify that similarity of performance exists between the two CMTs. Figure 2-1 shows a sketch of the CMT test relative to the AP600 Plant. Note that the actual pipe routing is not fully represented in this sketch.

The assumptions used in this analysis are:

1) Single-phase recirculation
2) One-dimensional flow
3) Linear interpolation of the density gradient in the CMT
4) Linear interpolation of the density gradient in the CMT test reservoir
5) Essentially zero velocity in the reactor vessel downcomer annulus
6) Loss coefficients are independent of Reynolds number
7) Quasi-steady state conditions

The generalized mechanical energy balance equation (see Bennett and Meyers) is given as

$$\frac{\Delta P}{\rho} + \frac{\Delta U_b^2}{2g_c} + \left(\frac{fL_f}{D_h} + K\right)\frac{U^2}{2g_c} + \frac{g}{g_c}\Delta L + W_s = 0 \qquad (2\text{-}14)$$

for the generalized system equation, where W_s is the rate of shaft work and is set to zero. Since the starting point and end point of the calculations are the same; then

$$\frac{\Delta P}{\rho} = 0 \qquad (2\text{-}15)$$

Expanding Equation 2-14 around the piping network using the component density gives

$$\frac{\rho_2 U_{DVI}^2}{2g_c} - \frac{\rho_1 U_{CL}^2}{2g_c} + \left(K_{CL_N} + \frac{fL_f}{D_h}\right)_{CL} \rho_1 \frac{U_{CL}^2}{2g_c} + \left(K_T + K_{CMT_N} + \frac{fL_f}{D_h}\right)_{BL} \rho_1 \frac{U_{BL}^2}{2g_c} +$$

$$\left(K_{CMT_{EX}} + K_{CKV} + K_{DVI_N} + \frac{fL_f}{D_h}\right)_{DVI} \rho_2 \frac{U_{DVI}^2}{2g_c} + \frac{g}{g_c}\rho_1 L - \frac{g}{g_c}\rho_2 L = 0 \qquad (2\text{-}16)$$

where ρ_1 is the hot RCS and balance line flow and ρ_2 is the cold CMT fluid density state.

The form loss coefficients and velocities are defined in the nomenclature in Section 7.1.

Equation 2-16 can be further simplified noting that the volume flow is preserved, that is

$$U_{CL}A_{CL} = U_{BL}A_{BL} = U_{DVI}A_{DVI} = Q_\ell \qquad (2\text{-}17)$$

Transposing the gravity head term to the left side of the equation and using Equation 2-17; the system Equation 2-16 becomes

$$\frac{g}{g_c}L(\rho_2 - \rho_1) = \frac{Q_\ell^2}{2g_c}\left\{\left[\left(K_{CLN} + \frac{fL_f}{D_h}\right)_{CL} - 1\right]\frac{\rho_1}{A_{CL}^2} + \right.$$

$$\left[K_T + K_{CMT_N} + \left(\frac{fL_f}{D_h}\right)_{BL}\right]\frac{\rho_1}{A_{BL}^2} + \qquad (2\text{-}18)$$

$$\left.\left[K_{CMT_{EX}} + K_{CKV} + 1\ K_{DVI_N} + \left(\frac{fL_f}{D_h}\right)_{DVI}\right]\frac{\rho_2}{A_{DVI}^2}\right\}$$

As the CMT recirculates, the top of the CMT will fill with the less dense, hot fluid from the cold leg at density ρ_1. Recirculation will end when all of the denser liquid, ρ_2, has been replaced with the less dense ρ_1 fluid. To represent the decrease in the driving head the buoyant term becomes

$$\frac{g}{g_c}\left[\left\{\left(L - L_1\right)\rho_2 + L_1\rho_1\right\} - \rho_1 L\right] \qquad (2\text{-}19)$$

which simplifies to

$$\frac{g}{g_c}\left[\left(L - L_1\right)\left(\rho_2 - \rho_1\right)\right] \qquad (2\text{-}20)$$

where L_1 is the height of less dense liquid ρ_1 in the CMT, and L is the overall height. This expression has the correct limits since at the beginning of recirculation, L_1=0, and the full driving head is available, while when L_1=L, there is no driving head and recirculation ends.

The value of L_1 can be calculated as

$$L_1 = \int_0^t \frac{\dot{m}(t)\, dt}{\rho_1 A_{CMT}} \qquad (2\text{-}21)$$

where A_{CMT} is a function of L_1 for the CMT heads and $\dot{m}(t)$ is the mass flow into the CMT. Equation 2-21 must be solved in an iterative fashion for the CMT head volume, but can be directly solved for the cylindrical portion.

A similar calculation is used for the steam/water reservoir in the CMT test since the volume is much smaller than the volume of the reactor system. In this case, the driving head will also decrease as the reservoir fills with the denser ρ_2 fluid. This will result in a faster decreasing circulation rate for the CMT test, relative to the AP600. In the AP600, the colder CMT water that enters the downcomer can fall or flow downward to the core inlet. There is less of a chance that it would act to diminish the driving head, as in the CMT test.

The hydraulic resistances for the experiment were measured in the pre-operational tests and were found to be very close to standard textbook values. The current design values for the AP600 CMT balance line and DVI line resistances were used, as well as an estimate for the reverse flow cold leg nozzle loss and the DVI nozzle expansion. Equations 2-18, 2-20, and 2-21 were programmed for the AP600 CMT and the CMT test facility.

Figure 2-2 shows the mean flow rate as a function of time for the AP600 CMT balance line circuit. Figure 2-3 shows the development of the hotter, less dense fluid level in the CMT as it drains. The dominant terms in AP600 CMT mass flow equation are the form losses in the circuit. The frictional terms are second order effects.

The same figures are shown for the CMT test facility. Figure 2-4 shows the mass flow rate as a function of time for the CMT test circuit. Figure 2-5 shows the development of the hotter liquid layer in the CMT test vessel. The dominant terms in the CMT test are the line frictional losses since there are many more L/D's in the test facility compared to the plant.

[

]a,c

Figure 2-6 shows the recirculation mass flux ratio of the CMT test to the AP600 Plant at 1100 psia. As the figure indicates, the CMT recirculates at [ ]a,c of the mass flux of the plant; then as time increases, it decreases to [ ]a,c. This is due to the increase in the cold level in the test reservoir, which decreases the test driving head relative to the plant. As a result, the test mass flow decreases at a faster rate in the test than in the plant. The calculated hot liquid layer in the CMT test reservoir and the plant CMT are shown in Figure 2-7 at 1100 psia. Similar response occurs for the first 250 seconds between the test and plant, after which the hot layer builds up faster in the test than in the plant. Figures 2-6 and 2-7 are repeated at 2250 psia conditions in Figures 2-8 and 2-9 for high pressure performance of the CMTs (more typical of operational transients) and similar behavior is observed.

2.2 DISCUSSION OF CMT RECIRCULATION SCALING

Since the CMT test can simulate the full pressure and temperature operation of the plant, the density differences are preserved. Since the heights are preserved, the buoyant expression in Equation 2-2 is preserved between the test and the plant, such that the [ ]a,c, as given in equation 2-12. This is confirmed by the ratio of the CMT mass flux ratio that is nearly unity.

The resistances of the plant are calculated design values, not measured, that the test only approximately simulated. Also, the resistances in the test are dominated by frictional pressure drop, not form losses, which would make them more flow or Reynolds-number dependent. That is, as the flow decreases, the Reynolds number will decrease, increasing the friction factor. [

]a,c

A more significant effect is the build up of the cold liquid layer in the steam/water reservoir tank in the test. There is no counterpart for this component in the AP600 reactor systems since the flow from the CMT can enter the core. In the test, the increase in the cold liquid layer in the reservoir will

decrease the net driving head for the test recirculation, relative to the plant. However, since the reservoir has an area of 3.5 times as large as the CMT, the effect will be small, but noticeable.

The hot liquid layer build up in the test can also be examined from a geometric basis for the test CMT and the plant CMT. The scaling approach used in the CMT test was to choose an inside diameter scale ratio of

[ ]^{a,c}

Using this as a scale ratio, S, the areas of the inlet nozzle were preserved in the same fashion such that

$$d_{N_m} = S\, d_{N_p} \tag{2-23}$$

or

$$A_{N_m} = S^2 A_{N_p} \tag{2-24}$$

Since the scaling approach preserves the full pressure and full height, and the line resistances are similar to, but not exactly the same, the mass flux recirculation ratio, as shown in Figure 2-6, is nearly unity.

Therefore, the mass flow in the CMT test should be related to the plant mass flow as

$$\rho U)_m \cdot A_{N_m} \cong \rho U)_p\, A_{N_p} \cdot S^2 \tag{2-25}$$

Since full height simulation was used, and the line resistances are similar, the time scale for the test is similar to the plant, that is

$$t_m = \frac{L_m}{U_m} \cong t_p = \frac{L_p}{U_p} \tag{2-26}$$

at least until the CMT test tank, which is 10 feet high, is filled with hot water.

Therefore, the development of the hot liquid layer in the CMT test, relative to the plant, is given as

$$\Delta t\ \rho U A_N\Big)_m = \rho A_m(L_m)\Delta L_m \tag{2-27}$$

Where $A_m(L_m)$ is the cross section area of the CMT in the test head region and ΔL_m is the layer thickness. If the tank has drained to the cylindrical portion then the cross sectional area is a constant. A similar expression can be written for the plant as

$$\Delta t\ \rho U A_N\Big)_p = \rho A_p(L_p)\Delta L_p \tag{2-28}$$

Since time is approximately preserved, both Equations 2-26 and 2-27 can be solved for Δt and equated giving

$$\frac{\rho A_m(L_m)\Delta L_m}{\rho U A_N)_m} = \frac{\rho A_p(L_p)\Delta L_p}{\rho U A_N)_p} \tag{2-29}$$

Using Equations 2-24 and 2-25, Equation 2-29 reduces to

$$\frac{\Delta L_m}{\Delta L_p} = \frac{A_p(L_p)}{A_m(L_m)}\ \frac{\rho U)_m}{\rho U)_p}\ \frac{A_{N_m}}{A_{N_p}} \tag{2-30}$$

or

$$\frac{\Delta L_m}{\Delta L_p} = \frac{A_p(L_p)}{S^2 A_m(L_m)}. \tag{2-31}$$

That is, the hot layer development in the test should be approximately the same as that in the plant, if the test and plant dome or head regions are geometrically similar. Figure 2-10 shows the difference in the cross section area of the plant CMT and the test facility CMT. As the figure indicates, there are

differences in these areas that will affect the thickness of the hot water layer as it develops. In general, however, the test article is a reasonable approximation of the plant. Resistance differences between the test and the plant can affect the mass flux ratio, which can alter the layer development.

As the CMT recirculates and hot water replaces the cold water in the tank, there will be heat transfer between the colder CMT walls and the hot water layer. The scaling effects of the wall heat transfer in the CMT test and the AP600 CMT were estimated for the recirculation period. Because the CMT tanks drain slowly, the convective velocity past the walls is small, approximately 0.008 to 0.016 ft/sec, depending on whether the tank is in the recirculation or draining mode, with vapor in the cold leg balance line. The heat transfer at the CMT inside wall surface from the hot CMT liquid layer could either be forced convection or natural convection depending on the temperature difference between the hot recirculated CMT liquid temperature and the CMT walls, as well as the thickness of the hot CMT liquid layer. To evaluate which mode of heat transfer dominates, the ratio

$$\frac{Gr}{Re^2} >><< 1 \tag{2-32}$$

where

$$Gr = \frac{\beta g (T_b - T_w) Z^3}{\nu^2} \tag{2-33}$$

where $(T_b - T_w)$ is the temperature difference between the hot fluid temperature and T_w is the CMT inside wall temperature. Z is the thickness of the hot liquid layer inside the CMT. The Reynolds number is based on the inside diameter for the CMT.

Using the recirculation mass flow, a tank Reynolds number can be calculated as

$$Re_T = \frac{\dot{m} D_T}{A_T \mu} \tag{2-34}$$

If Equation 2-34 is evaluated at 400 seconds; the AP600 Plant Reynolds number becomes

$$R_{e_T}\Big)_P = 62000 \tag{2-35}$$

and the CMT model Reynolds number is

$$R_{e_T}\Big)_m = 6750 \tag{2-36}$$

Both the AP600 and the test CMT are in a turbulent flow regime; a turbulent heat transfer convective correlation such as Dittus-Boelter (1930) is applicable. The Grashoff number was calculated for a range of hot liquid to CMT wall temperature differences, and for different hot liquid layer thickness, the ratio of Gr/Re^2, given in Equation 2-32, was evaluated over this range and was found to be greater than 1 for all cases; indicating that the heat transfer between the cold CMT wall and the hot liquid would be by natural convection.

The Π group that examines the convective heat transfer is the Nusselt number, defined as

$$Nu = \frac{hZ}{R} = 0.021\ Ra_L^{0.4} \tag{2-37}$$

which is given by Eckart and Jackson (1951) for turbulent flow where the Raleigh number is given in terms of the Grashoff number and the Prandtl number as

$$Ra_L = Gr_L \cdot Pr \tag{2-38}$$

such that

$$Nu = \frac{hZ}{k_\ell} = 0.02\ (Gr_L \cdot Pr)^{2/3} \tag{2-39}$$

[

a,c

]

Since the fluid properties are preserved, the ratio of the heat transfer coefficients becomes

$$\frac{h_m}{h_p} = \left[\frac{(T_b - T_w)_m}{(T_b - T_w)_p}\right]^{.4} \left(\frac{Z_m}{Z_p}\right)^{.2} \qquad (2\text{-}41)$$

where it has been assumed that all physical properties are the same between the model and the AP600 test. Since the model CMT will experience the same wall and fluid temperature range as the AP600 CMT; and since the development of the hot liquid layer is very similar between the model and plant CMT, the heat transfer coefficient ratio is

$$\frac{h_P}{h_m} = 1.0 \qquad (2\text{-}42)$$

which indicates that the experiment will yield natural convective heat transfer data in the recirculation phase that is approximately the same as the AP600 Plant CMT.

If the heated liquid layer is very thin, less than 0.3 feet, then the ratio given in Equation 2-32 is closer to unity for the plant CMT. For the same hot water layer thickness, the model CMT will tend to remain in the free convection compared to the plant, since the test CMT Reynolds number is smaller due to the diameter difference. However, this situation only occurs when the heated CMT water level is very small. Natural convection heat transfer will dominate all other cases.

2.3 CONCLUSION ON CMT TEST FACILITY RECIRCULATION SCALING BEHAVIOR

The system of equations that govern the CMT recirculation behavior were normalized and the [

]^{a,c}. Since full

pressure, full height is preserved in the test, and the resistances are also preserved, these dimensionless ratios were near unity for the model CMT. This indicates that the test CMT will preserve the recirculation thermal-hydraulic phenomena expected in the plant CMT.

In addition, a one-dimensional flow model has been used to calculate the behavior of the AP600 CMT and the CMT test facility natural circulation behavior. The calculated recirculation flows were normalized and compared between the test facility and the plant. The hot water layer development in the CMT was also calculated for both the test and the plant CMT and compared. The comparison of the calculated recirculation flows (mass flux) and the hot water layer were very similar between the test and the AP600 CMT. If the PIRT table, provided as Table 1-1, is reviewed under the CMT recirculation phenomena testing, the natural circulation of the CMT and the cold leg balance line behavior is well simulated. The CMT wall heat transfer to the CMT liquid, due to the recirculation, has also been assessed showing that the CMT test will yield natural convective heat transfer coefficients similar to those expected for the AP600 Plant CMT. Therefore, the water to CMT wall liquid heat transfer phenomena, identified in the PIRT, will be addressed in the tests, and the resulting data will be available for computer code validation.

The liquid mixing effects of the CMT balance leg, the condensate, and CMT liquid were not assessed. However, since the hot liquid layer in the test closely approximates the AP600 Plant, and the recirculation mass flows are similar, the mixing behavior of the CMT test and the plant should be similar such that this particular phenomena will be captured. The flashing effects of the test CMT and the AP600 Plant CMT were also not specifically calculated. However, since the hot liquid layer development is similar in the CMT test model compared to the plant; and since the experiments will cover the full pressure range of operation as the plant, it is expected that the flashing effect will be similar between the test and the plant such that this phenomena on the PIRT chart will be addressed for code validation.

In conclusion, the scaling for the CMT test has shown that the same effects observed in the plant recirculation behavior can be represented adequately in the test such that the recirculation phenomena listed in the CMT PIRT will be captured in the CMT test facility.

a,c

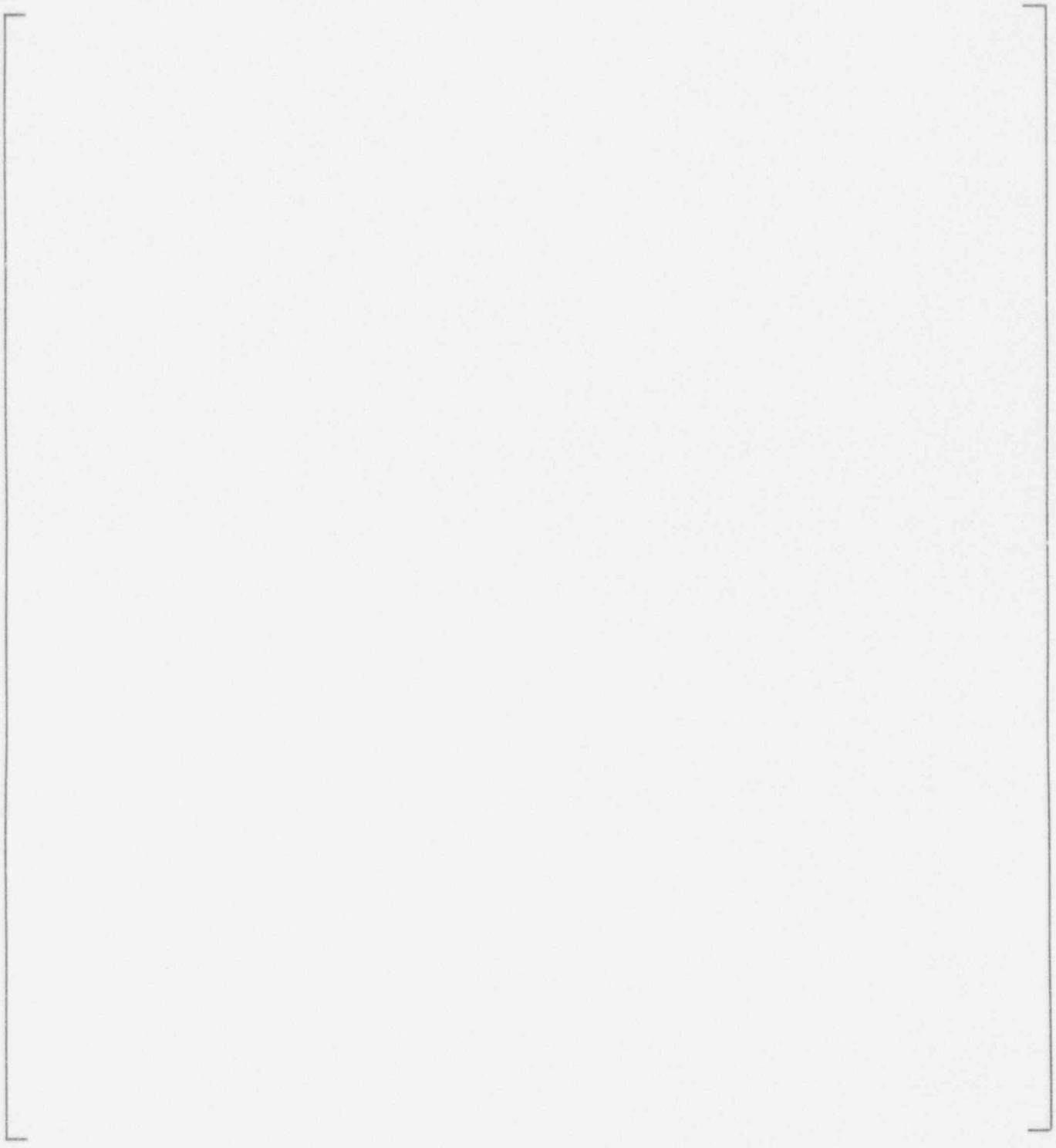

Figure 2-1 CMT Test Facility and AP600 Plant

a,c

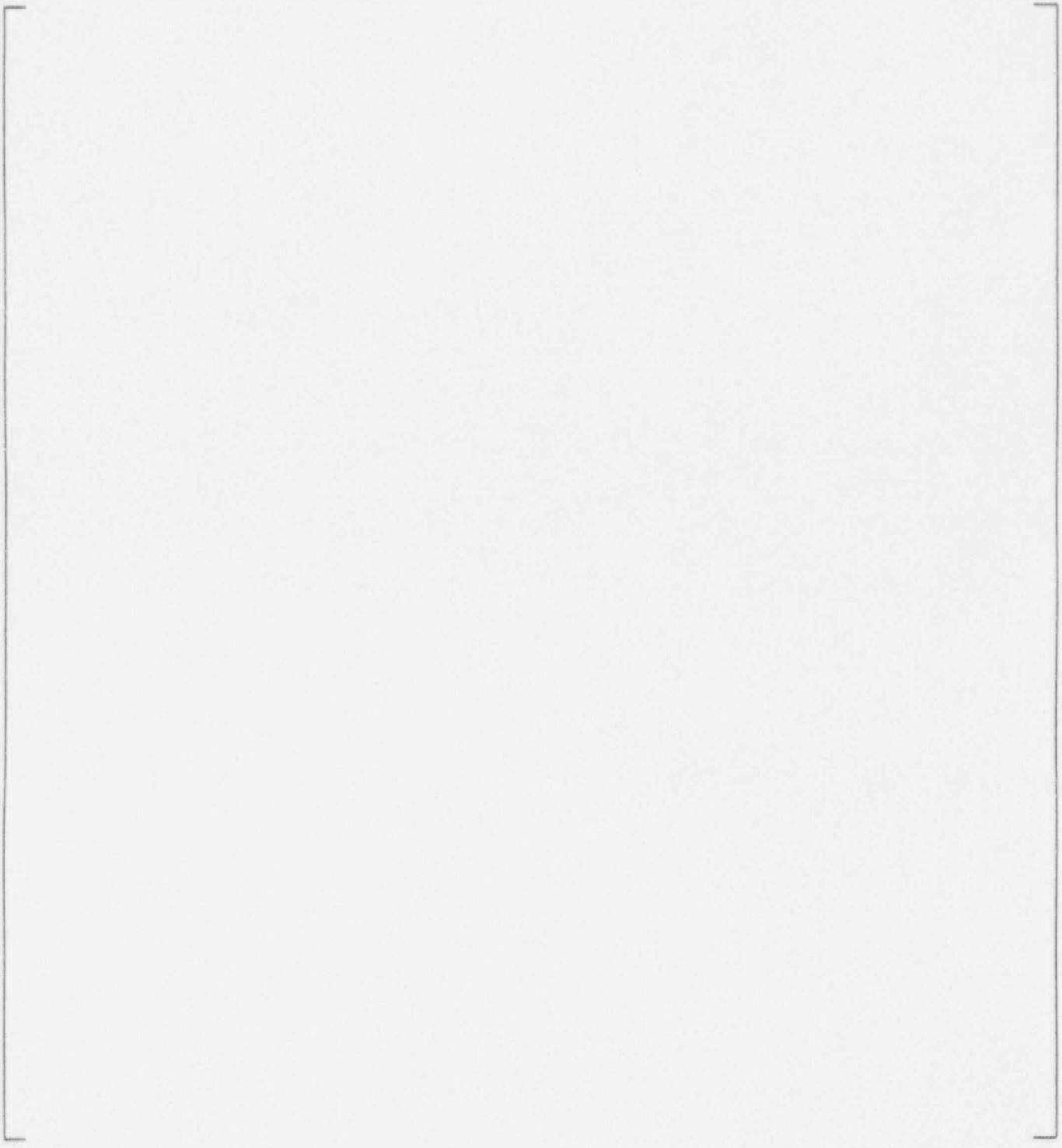

Figure 2-2 Calculated Recirculation Flow for the AP600 CMT at 1100 psia

a,c

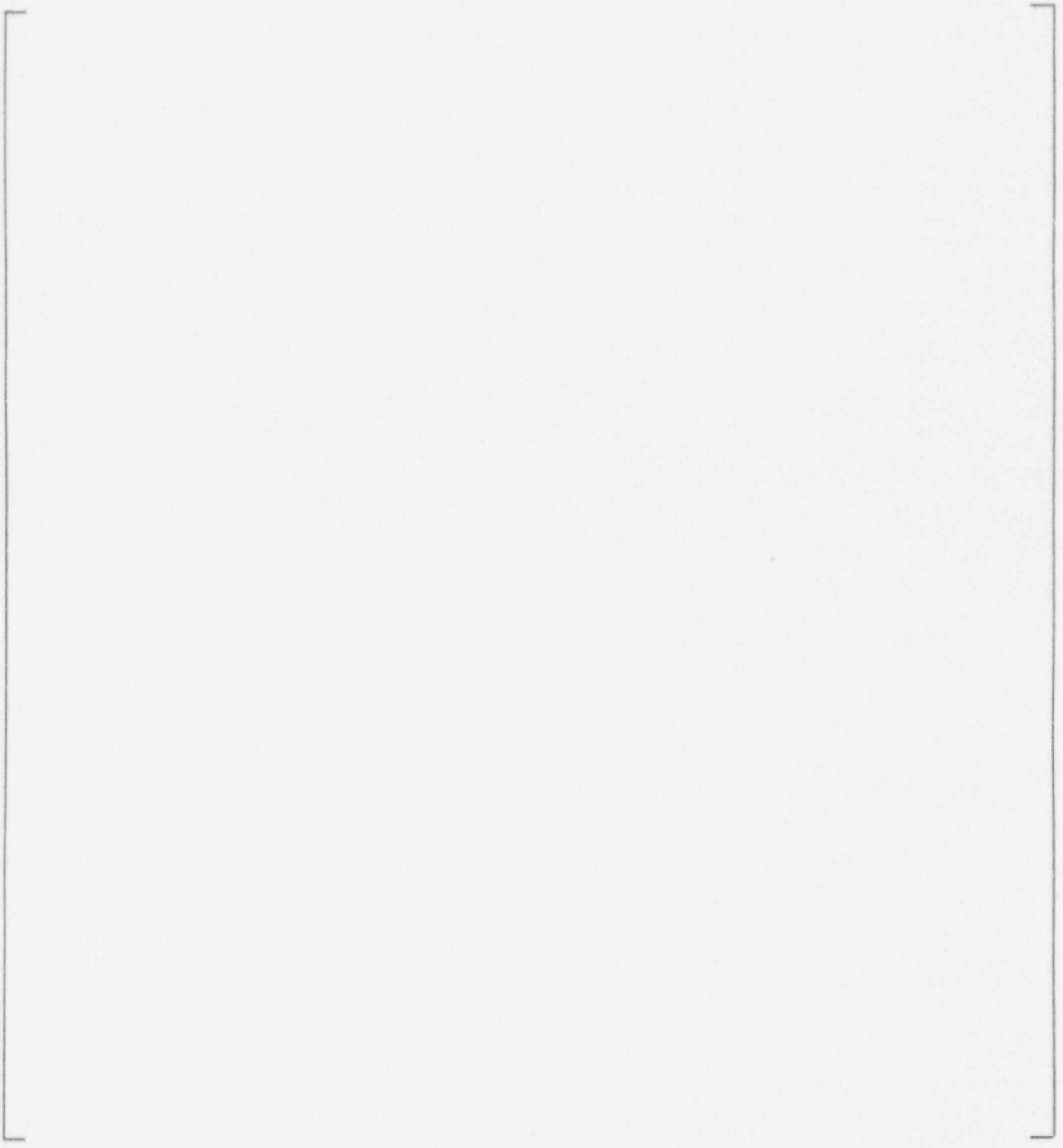

Figure 2-3 Calculation of the Hot Liquid Layer Thickness for the AP600 CMT at 1100 psia

a,c

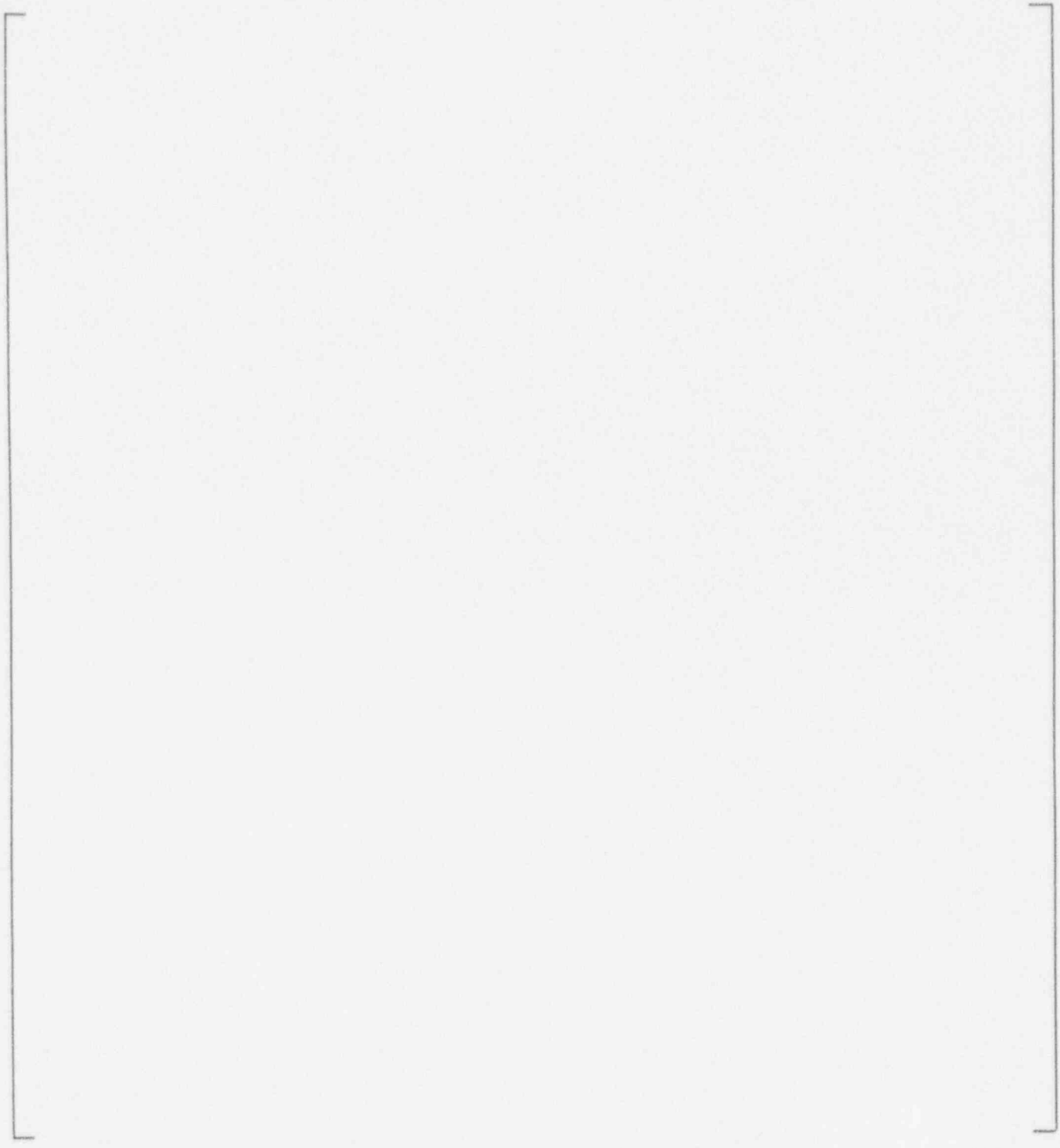

Figure 2-4 Calculation of the Recirculation Flow for the CMT Test Facility at 1100 psia

a,c

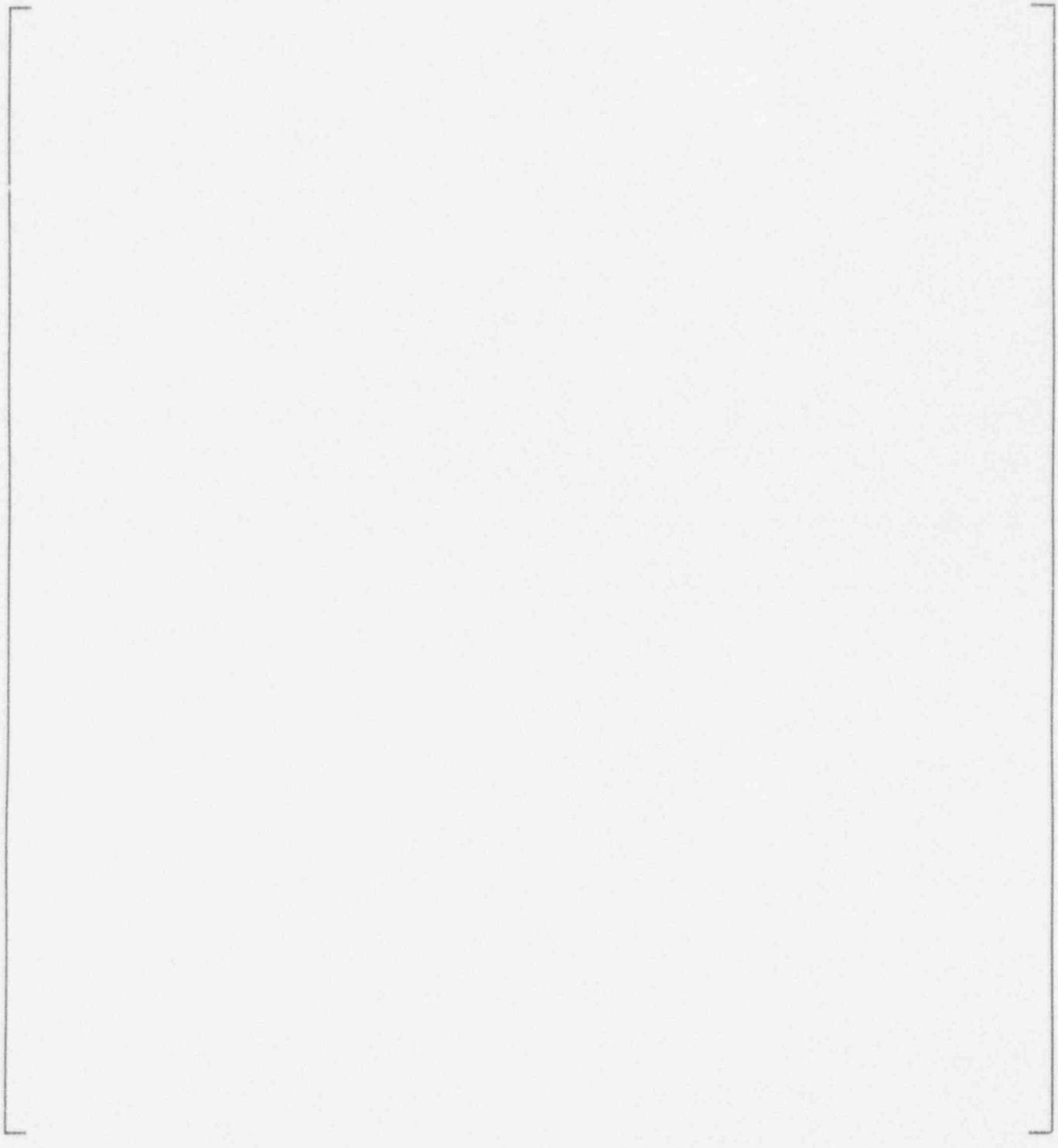

Figure 2-5 Calculation of the Hot Liquid Layer Thickness for the CMT Test Facility and Cold Liquid Layer Thickness in the Reservoir at 1100 psia

a,c

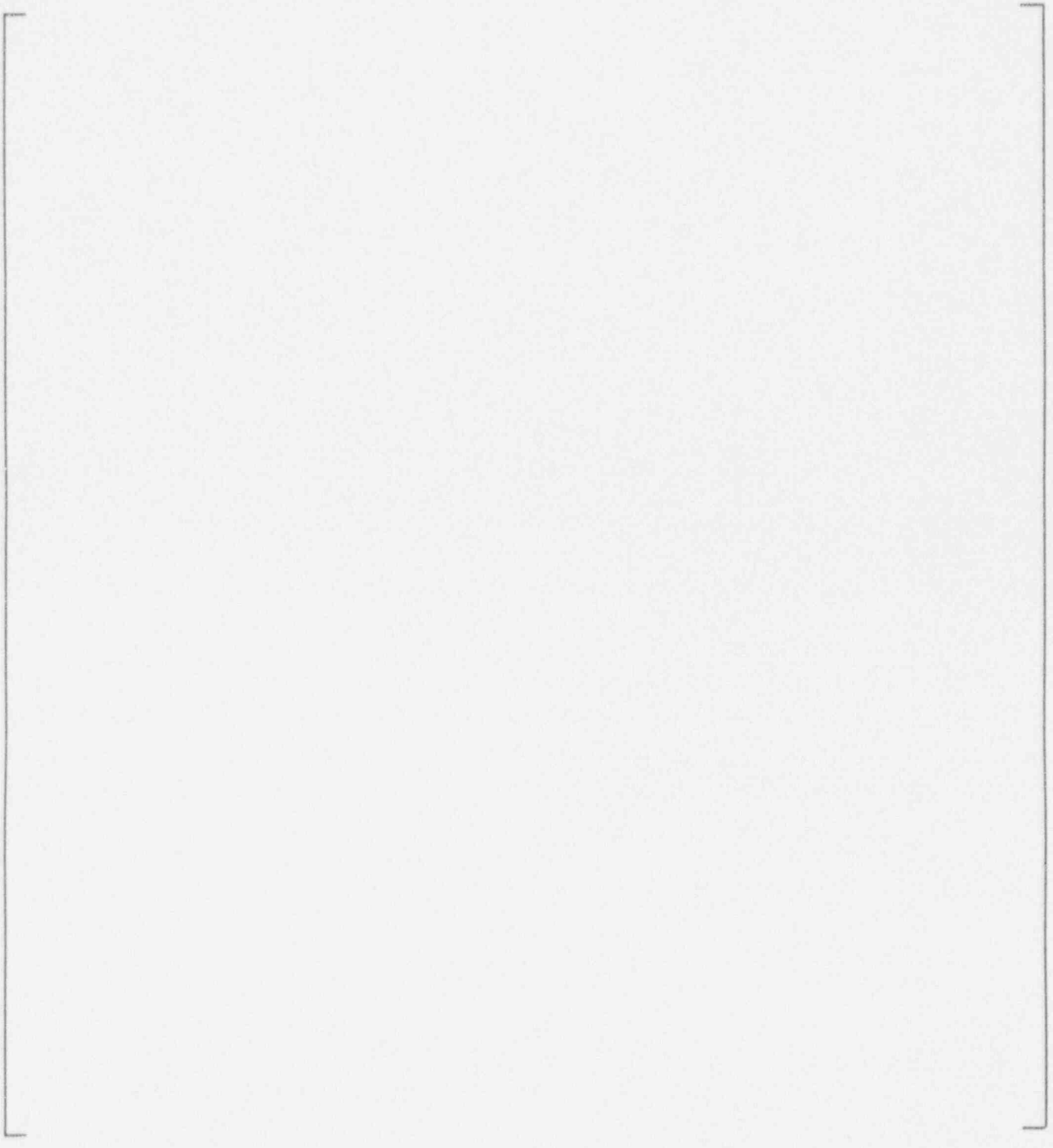

Figure 2-6 Recirculation Ratio of the CMT Test to the AP600 CMT at 1100 psia

a,c

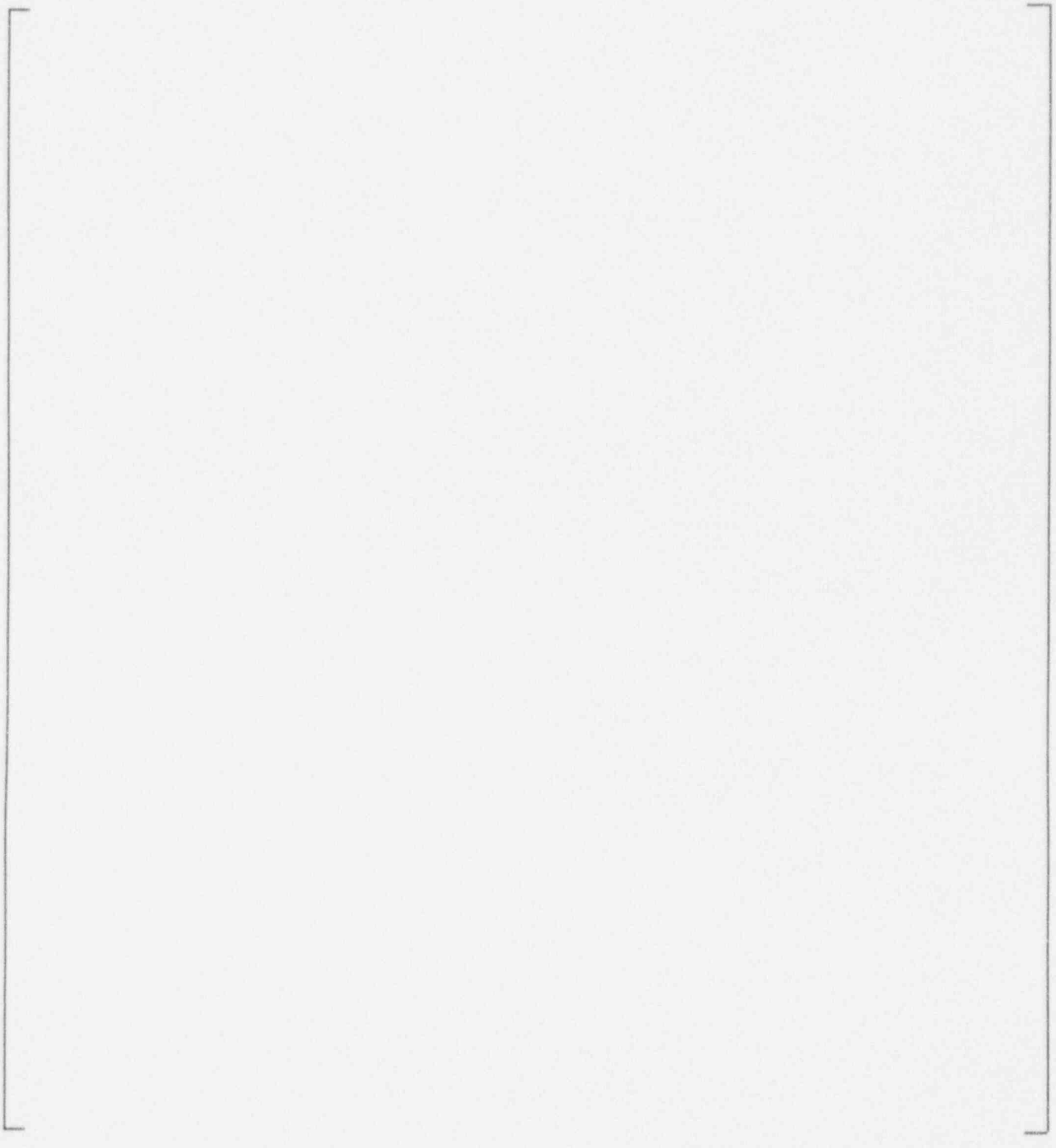

Figure 2-7 Comparison of the Hot Layer Thickness of the CMT Test and the Plant CMT at 1100 psia

a,c

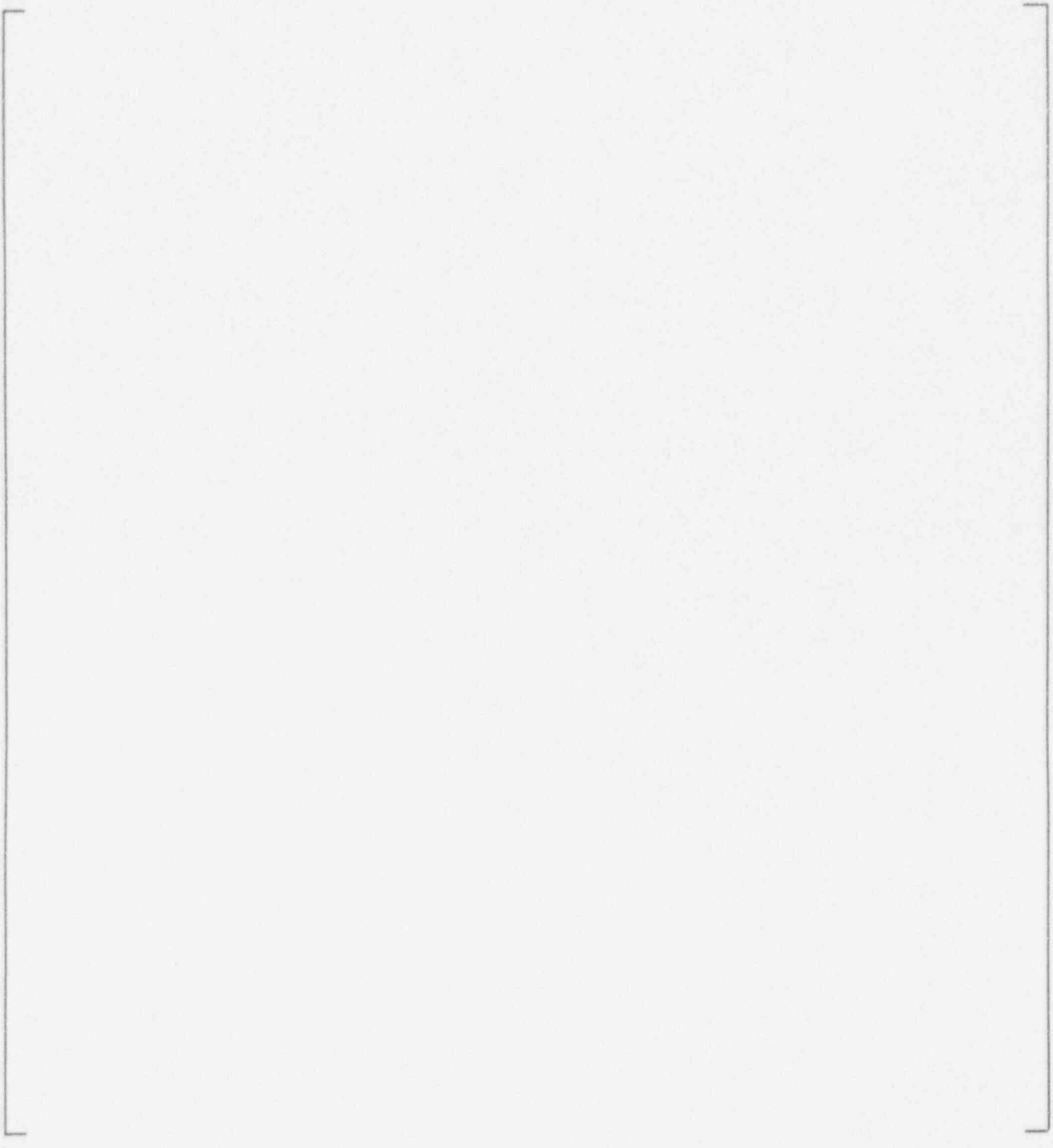

Figure 2-8 Comparison of the Recirculation Ratio of the CMT Test to the AP600 CMT at 2250 psia

a,c

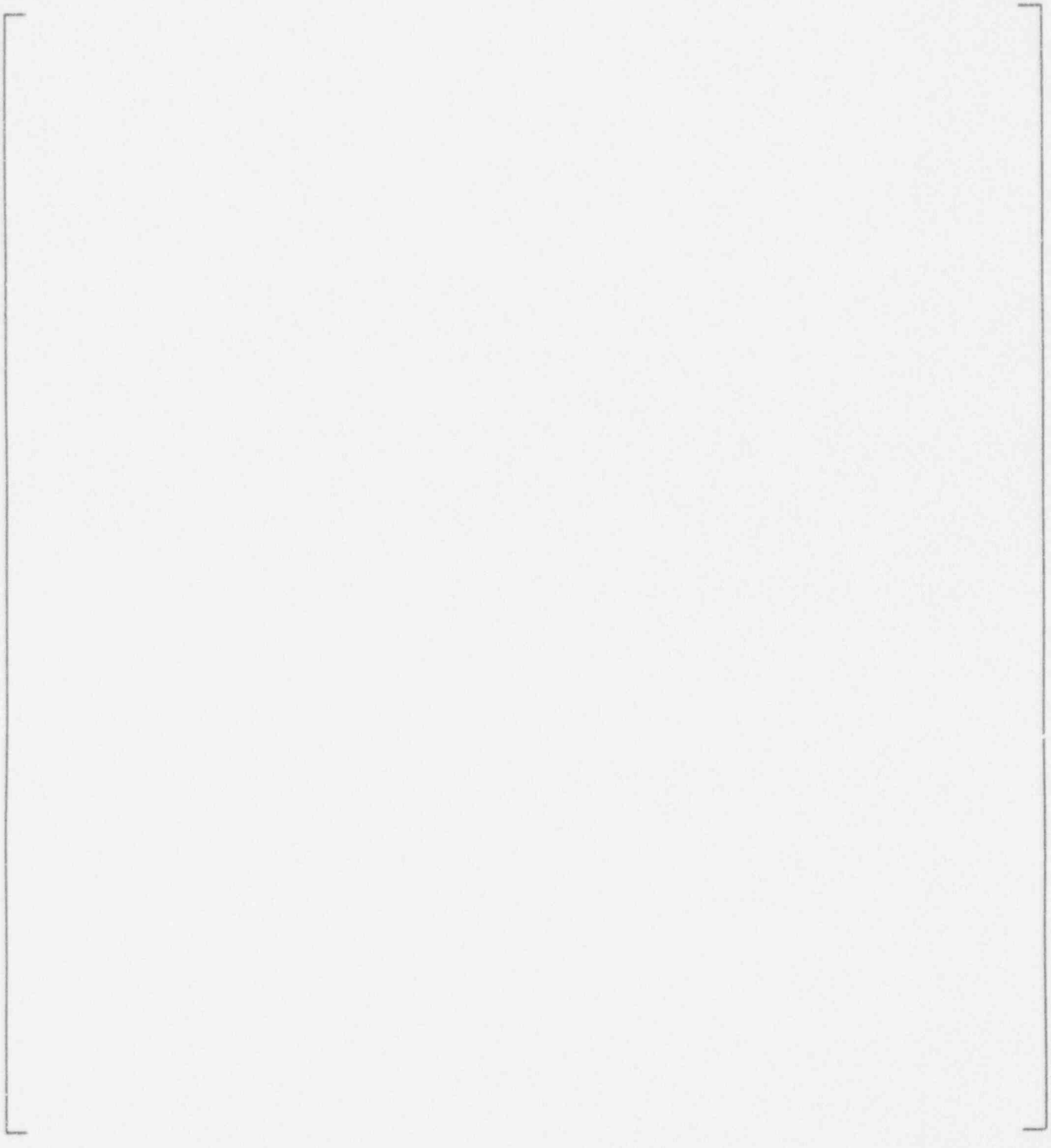

Figure 2-9 Comparison of the Hot Layer Thickness of the CMT Test and Plant at 2250 psia

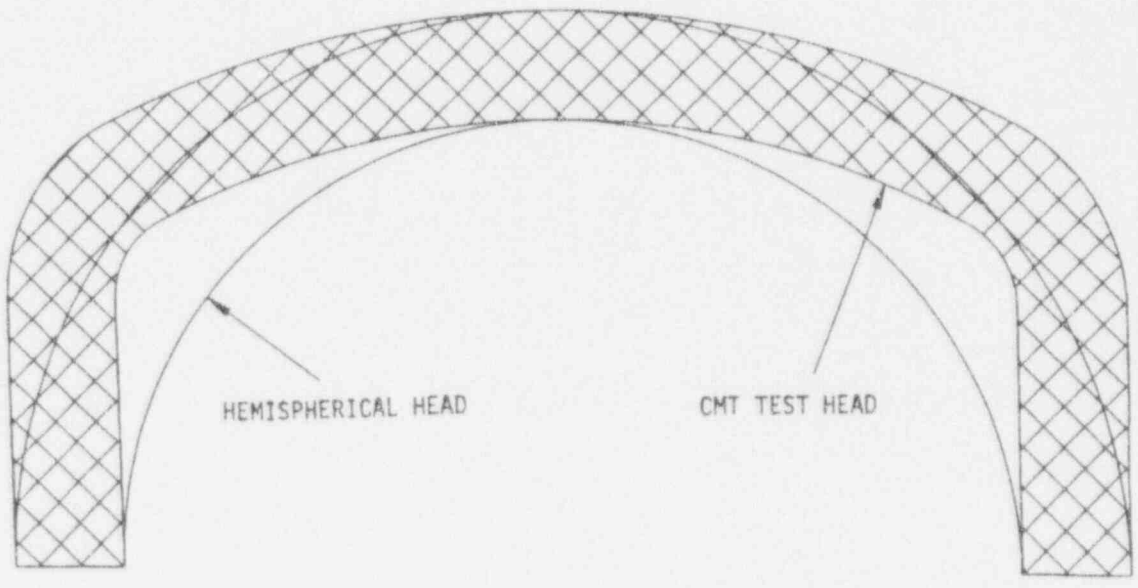

Figure 2-10 Comparison of AP600 Plant Head Cross Section Area and AP600 CMT Test Head Cross Section Area

3.0 CMT DRAINDOWN BEHAVIOR SCALING ASSESSMENT

One of the modes of operation of the CMT is the draining behavior during which the natural circulation flow path is broken and steam flows from the cold leg balance line and the pressurizer balance line to the CMT. The steam condenses on the cold CMT walls and water surface, drawing more steam into the CMT. As the condensation proceeds, the wall and water surfaces are heated and the tank drains. Eventually, the draining process approaches a volume replacement process and the tank drain rate is based on the elevation head within the tank.

This section will focus on the condensation processes in the CMT and will compare the estimated response of the AP600 Plant CMT to the CMT test facility to insure that the CMT test facility will capture the key thermal-hydraulic phenomena identified in the PIRT.

3.1 GOVERNING EQUATIONS FOR TANK DRAINING PROCESSES

This section uses as a basis the scaling methodology developed by Reyes (1993) for the CMT for the Oregon State University AP600 Low Pressure Integral Systems Test. A set of balance equations and dimensionless groups, applicable to draining processes in general, is developed. Figure 3-1 defines the control volume boundaries for the CMT. The system of equations that represent the tank and its draining are given as

Liquid Mass:

$$\frac{d}{dt}(\rho_\ell V_\ell) = \Delta[\rho Q] \tag{3-1}$$

Liquid Energy:

$$\frac{d}{dt}(\rho_\ell e_\ell V_\ell) = \Delta\left[\rho Q\left(e_\ell + \frac{P}{\rho}\right)\right] + q_t - W_t \tag{3-2}$$

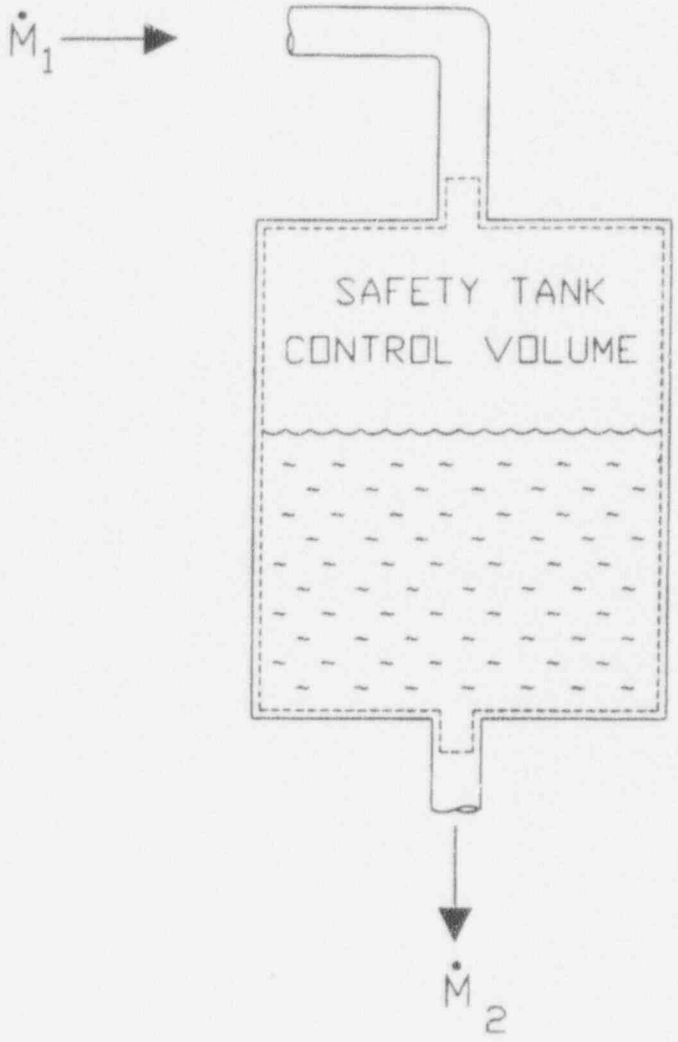

Figure 3-1 Control Volume Boundaries for CMT Draining Analysis

Solid Structure Energy:

$$\frac{d}{dt}(\rho_s V_s C_{vs} T_s) = H_{st}(T_s - T_\ell)a_{si} - H_{sa}(T_s - T_{amb})a_{sa} \qquad (3\text{-}3)$$

Equations 3-1 and 3-2 are the fluid conservation equations for the tank. In these equations,

ρ_ℓ	is the density of the liquid inside the control volume
V_ℓ	is the volume of liquid inside the control volume
$\Delta[\rho Q]$	is the net rate of fluid mass entering or leaving the control volume
q_t	is the net heat loss to the ambient
W_t	is the shaft work done by the liquid, and
e_ℓ	is the average liquid energy per unit mass. It consists of internal energy, kinetic energy, and potential energy as follows:

$$e_\ell = e_{int} + \frac{U^2}{2g_c} + \frac{gz}{g_c} \qquad (3\text{-}4)$$

The term,

$$\Delta\left[\rho Q\left(e_\ell + \frac{P}{\rho}\right)\right] \qquad (3\text{-}5)$$

is the net rate of liquid energy entering or leaving the control volume. It includes the work done by pressure on liquid flowing across the control surface boundaries. Equations 3-1 and 3-2 describe the average liquid mass and energy transfer for the control volume.

Equation 3-3 is the solid structure energy conservation equation. It is a lumped parameter description of the solid structure that encloses the control volume. It assumes a uniform temperature throughout the solid. This equation will be replaced by a more complete one-dimensional conduction equation in

subsequent sections to more accurately calculate the heat transfer into the CMT walls. H_{st} is the coefficient for convective heat transfer from the surface to the liquid inside the CMT and H_{sa} is the coefficient for the convective heat transfer from the surface to the ambient.

The following assumptions will be applied to the governing equations:

1. The liquid inside the control volume is inviscid and incompressible
2. There is no work done by the liquid
3. Changes in kinetic and potential energy internal to the liquid inside the control volume are small compared to its internal energy

The liquid volume inside a tank having a constant cross section area, A_{TANK} over the entire height of liquid, $L_\ell(t)$, is given by

$$V_t = A_{TANK} L_\ell(t) \tag{3-6}$$

This particular assumption will be modified when analyzing the plant CMT since a large fraction of the surface area and tank volume is contained within the heads of the tank.

Substituting Equation 3-6 into Equation 3-1 yields

$$\frac{d}{dt}(\rho_\ell A_{TANK} L_\ell) = \Delta[\rho Q] \tag{3-7}$$

Recognizing that the mass flow rate $\dot{m}$, equals ρQ, Equation 3-7 becomes:

$$\frac{d}{dt}(\rho_\ell A_{TANK} L_\ell) = \sum \dot{m}_1 - \sum \dot{m}_2 \tag{3-8}$$

Locations 1 and 2 are shown on Figure 3-1.

Applying the assumptions stated above to the liquid energy Equation 3-2 yields

$$\frac{d}{dt}(\rho_\ell A_{TANK} C_{v\ell} T_\ell L_\ell) = \sum (\dot{m}h)_1 - \sum (\dot{m}h)_2 + q_t \tag{3-9}$$

Furthermore, since all of the CMT tanks have a single drain line, Equations 3-8 and 3-9 can be simplified as follows:

$$\frac{d}{dt}(\rho_\ell A_{TANK} L_\ell) = \sum \dot{m}_1 - \dot{m}_2 \tag{3-10}$$

$$\frac{d}{dt}(\rho_\ell A_{TANK} L_\ell C_{v\ell} T_\ell) = \sum (\dot{m}h)_1 - \dot{m}_2 h_2 + q_t \tag{3-11}$$

Because each CMT has a pressurizer balance line and a cold leg balance line attached to the CMT head, the same simplification could not be applied to the inlet. These simplified equations are summarized in Table 3-1 and can be expressed in terms of dimensionless quantities using the initial and boundary conditions presented in Table 3-2.

Substituting the dimensionless quantities into Equations 3-3, 3-10, and 3-11 and dividing the liquid mass conservation equation by $(\dot{m}_2)_o$, the liquid energy conservation equation by $(\dot{m}_2 h_2)_o$ and the solid structure energy equation by $(H_{sa} a_{si} T_{amb})_o$ yields the non-dimensionalized balance equations listed in Table 3-3.

Table 3-1
Top-Down Subsystem Level Scaling Analysis: Control Volume Balance Equations for Safety Injection Tank Draining (with Simplifying Assumptions)

Liquid Mass:

$$\frac{d}{dt}(\rho_\ell A_{TANK} L_\ell) = \sum \dot{m}_1 - \sum \dot{m}_2 \qquad (3\text{-}10)$$

Liquid Energy:

$$\frac{d}{dt}(\rho_\ell A_{TANK} L_\ell C_{v\ell} T_\ell) = \sum (\dot{m}h)_1 - \dot{m}_2 h_2 + q_t \qquad (3\text{-}11)$$

Solid Structure Energy:

$$\frac{d}{dt}(\rho_s V_s C_{vs} T_s) = H_{st}(T_s - T_\ell)a_{si} - H_{sa}(T_s - T_{amb})a_{sa} \qquad (3\text{-}3)$$

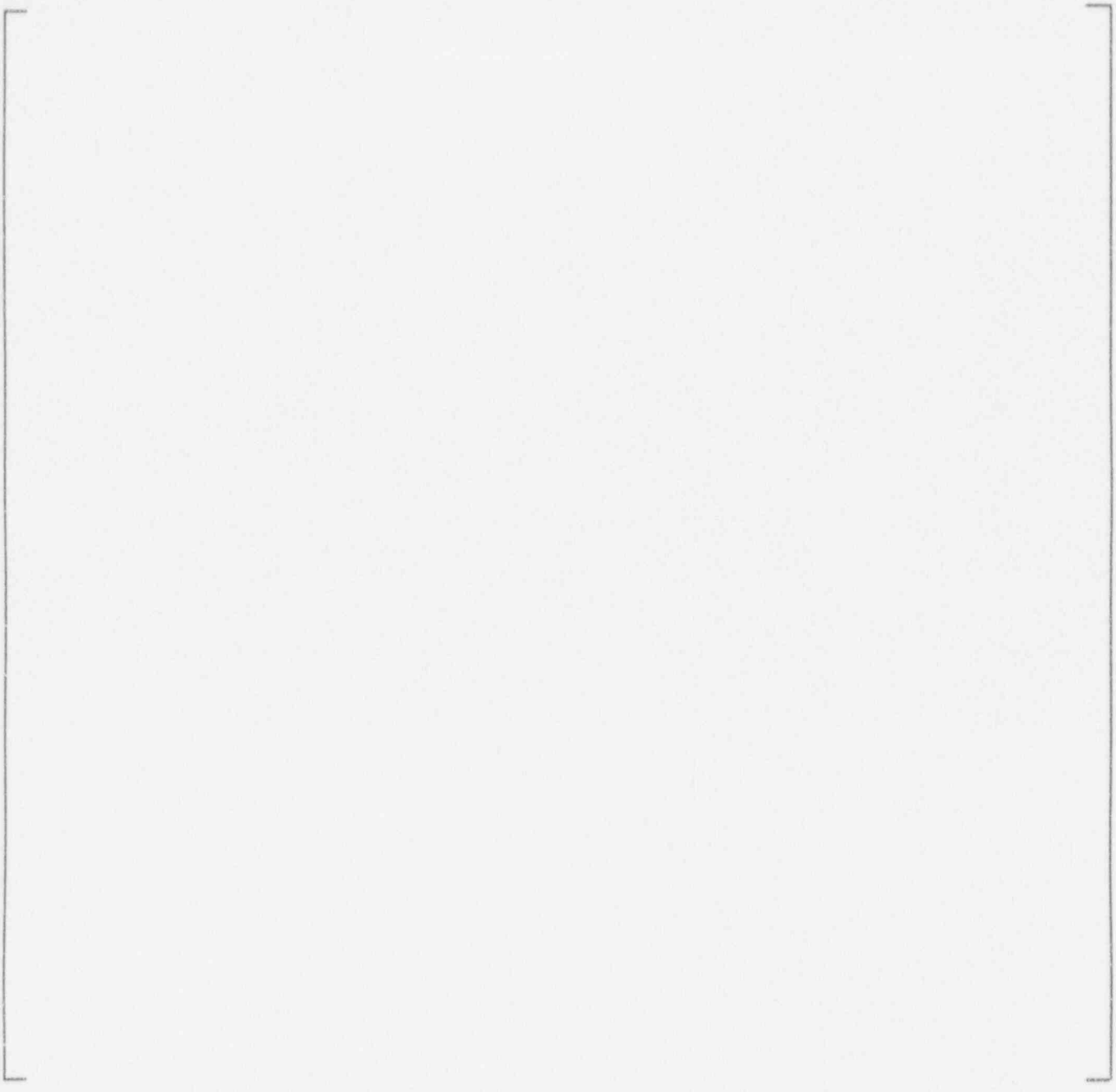

a,c

a,c

3.2 CMT TOP-DOWN SCALING ANALYSIS FOR CMT DRAINING

This section presents a more detailed scaling analysis for the CMTs, using the system equation derived in Section 3.1.

The phenomena of interest during the CMT draining process are given in the PIRT Table 1-1 and are:

- Condensation on cold steel surfaces
- Transient conduction in CMT walls
- Interfacial condensation on CMT liquid surface
- Dynamic effects of steam injection and mixing
- Thermal stratification and mixing of condensate with colder CMT water

Figure 3-2 is a flow diagram for the CMT condensation and draining pressures scaling analysis. First, a top-down scaling analysis is performed. The objective of the top-down scaling analysis is to: examine the transport time scaling constants and the characteristic time ratios that govern the CMT draining process and the transient wall temperature behavior; and, to compare the CMT test facility to the AP600 Plant CMT.

Following the top-down scaling analysis, a bottom-up scaling analysis is performed to scale specific processes including wall condensation heat transfer and steam jet-liquid interface interactions.

The CMT test facility parameters that have to be assessed to address the phenomena of interest to the AP600 Plant CMT draining process are as follows:

1. Metal Mass
2. Internal Volume
3. Length
4 Diameter
5. Heat Transfer Time Constant

Other parameters that affect the CMT test facility recirculation behavior are discussed in Section 2.1.

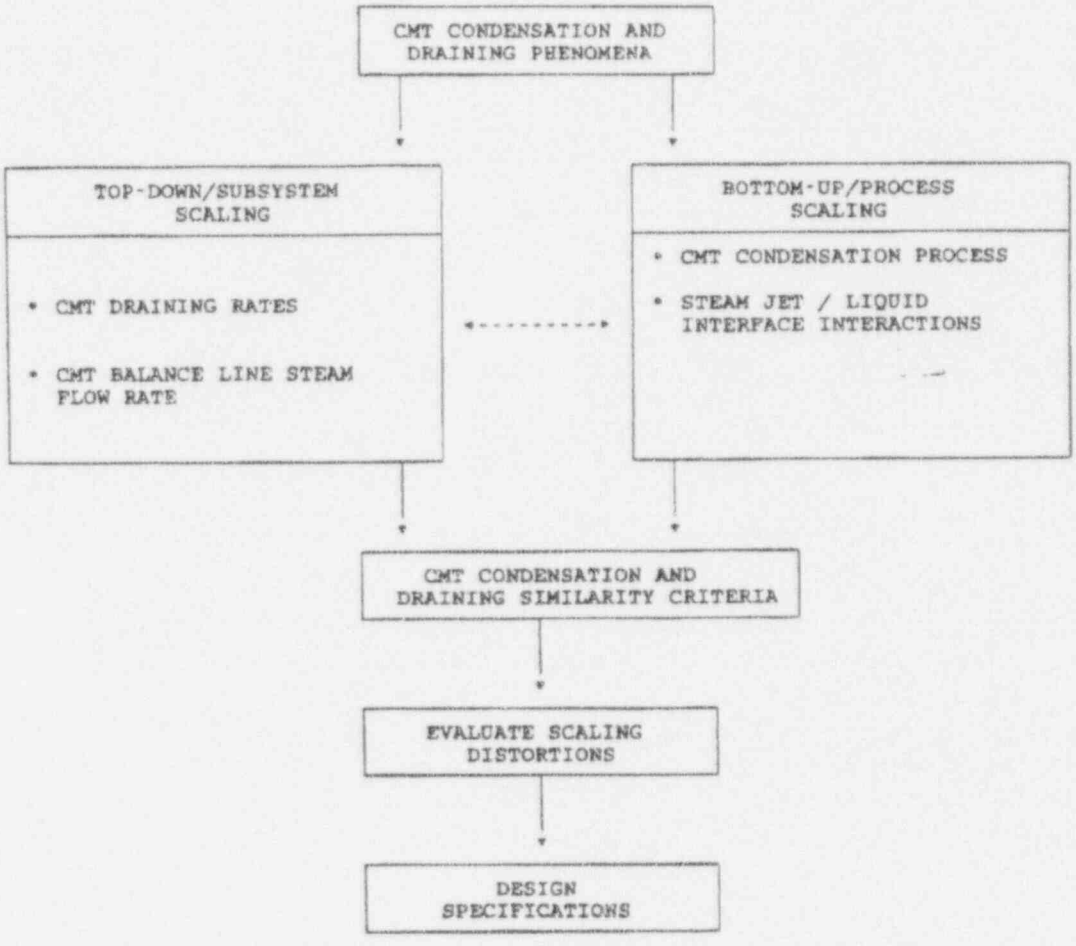

Figure 3-2 Scaling Analysis Flow Diagram for CMT Condensation and Draining Processes

The CMT injection process is highly coupled to primary system behavior. The CMTs are maintained at system pressure by a PBL that permits steam, either from the pressurizer or from the cold legs (in the event of a LOCA), to pressurize the CMT. The rate of steam flow into the CMT is dictated by the rate at which the steam condenses on the CMT inside wall and liquid surfaces. As more steam is condensed, the local pressure at the top of the CMT drops and more steam will flow to the CMT. If steam jetting or mixing occurs, it can disturb the liquid surface, which can induce additional condensation which, in turn, will induce additional steam flow into the CMT. Since the wall and liquid surfaces are initially at ambient temperature, steam condensation is expected to be significant.

The coupled behavior of the CMTs makes scaling the CMT injection and draining processes challenging because rapid condensation can induce additional steam flow, which produces even more condensation. This section develops the similarity criteria needed to scale the various processes occurring in the CMT during draining. The general balance equations presented in Table 3-1 were developed for the control volume depicted in Figure 3-1. These balance equations will now be made specific for the CMTs, and additional detail will be added to the original equations to more accurately calculate the thick wall condensation and heat up effects.

For the CMTs, the inlet flow rate is given by $\dot{m}_{BAL}$, the steam mass flow rate through the PBLs. The flow leaving the CMTs is given by $\dot{m}_{CMT}$, the CMT injection mass flow rate. Thus, Equation 3-10, the liquid mass balance equation, can be written as

a,c

[ ]

where A_t is the horizontal liquid surface area in the cylindrical portion of the CMT, where the tank is filled to some level L_t. To evaluate $\dot{m}_{BAL}$, it is necessary to perform an energy balance on the steam entering the CMT head. Figure 3-3 depicts an idealized view of the condensation processes within the CMT. It is assumed that steam enters the CMT at saturated conditions. The steam contacts the cold

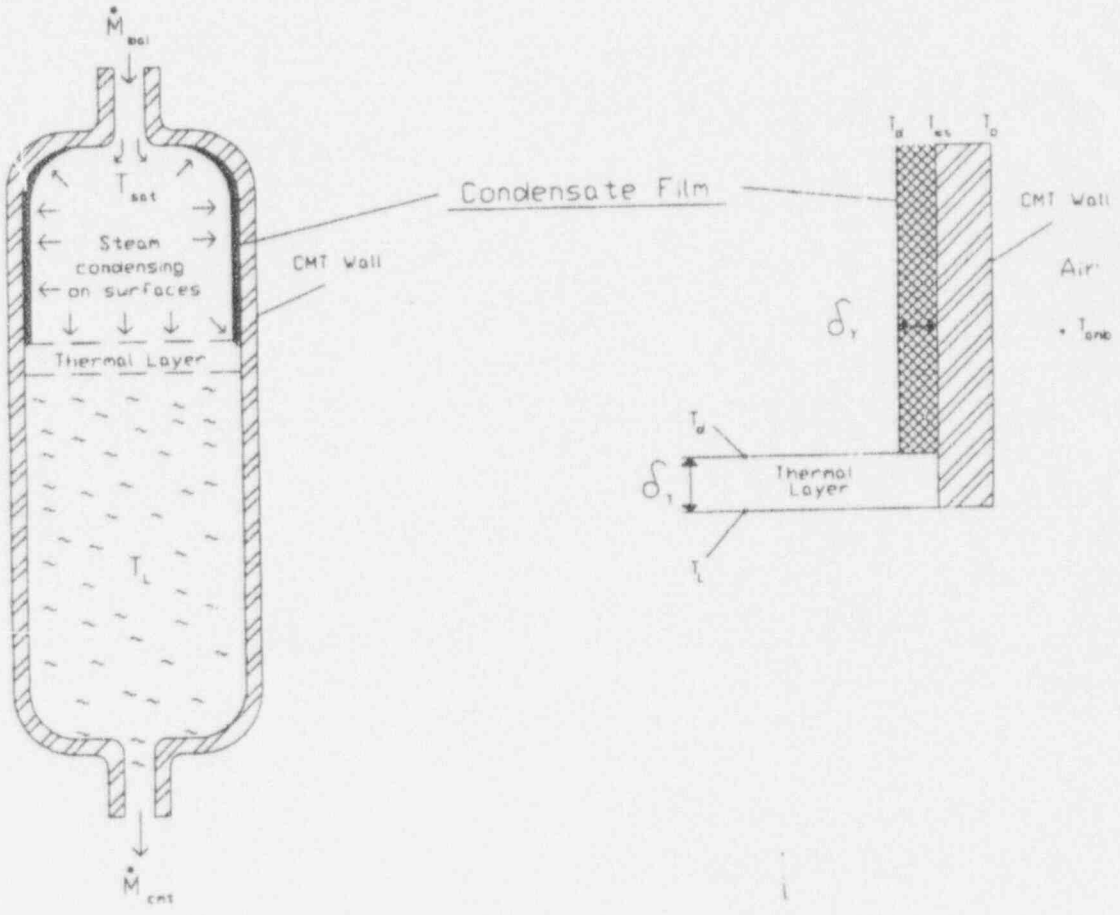

Figure 3-3 Idealized Model for Scaling CMT Condensation Behavior

CMT walls, where it condenses to form a liquid film. The liquid film flows down the wall and eventually mixes with the bulk of the fluid. The steam also contacts the initially cold liquid surface. Depending on the momentum flux of the steam jet entering the top of the CMT, the liquid interface may be quiescent, wavy, or, the steam can jet into the liquid, which enhances the condensation. The type of interface will significantly impact the extent of condensation on the liquid surface. Steam condensation on the liquid surface and wall condensate film draining to the surface will cause a thermal layer to develop at the steam-liquid interface. The thickness and temperature of this layer will affect the liquid surface condensation rate. Writing an energy balance for the steam in terms of these two condensation mechanisms yields

[a,c]

where it is assumed that the steam gives up only its latent heat, h_{fg}. In this equation, q_{WS} is the energy transferred to the condensate film on the CMT walls and q_{LS} is the energy transferred to the liquid surface. The amount of energy transferred to the liquid film is given by

$$q_{WS} = H_{LF} a_{ws} (T_d - T_{ws}) \tag{3-26}$$

where H_{LF} is a heat transfer coefficient for condensation of steam on vertical surfaces. This coefficient will be obtained in the bottom-up scaling analysis. a_{ws} is the total CMT wall surface area exposed to the steam and $(T_d - T_{ws})$ is the temperature difference across the condensate film, as depicted in Figure 3-3, and depends on the liquid level in the tank.

The amount of energy transferred to the liquid surface, q_{LS}, can be estimated by

$$q_{LS} = \left[H_{LS} + \frac{k_f}{\delta_T} \right] (T_d - T_f) A_t \tag{3-27}$$

where H_{LS} is a condensation heat transfer coefficient that depends on interfacial structure and steam flow rates over the liquid surface, δ_T is the depth of the thermal layer through which heat conduction occurs, and k_ℓ is the thermal conductivity of the liquid. If the surface is heated such that no waves or steam jetting occur, or a thick hot liquid layer exists, the condensation at the surface is small and conduction is insignificant. If there is significant surface condensation, due to the steam jetting into the water or to mixing with the cold water, the condensation effects are still negligible relative to the direct condensation heat transfer.

Substituting Equations 3-26 and 3-27 into 3-25 and solving for the balance line mass flow rate yields

[a,c]

where the conduction effects are ignored.

Substituting Equation 3-28 into 3-24 yields

[a,c]

This equation directly relates the rate of change (draining) of the CMT to the condensation processes on the walls and surfaces.

Equation 3-29 is one of the governing equations for CMT scaling.

The liquid energy equation, Equation 3-11, can also be made specific to CMT draining by implementing the definition of $\dot{m}_{BAL}$ provided by Equation 3-28. Thus, the CMT liquid energy equation becomes:

$$\frac{d}{dt}\left(\rho_\ell A_t L_\ell C_{v\ell} T_\ell\right) = (\dot{m}h)_{BAL} - (\dot{m}h)_{CMT} \qquad (3\text{-}30)$$

where the heat loss from the tank, q_t, is assumed to be negligible.

Substituting Equation 3-28 into 3-30 yields

[ ] a,c

Because the CMT walls are thick structures that are initially at room temperature, a more detailed solid structure energy equation will also be considered in this analysis. For the CMTs, the structure energy equation is written as follows

$$\frac{\partial}{\partial t}\left(\rho_s V_s C_{vs} T_s\right) = \frac{1}{r}\frac{\partial}{\partial r}\left(r k_s \frac{\partial T_s}{\partial r}\right) \tag{3-32}$$

which assumes one-dimensional heat transfer in the CMT wall. The boundary conditions become

$$k_s \frac{\partial T_s}{\partial r})_{r=R_1} = H_{LF}\,(T_d - T_{ws}) \tag{3-33}$$

at the inner surface where condensation is occurring with the transient wall surface temperature T_{ws}. The outer wall boundary condition is

$$k_s \frac{\partial T_s}{\partial r})_{r=R_o} = 0 \tag{3-34}$$

where it is assumed that the heat transfer from the outer surface of the tank is assumed to be sufficiently small, such that the tank is adiabatic.

The use of the one-dimensional conduction equation permits a more accurate assessment of the wall heat up and condensation effects and, therefore, the draining behavior of the CMT. This is particularly important because the AP600 Plant CMT has a [ ]^{a,c} wall thickness, while the CMT test has a

wall thickness of [ ]^{a,c} Cylindrical coordinates are used for the CMT wall conduction calculation, spherical coordinates are used for the AP600 CMT head, and a modified spherical coordinate system is used for the ellipsoidal head of the CMT test facility, to calculate the wall and head heat up rates.

It should be noted that the CMT wall surface participating in the energy exchange process is limited to that section of the tank that has its inner wall surface exposed to steam. As the CMT drains, more surface is exposed and, hence, condensation on the walls should increase.

Equations 3-29, 3-31, and 3-32 will form the basis of the top-down scaling analysis. These equations are listed in Table 3-4 for purposes of future reference.

Equations 3-29, 3-31, and 3-32 can be made dimensionless using the CMT boundary, initial, and geometry conditions given in Table 3-5. Applying these conditions and dividing the liquid mass equation by $(\dot{m}_{CMT})_0$ yields the dimensionless equations presented in Table 3-6. The structure conduction equation can be put into a dimensionless form as given in Table 3-7, which yields the Biot number and the Fourier number defined as

$$B_i = \frac{H_{LF}L}{k_s} = \frac{H_{LF}\left(R_o - R_i\right)}{k_s} \tag{3-39}$$

and

$$F_o = \frac{k_s t}{\rho_s C_{vs} L^2} = \frac{\alpha t}{\left(R_o - R_i\right)^2} \tag{3-40}$$

which characterizes the conduction process in the CMT wall and dome.

Table 3-7 lists the CMT drain time constant, the solid structure specific frequency, and the characteristic time ratios.

Table 3-4
Balance Equations for Top-Down Scaling Analysis of the CMTs

[a,c]

Solid Structure Energy:

$$\frac{\partial}{\partial t}(\rho_s V_s C_{vs} T_s) = \frac{1}{r}\frac{\partial}{\partial r}(r k_s \frac{\partial T_s}{\partial r}) \qquad (3\text{-}32)$$

Where the boundary conditions are:

$$k_s \frac{\partial T}{\partial r})_{r=R_i} = H_{LF}(T_d - T_{ws}) \qquad (3\text{-}33)$$

and

$$k_s \frac{\partial T}{\partial r})_{r=R_o} = 0 \qquad (3\text{-}34)$$

[a,c]

[ ] a,c

[ ] a,c

The CMT liquid balance equations implement the same time scale, $\tau_{CMT,0}$. This permits direct comparisons of the Π groups. The time scale for the solid energy equation, $\tau_{s,CMT}$, differs from the CMT liquid time scale. The ratio of these time scales is written as follows

[ ] a,c

When $\varepsilon_{CMT,t}$ <<1, the CMT liquid variables change more rapidly than those of the solid, that is, the CMT drains before the CMT walls are significantly affected. When $\varepsilon_{CMT,t}$ >>1, the solid variables change more rapidly than those of the liquid because the draining rate is so slow that the CMT walls are directly affected. Thus, the time scale ratio presented in Equation 3-51 indicates the degree of coupling between the liquid transport phenomena and the heat transport phenomena in the CMT walls.

The characteristic time ratios presented in Table 3-7 can be used to develop the set of similarity criteria needed to assess the CMT transport process of interest.

3.3 BOTTOM-UP SCALING ANALYSIS FOR CMT TRANSIENT PROCESSES

The CMT systems equations provided in Table 3-4 will give the thermal-hydraulic response of the CMT. The heat transfer coefficients are key ingredients and are assumed for the wall condensation and the direct condensation on the liquid surface.

3.3.1 Condensation on CMT Walls

It is assumed that film condensation exists on the CMT walls. The condensation heat transfer coefficient is a function of the film Reynolds number; defined as

$$Re_{\Gamma} = \frac{4\Gamma}{\mu_f} \tag{3-52}$$

where Γ is the film flow per unit width. The wall condensation model used in the CMT scaling analysis was to use the Nusselt (1916) laminar film condensation coefficient for $Re_{\Gamma} \leq 2000$; given as (see Kreith, 1962)

$$\bar{H}_{LF} = 0.94 \left[\frac{\rho_\ell g h_{fg} k_f^3}{\mu_f L \left(T_d - T_{ws}\right)} \right]^{1/4} \tag{3-53}$$

where

$$T_d = \frac{T_{ws} + T_{sat}}{2} \tag{3-54}$$

such that

$$T_d - T_{ws} = \frac{1}{2}\left(T_{sat} - T_{ws}\right) \tag{3-55}$$

and T_{ws} is the surface temperature which is calculated from the one-dimensional CMT wall conduction solution. For turbulent film condensation, the modified Colburn (1933) correlation is used, as recommended by Kreith (1962). The correlation is given as

$$H_{LF} = 0.056 \left(\frac{4\Gamma_c}{\mu_f} \right)^{.2} \left(\frac{k_f^3 \rho_f^2 g}{\mu_f^2} \right)^{\frac{1}{3}} Pr_f^{\frac{1}{2}} \qquad (3\text{-}56)$$

This is a local correlation since Γ_c is the local film flow. However, in the CMT heat transfer analysis, an average film flow is calculated separately for the dome region and for the combined dome and cylindrical wall region. Therefore, the Γ_c in Equation 3-56 represents the average film flow, such that the heat transfer coefficient is also taken as an average, over these regions.

3.3.2 Condensation on Liquid Surfaces

The value of the condensation heat transfer coefficient for the steam on the cold CMT water is an unknown. The CMT tests have been specifically designed to measure this parameter, as will be discussed in Section 4.0, CMT Test Matrix. To estimate the magnitude and the effects of the liquid surface condensation heat transfer, two models were examined for both the plant CMT and the model to see how the model CMT responds relative to the plant.

In the first case, the turbulent film condensation coefficient from Grigull (1942) as recommended in the text book by Bird, Stewart, and Lightfoot (1960) was used to model the CMT water surface condensation heat transfer coefficient. The value for the coefficient is given as

$$H_{LS} = 0.003 \left[\frac{k_f^3 \rho_f^2 8 (T_d - T_{WS}) L}{\mu_f^3 h_{fg}} \right]^{1/2} \qquad (3\text{-}57)$$

There are some desirable features that the correlation given in Equation 3-57 exhibits. As the liquid surface heats up, the heat transfer coefficient will decrease because the temperature difference is in the numerator. Examining Equation 3-53 for the laminar film condensation, the heat transfer coefficient will approach unrealistically large values at low temperature differences. The other feature that Equation 3-57 has is a characteristic length L, which can represent the effects of scale for the different CMTs. For the calculations presented in this report, the characteristic length term given in Equation 3-57 is taken as the CMT diameter, either for the plant or for the experiment.

Using the system of equations provided in Table 3-4, and the condensation coefficients given in Equations 3-53, 3-56 and 3-57, the CMT wall and liquid surface condensation was calculated for the plant CMT and the test CMT. The Π groups and ratios were also calculated to compare how well the test matched the response of the plant.

A more mechanistic correlation for the liquid surface condensation has been proposed by Bankoff (1982) for steam flowing countercurrent to a liquid flow on a flat channel. This particular correlation represents condensation as a hydrodynamically-controlled process such that as the condensation increases, it will draw in more steam flow and further increase the condensation heat transfer coefficient. Bankoff's correlation is given as

$$H_{LS} = 0.061 \frac{k_f}{\eta} Re_t^{1.12} Pr^{\frac{1}{2}} \qquad (3\text{-}58)$$

where η is the maximum interfacial wave amplitude, the turbulent Reynold's number is given by

$$Re_t = \frac{U_f \eta}{\nu_f} \qquad (3\text{-}59)$$

where U_f is the steam friction velocity parallel to the liquid surface. The Bankoff correlation is very difficult to use for the CMT condensation process since the steam flow pattern with the CMT is unknown.

However, the Bankoff correlation does indicates that it is important to consider the interfacial structure for the liquid surface condensation behavior in the CMT and conversely, the interfacial structure can significantly influence the condensation rate on the liquid surface. During CMT draining, steam entering the CMT through the balance lines will impinge on the liquid surface. Depending on the momentum flux of the steam jet, interfacial waves may form on the liquid surface and propagate radially outward from the disturbance region and impact the CMT walls. [

]^{a,c}

These effects have been observed by Belyayev and Dyadyakin (1989) for a vertical jet impacting horizontal liquid surfaces.

For an incompressible, inviscid liquid, impinged upon by a steam jet, Lamb's (1932) analysis of the wave height at the radial boundary of the disturbance is determined by the following force balance

$$\rho_\ell g\eta = \frac{1}{2}\rho_j u_j^2 \tag{3-60}$$

where surface tension has been neglected and η is the height of the wave formed at the edge of the disturbance, ρ_ℓ is the liquid density, ρ_j is the steam density and u_j is the velocity of the jet. Rearranging this equation and writing it in terms of the wave height yields

$$\eta = \left[\frac{\rho_j u_j^2}{\rho_\ell}\right] \tag{3-61}$$

This equation can also be written in terms of the mass flow rate through the balance lines as follows

$$\eta = \left[\frac{\dot{m}_{BAL}^2}{\rho_j \rho_\ell a_j^2}\right] \tag{3-62}$$

[

]^{a,c} Lamb (1932) develops the following equation for wave group velocity as

$$u_{wave} = \frac{1}{2}\left[\frac{g\lambda}{2\pi}\right]^{1/2} \tag{3-63}$$

where λ is the wavelength that approximately characterizes a group of waves. Lamb assumes that the wavelength is proportional to ℓ_B, the breadth of the wave generated at the disturbance front.

Writing the wave group velocity and wavelength, ℓ_B, in terms of a model to prototype ratio yields

$$\left[u_{wave}\right]_R = \left[\ell_B^{1/2}\right]_R \tag{3-64}$$

[

]

[ ] a,c

Substituting this result into the wave group velocity ratio yields

$$\left[u_{wave}\right]_R = \left[\frac{D_j}{\eta^{1/2}}\right]_R \tag{3-68}$$

Substituting in the relation for η_R from Equation 3-62 and assuming that the jet diameter is proportional to the CMT nozzle diameter, $D_j = D_{in,CMT}$ yields

$$\left[u_{wave}\right]_R = \left[\frac{D_j}{\frac{\dot{m}_{Bal}^2}{2\rho_g \rho_\ell a_j^2 g_c}}\right]_R \tag{3-69}$$

[ ] a,c

The equations that represent the wave height, wave group velocity, and wave propagating time scale ratios for the CMT liquid interface are summarized in Table 3-8. These equations will be used to compare the test CMT to the AP600 CMT.

Table 3-8
CMT Interfacial Wave Scaling Ratios

$$\eta_R = \left[\frac{\dot{m}_{Bal}^2}{\rho_j \rho_\ell a_j^2}\right]_R \quad (3\text{-}71)$$

$$\left[u_{wave}\right]_R = \left[\frac{\frac{D_j}{\dot{m}_{Bal}^2}}{2\rho_g \rho_\ell a_j^2 g_c}\right]_R \quad (3\text{-}72)$$

a,c

3.4 COMPARISON CALCULATIONS OF THE AP600 PLANT CMT DRAINING BEHAVIOR AND THE CMT TEST DRAINING BEHAVIOR

The equations that describe the CMT draining behavior are provided in Table 3-4. The dimensionless versions of these equations are provided in Table 3-6 and indicate the dimensionless Π groups that should be preserved between the test and the plant. These equations were programmed and solved to estimate the plant and test CMT behavior. Several assumptions were made in solving the system of equations:

a,c

3.4.1 Calculated Results for Wall and Surface Condensation Behavior for the AP600 CMT and the Test CMT

The first series of calculations examine the CMT dome and wall heat up due to the film condensation on those structures. Figure 3-4 shows the plant inside wall surface temperatures at different liquid levels in the CMT. As the figure indicates, the inside wall temperature quickly heats up to nearly the saturation temperature of 556°F for all exposed metal surfaces. The average wall temperature for the plant dome and the cylindrical wall portion, shown in Figure 3-5, indicates that while the surface quickly heats, the average wall temperature significantly lags behind the surface, due to the heat conduction through the thick walls. [

]^{a,c} The CMT test model dome and wall temperatures are shown in Figures 3-6 and 3-7. As Figure 3-6 indicates, the model inside surface temperatures quickly heat up to nearly the saturation temperature, faster than the plant inside wall temperatures, for all liquid levels investigated. Figure 3-7 shows the average wall temperatures for the CMT model. The model average wall temperatures heat up to the saturation temperature quicker than the average wall temperatures of the plant. [

]^{a,c} Therefore, a time scale exists between the plant and the CMT model for the wall condensation. The time scale will be discussed in the following sections.

Figure 3-8 shows the calculated wall condensation coefficient for the plant CMT at different levels. The heat transfer is initially large, then decreases as the CMT dome and wall temperatures increase. For the first 1800 seconds the condensation heat transfer is in the turbulent regime for both the dome and the cylindrical walls. After 1800 seconds, the dome has heated sufficiently that the condensation film flow is in the laminar regime and the correlation changes to Nusselt laminar film condensation. A similar behavior can be observed in the literature from Kreith (1962), as seen in Figure 3-9. A similar plot of the CMT model wall condensation heat transfer coefficient is shown in Figure 3-10. [

]^{a,c}

Figure 3-11 shows the plant wall condensation mass flow rates for different water levels in the CMT. As the figure indicates, the more surface area that is exposed, the larger the condensate flow rate. All values decrease with time as the structure heats up. Figure 3-12 shows the model CMT wall condensate flow rates at different water levels in the tank. [

]^{a,c}

As shown in Table 3-7, the dimensionless parameters that characterize the wall condensation are given by the Biot and Fourier Numbers. One method of assessing the differences between the AP600 Plant CMT wall condensation behavior and the CMT model wall condensation behavior, is to examine the ratio of the product of the Biot and Fourier numbers for each CMT. That is, define a new Π group as

$$\Pi_{cond} = \frac{B_i F_o)_m}{B_i F_o)_p} \tag{3-74}$$

The product of $B_i F_o$ is used for solving transient conduction problems, where the internal conduction resistance is negligible and the average structure temperature can be used. [

]^{a,c}

Equation 3-74 can be written as

$$\Pi_{cond} = \frac{\left.\frac{H_{HL}(R_o-R_i)}{k_s}\ \frac{\alpha t}{(R_o-R_i)^2}\right)_m}{\left.\frac{H_{HL}(R_o-R_i)}{k_s}\ \frac{\alpha t}{(R_o-R_i)^2}\right)_p} \tag{3-75}$$

[ ]^{a,c}

If we assume that the heat transfer coefficient is similar, the materials are the same, and $R_o - R_i$ is the wall thickness, then Equation 3-75 reduces to

$$\frac{\left.\frac{t}{R_o - R_i}\right)_m}{\left.\frac{t}{R_o - R_i}\right)_p} = 1 \qquad (3\text{-}76)$$

[

]^{a,c}

The heat transfer to the CMT liquid surface was also calculated for the plant CMT and the model CMT, assuming a 3-foot mixing depth and using the Gregull (1942) condensation correlation from Bird, Stewart, and Lightfoot (1960). The assumption of the 3-foot depth is artificial since the true depth is unknown. [

]^{a,c} Figure 3-13 shows the calculated liquid temperature for the plant CMT for different water levels but the same mixing depth (3 feet). The change in the CMT water level has only a secondary effect on the water temperature due to the geometry of the CMT dome and cylindrical portion of the tank. [

]^{a,c} As seen in Figure 3-13, the liquid temperature approaches the saturation temperature of 556°F as time increases. The liquid temperatures are slightly higher for the lower liquid levels since there is an increase in the total wall condensate (due to the increase in the wall area at lower water levels), that flows into the original CMT liquid and mixes; thereby more quickly heating it to higher temperatures. The calculated heat transfer at the water surface for the plant is shown in Figure 3-14, using the Gregull (1942) correlation from Bird, Stewart, and Lightfoot. [

]^{a,c} The lower three curves in Figure 3-14 are for positions located in the dome, while the top two curves are for positions in the cylindrical portion of the tank. The variations in the curves are due to the different amount of cold water available for mixing with the steam flow. Also, the characteristic length used in the water surface correlation is the tank diameter, which, compared to the cylindrical portion of the tank, is smaller in the dome region. The condensate flow rate resulting from the condensation on the liquid surface is shown in Figure 3-15. As indicated in Figures 3-13, 3-14, and 3-15, as the water surface temperature increases, the condensation heat transfer and resulting condensate flow decreases. The total condensate flow rate from both the plant CMT walls and the water surface is shown in Figure 3-16. [

]^{a,c}

Similar calculations have been performed for the AP600 CMT test using the same 3-foot mixing assumption for the water surface condensation calculation. Figure 3-17 shows the calculated liquid temperatures for different levels in the test CMT. The calculated results, as shown in subsequent figures, [

]^{a,c} As a result, the calculated CMT water temperatures show more of a spread for different water levels in the test CMT tank since the wall surface area, which is exposed to the steam, increases with decreasing water levels, thereby increasing the wall condensation. Figure 3-18 shows the calculated surface condensation heat transfer coefficient for the model. The model heat transfer coefficient transitions to the laminar correlation, whereas the plant CMT calculation indicates that the condensation is in the turbulent regime. The water surface condensate mass flow rate for the model using the 3-foot mixing depth assumption is shown in Figure 3-19. The total wall and water condensate flow rate is shown in Figure 3-20. [

]^{a,c}

To determine the behavior of the test or model CMT relative to the plant CMT, the relationships given by Equations 3-45 to 3-50 were examined. [

]^{a,c}

[

]^{a,c} The denominator in each equation is given as

$$\dot{m}_{CMT} h_{fg} \qquad (3-77)$$

which represents the energy of the drain flow out of the CMT. However, since the calculations are assuming a constant liquid level in the CMT, the drain rate is nearly equal to the CMT balance line flow as given by Equation 3-24. For these calculations, the balance line flow is the total steam flow rate into the CMT.

Two approaches were used to compare the test CMT to the plant CMT. [

]^{a,c} The first approach is discussed below and the second in Section 3.4.1.2, Condensation Π Groups and their Ratios.

3.4.1.1 Normalized Condensate Comparisons

In the first approach the wall surface condensate rate, shown in Figures 3-11 and 3-12, was divided by the wall surface area (which is exposed for the assumed different liquid levels) to obtain a wall condensate mass flux. This normalizes the condensation heat transfer on the actual surface area and permits comparisons between the test CMT and the plant CMT. A similar approach was used for the water surface condensate rate given in Figure 3-15 and 3-19, except that the water surface cross section area was used to divide the condensate mass flow for the plant and the test. The ratio of the wall condensate mass flux is plotted in Figure 3-21 for the CMT model and the AP600 Plant CMT.

[

]a,c

[

]a,c

The ratio of the water surface condensate mass flux is plotted in Figure 3-22 for the model and the plant. [

]a,c

Comparing the calculated heat transfer coefficients for the plant and the model, as shown in Figures 3-14 and 3-18, indicates that [

]a,c

Figure 3-23 shows the ratio of the total wall and water surface condensate flow rates for the model CMT relative to the plant CMT. [

]a,c

Additional sensitivity studies were performed to examine the effects of different assumed water mixing depths on the water surface condensation. The CMT water level was kept at 95 percent, that is, the tank was assumed to have a water volume equal to 95 percent of the total tank volume. The level assumption determines the surface areas, both water and metal, available for steam condensation. The mixing depth was varied from 3 inches to 3 feet. Figure 3-24 shows the calculated water temperatures for the AP600 CMT. [

]a,c

Figure 3-25 shows the calculated condensate flow rates for the water surface condensation. [

]^{a,c} As the mixing depth increases, the condensation on the water surface continues, but at a decreasing rate. The total wall and water surface condensation can be calculated at this level using the previous wall condensation values. Figure 3-26 shows the calculated total condensate flow rate for the different assumed mixing depths. [

]^{a,c}

3.4.1.2 Condensation Π Groups and Their Ratios

The second method of comparing the test CMT condensation behavior to the plant CMT condensation behavior was to directly calculate the Π groups from the dimensionless equations.

The condensation Π groups have been defined in Equations 3-45 and 3-46 in Table 3-7. The comparisons made in Section 3.4.1.1 of the normalized condensate mass fluxes ratios for the CMT test to the AP600 Plant CMT indicated that the test would capture the condensation phenomena of interest for the plant CMT. Additional comparisons will now be made using the condensate Π groups.

[

]^{a,c}

Figures 3-32 and 3-33 show the calculated Π_{Wcond} group for both the test CMT and the AP600 CMT Π group for a mixing depth of 3 feet and different CMT levels. Figure 3-34 shows the calculated ratio of the wall condensation Π groups for a mixing depth of 3 feet and different CMT levels.

[

]^{a,c}

The liquid surface condensation Π group for both the test CMT and the plant CMT is shown in Figures 3-35 and 3-36 using the Bird, Stewart, and Lightfoot correlation for a CMT level of 90 percent and different mixing depths. The Π ratio is given in Figure 3-37 for the surface condensation effects. [

]^{a,c}

A similar series of figures have been generated with the CMT level at 95 percent for different assumed mixing depths. Figures 3-38 and 3-39 compare the AP600 CMT wall condensation Π group and the CMT test wall condensation Π group, respectively. Figure 3-40 compares the wall condensation Π group ratio. The same behavior is seen in Figure 3-40 as was observed in Figure 3-34 for the 3-foot mixing depth. The surface condensation Π groups for the plant CMT and the test CMT at a level of 95 percent and for different mixing depths are shown in Figures 3-41 and 3-42, respectively. The Π group ratio for the surface condensation is given in Figure 3-43. [

]^{a,c}

3.4.2 Calculated Interfacial Parameters

The solution of Equation 3-28 results in the steam flow into the CMT for a given liquid level and assumed mixing depth within the tank. Using the calculated values of the inlet steam flow for different mixing depths, the inlet steam jet velocity can be calculated for both the CMT test and the plant CMT.

Using the inlet jet velocity, the wave heights were calculated from Equation 3-71 and the wave velocities were also calculated from Equation 3-72. The time constants, as defined in Equation 3-73, were also calculated for both the CMT test and the plant CMT. The ratios of the above parameters were calculated to investigate how well the CMT test could model the [ ]^{a,c} in the plant CMT.

Figure 3-44 shows the ratio of the CMT test to CMT plant jet velocities for a CMT level of 95 percent and different mixing depths. [

]^{a,c}

The ratios of the wave heights for the CMT level at 95 percent and different mixing depths are shown in Figure 3-45. [

]^{a,c}

The ratio of the calculated wave velocities is shown in Figure 3-46 for the test CMT and plant CMT with a level of 95 percent and different mixing depths. [

]a,c

The calculated time constants for the test CMT and the plant CMT are shown in Figure 3-47 for the CMT level of 95 percent and different mixing depths. [

]a,c

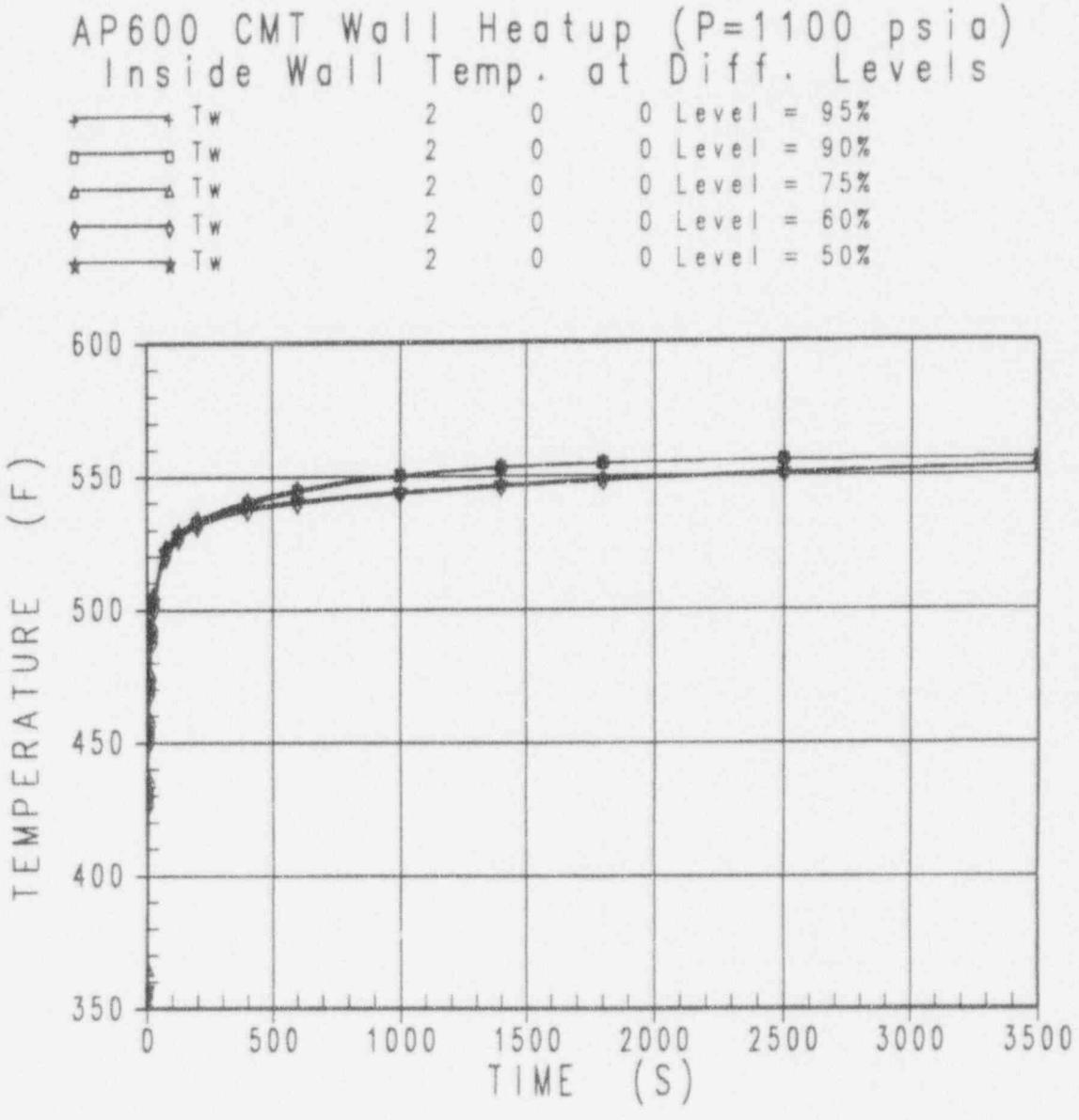

Figure 3-4 AP600 Plant CMT Inside Wall Temperatures for Different Levels

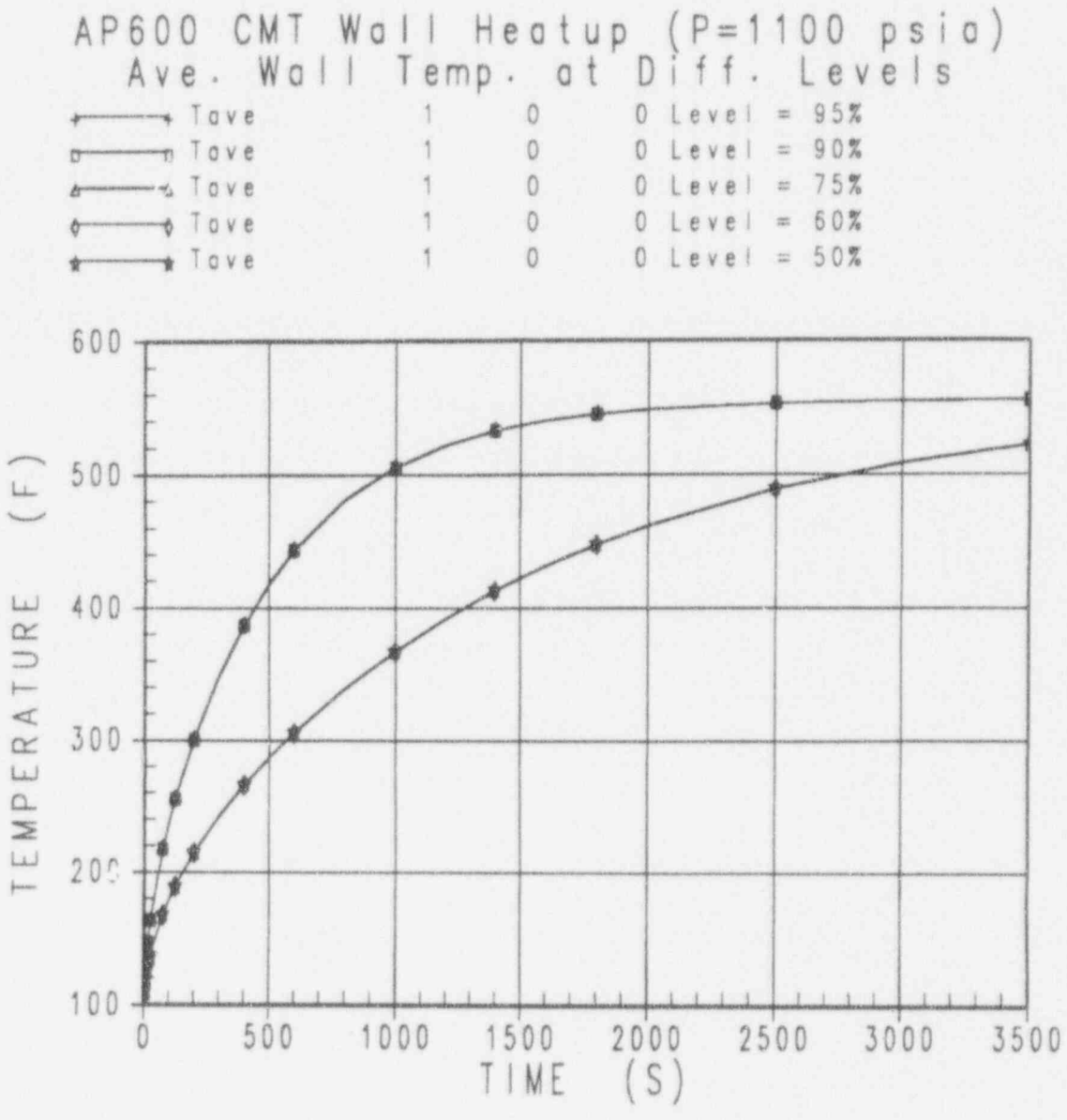

Figure 3-5 AP600 Plant CMT Average Wall Temperatures for Different Levels

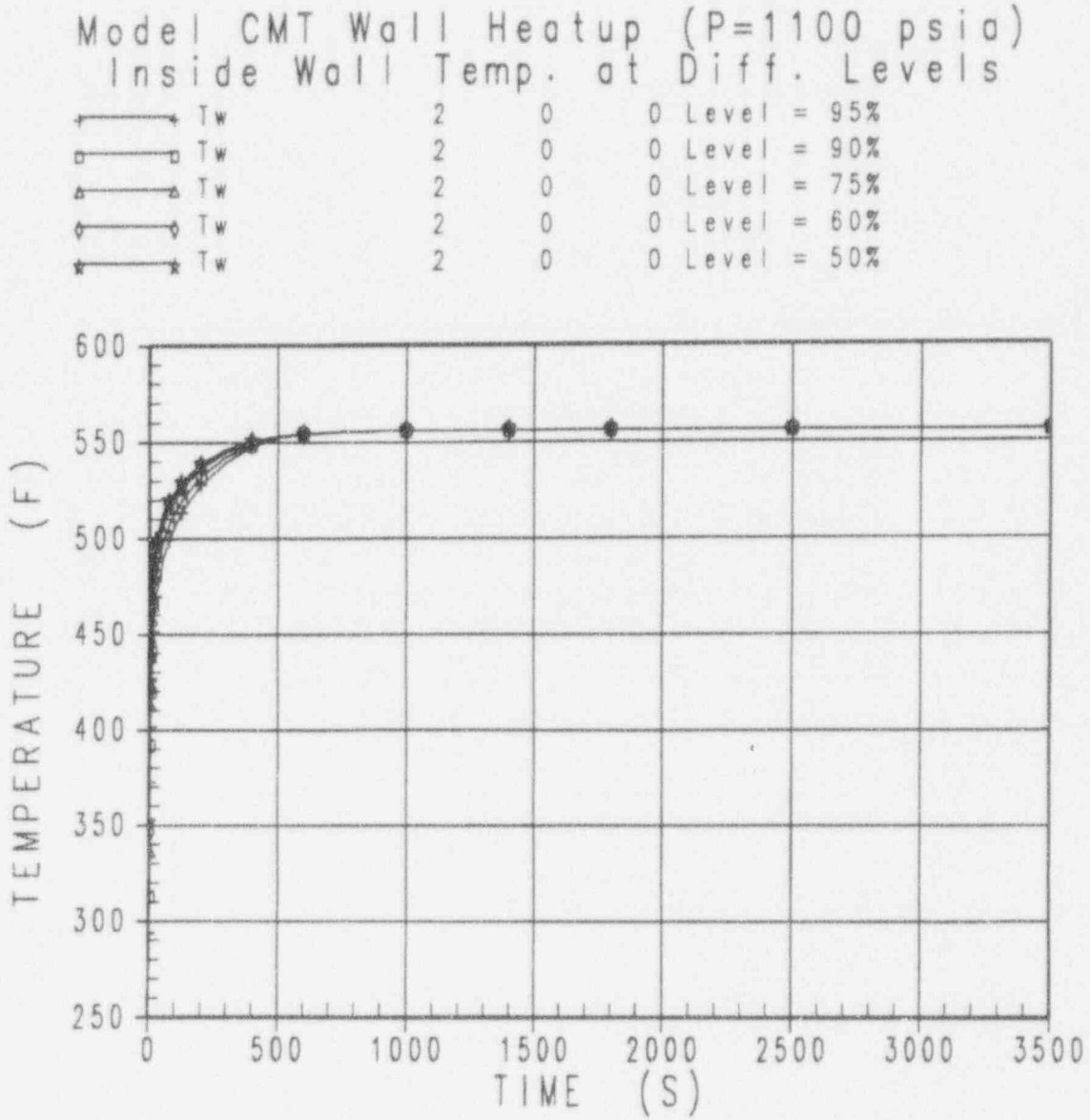

Figure 3-6 CMT Test Model Inside Wall Temperatures for Different Levels

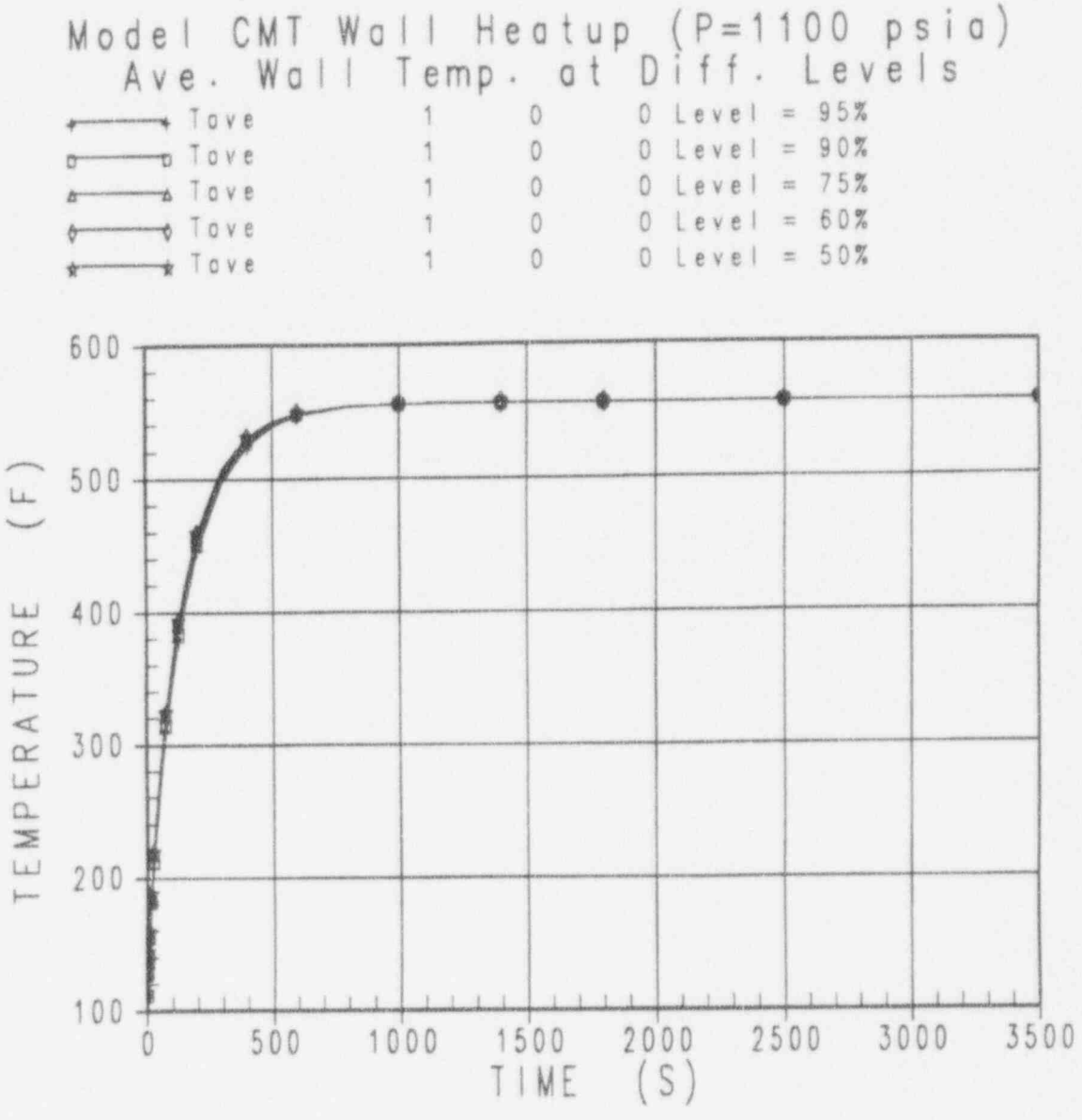

Figure 3-7 CMT Model Average Wall Temperatures for Different Levels

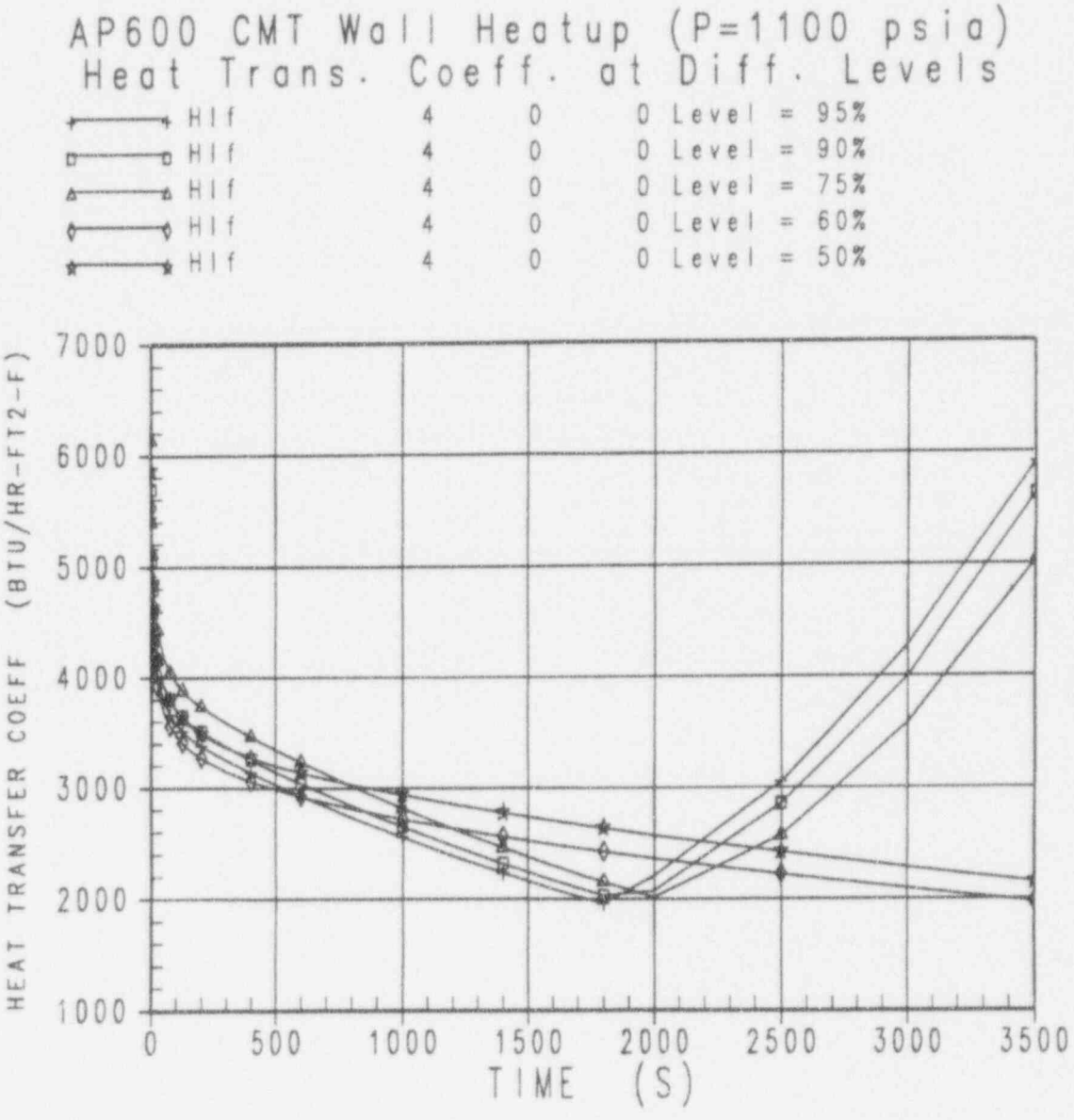

Figure 3-8 AP600 Plant Calculated Wall Condensation Heat Transfer Coefficient

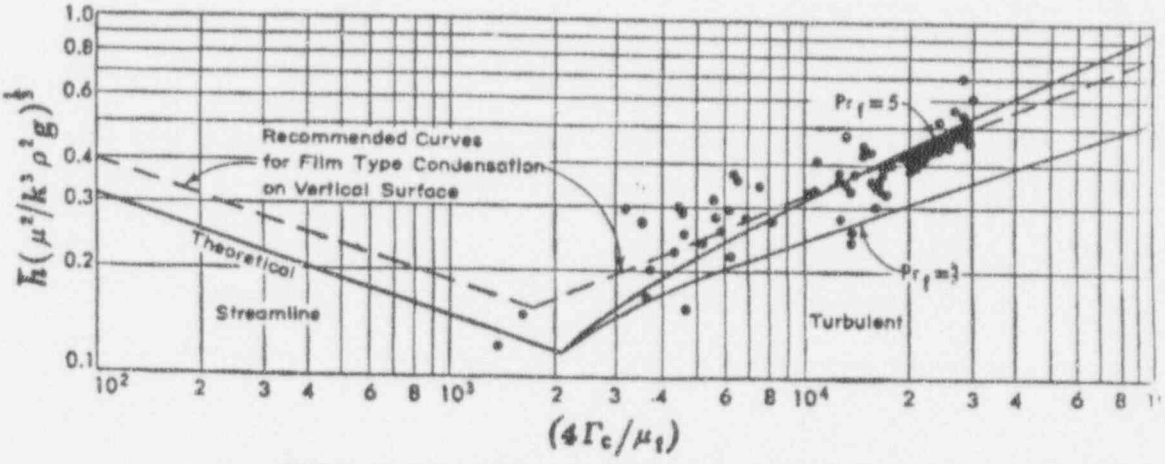

Effect of turbulence in film on heat transfer with condensation

Figure 3-9 Laminar and Turbulent Film Condensation Heat Transfer Coefficients (Kreith, 1962)

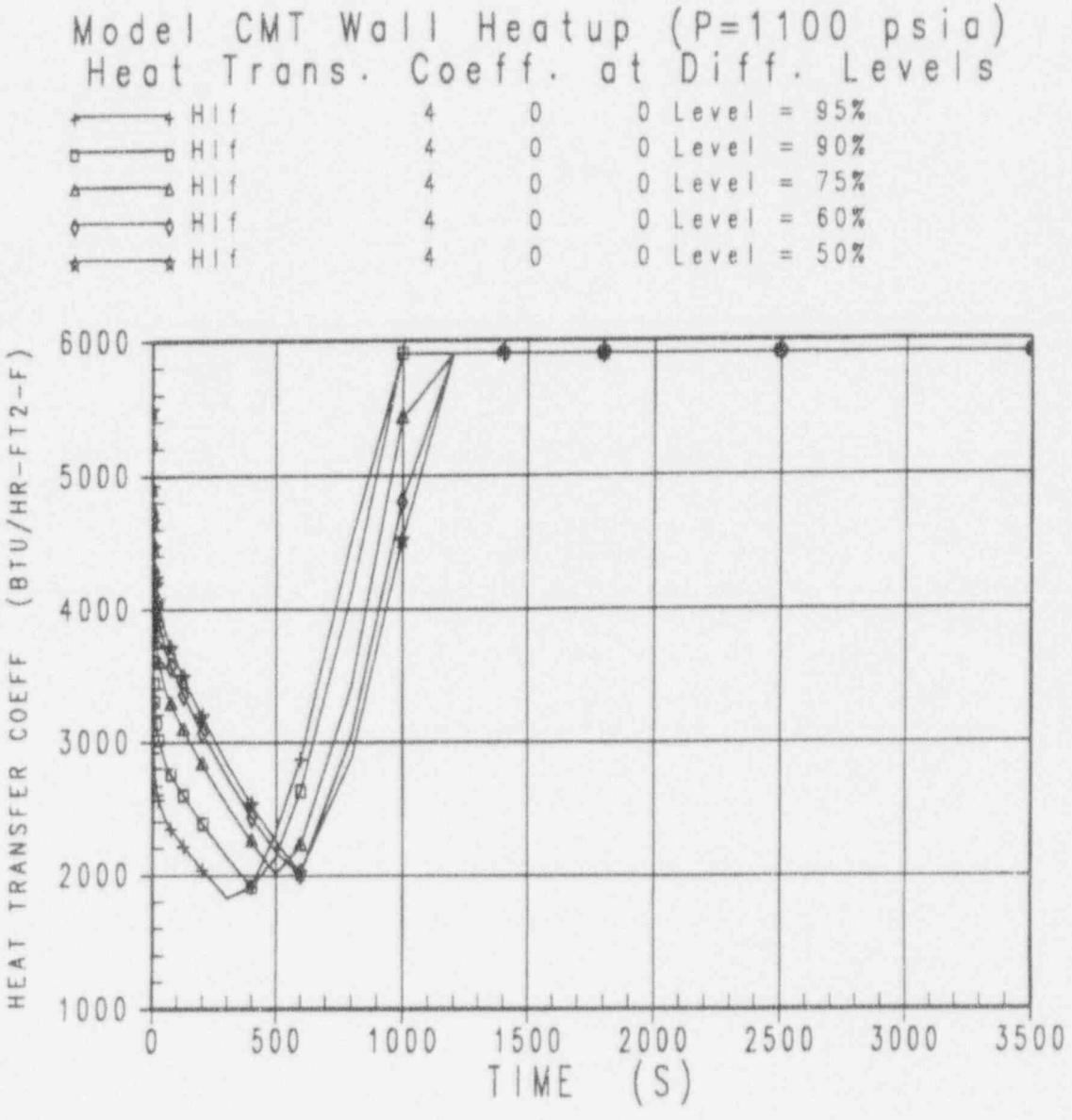

Figure 3-10 Calculated CMT Test Wall Condensation Coefficients

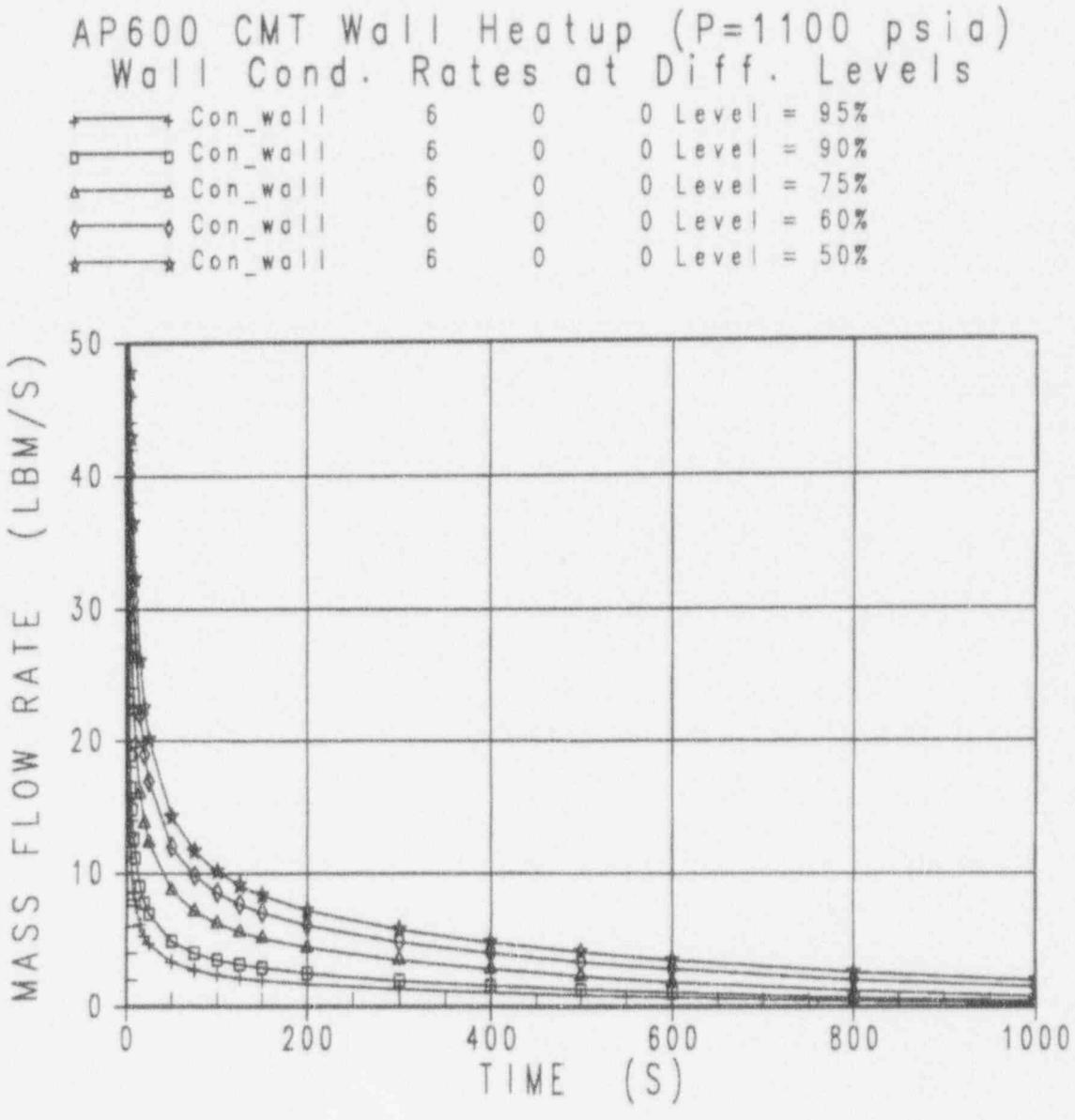

Figure 3-11 AP600 Plant Wali Condensate Flow Rate for Different Levels

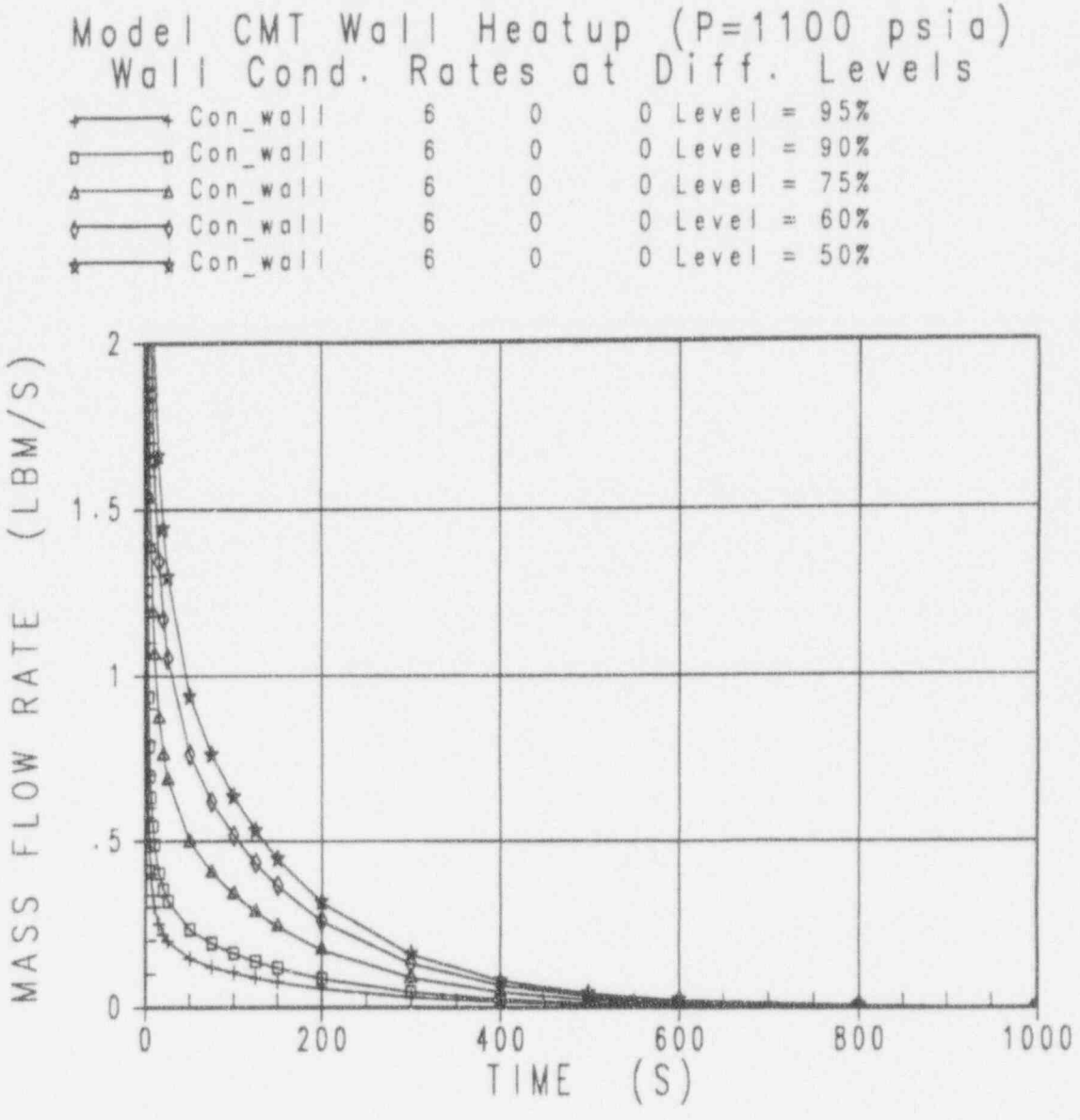

Figure 3-12 CMT Test Wall Condensate Flow Rates for Different Levels

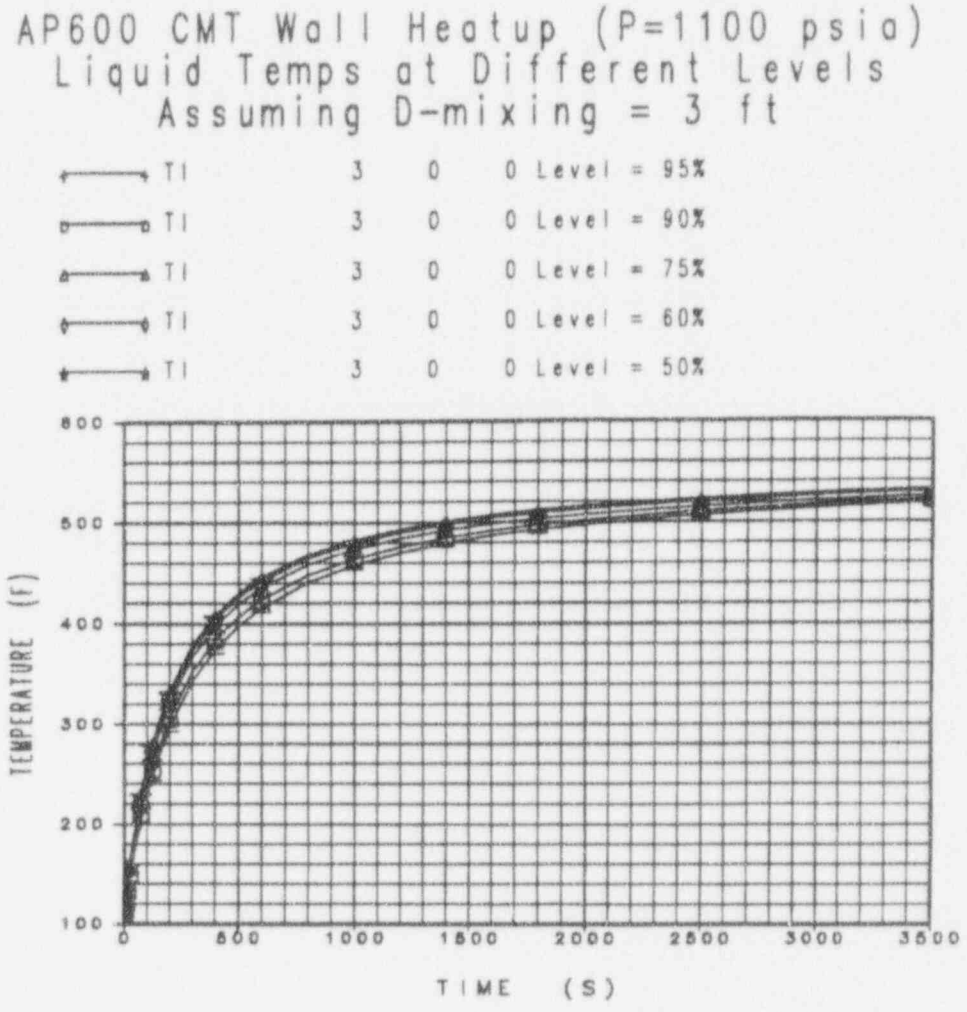

Figure 3-13 AP600 Plant Calculated CMT Water Temperature for Different Water Levels with a Mixing Depth of 3 Feet

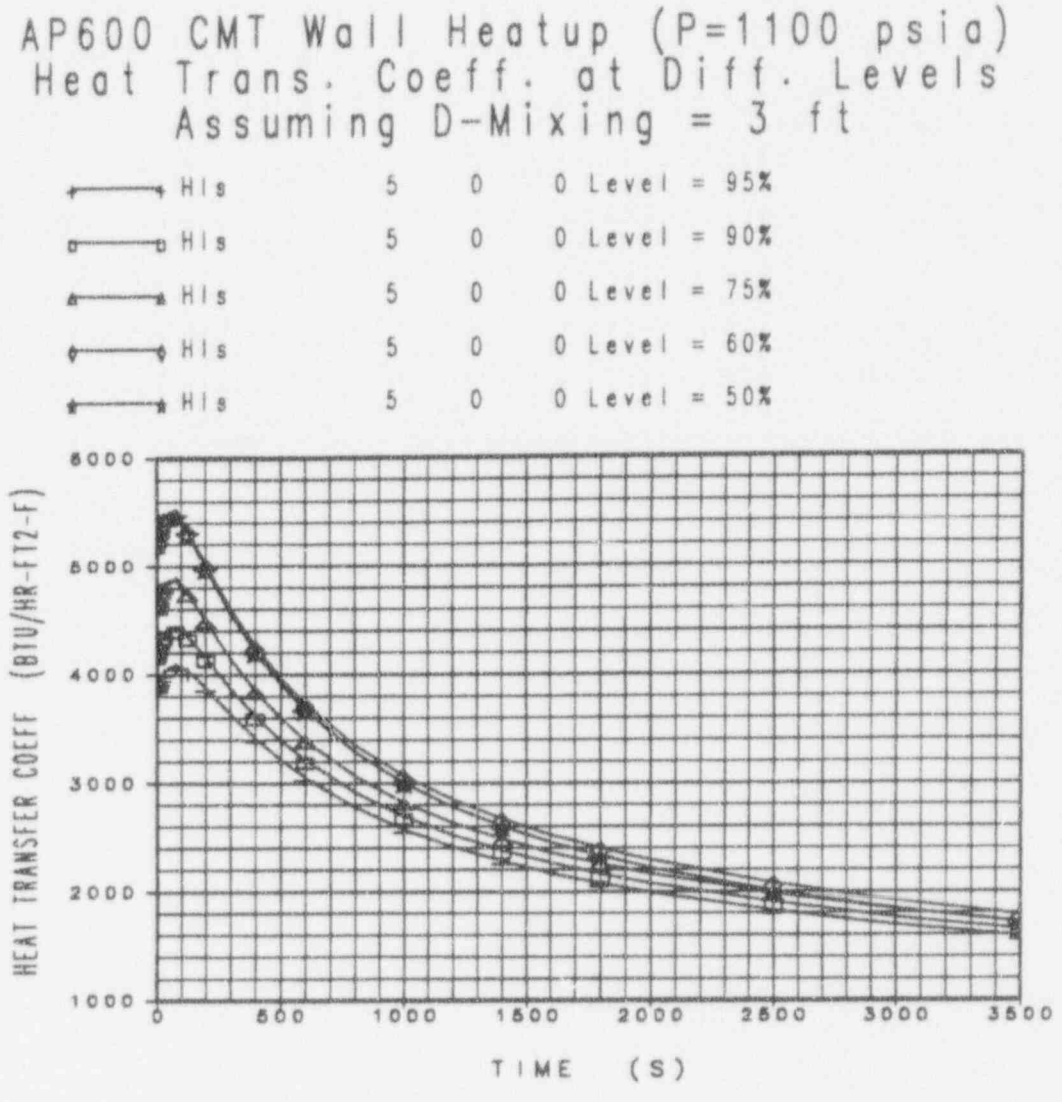

Figure 3-14 AP600 Plant CMT Calculated Water Surface Condensation Heat Transfer Coefficient for Different Water Levels and a Mixing Depth of 3 Feet

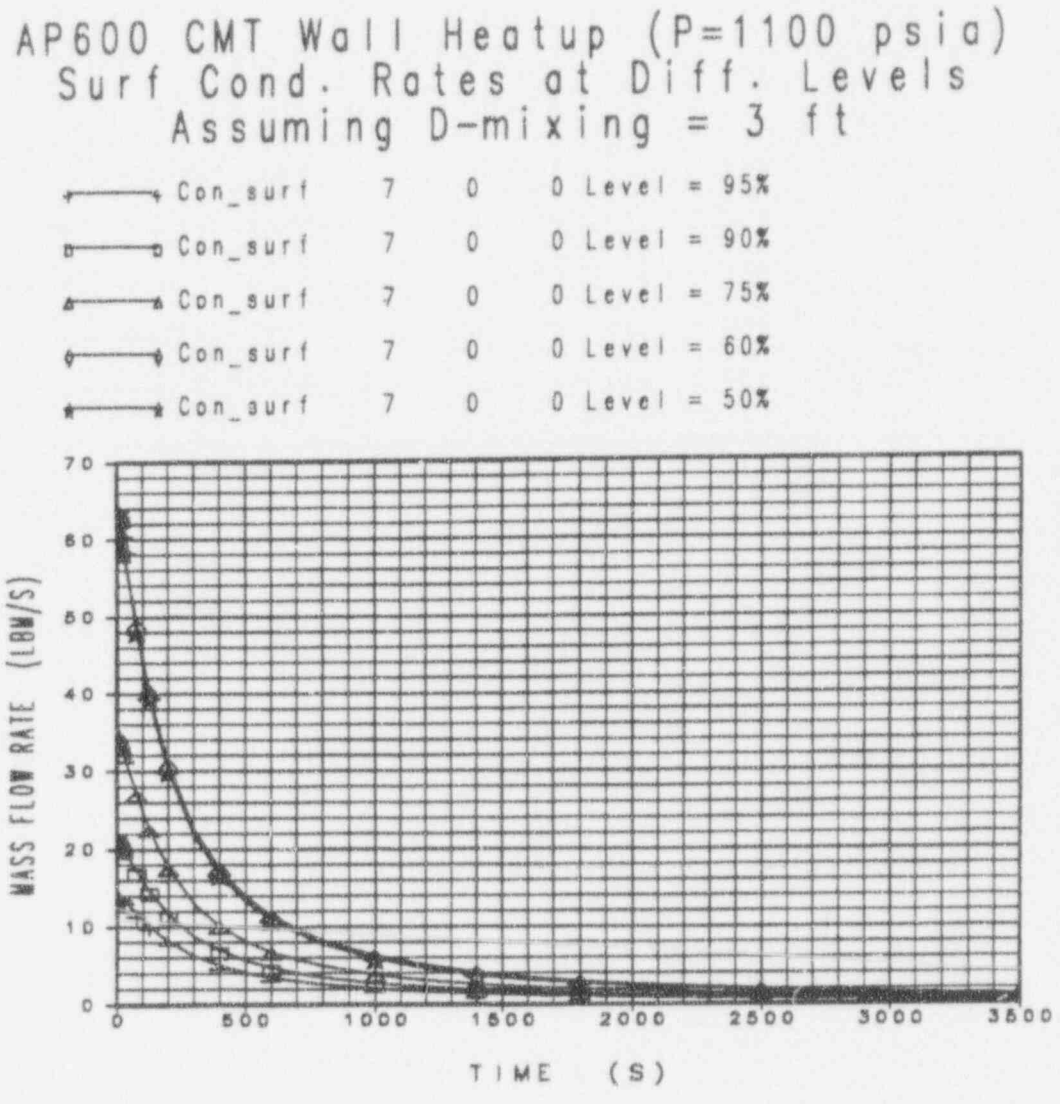

Figure 3-15 AP600 Plant Water Surface Condensate Flow Rates for Different Water Levels and a Mixing Depth of 3 Feet

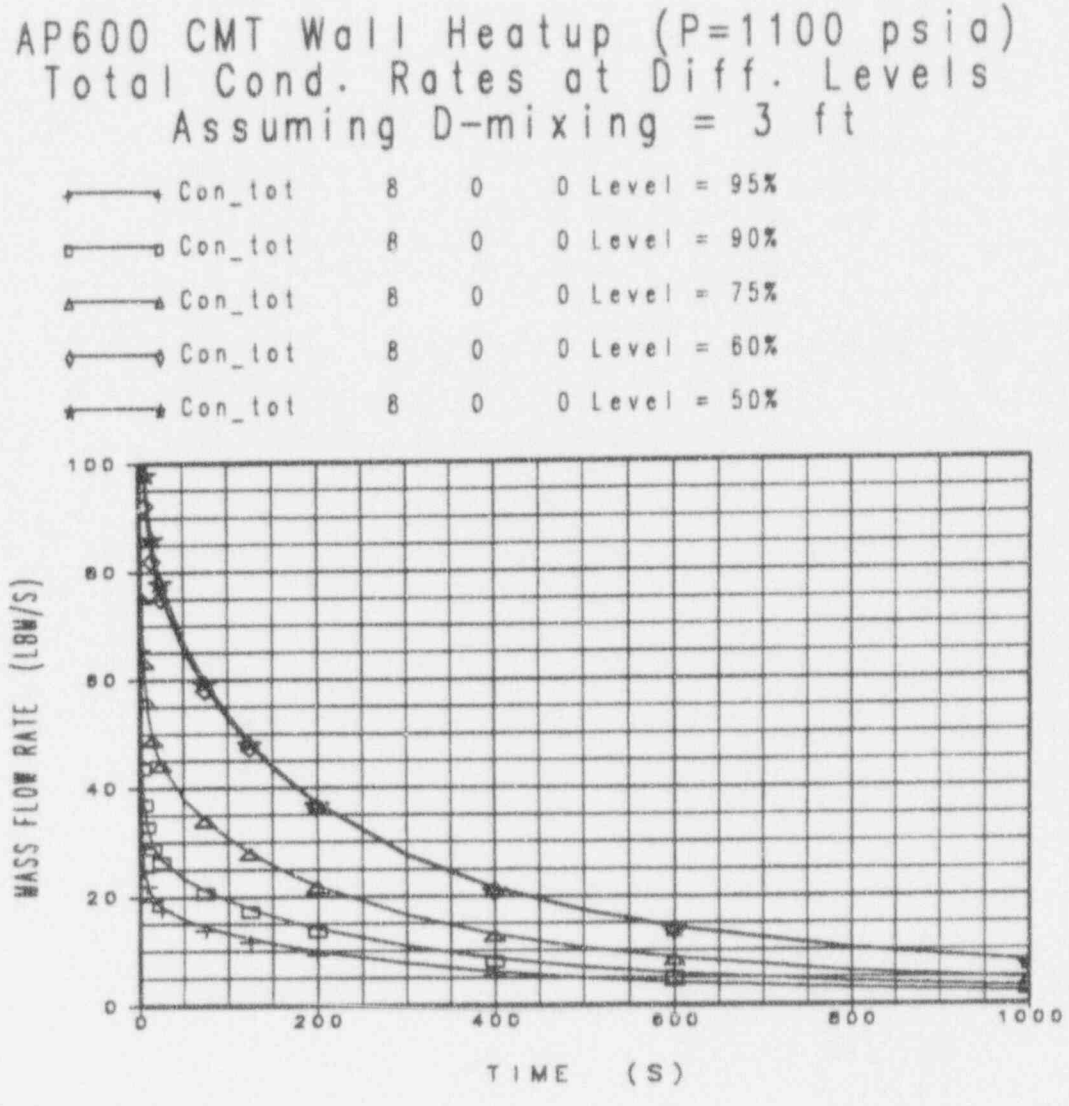

Figure 3-16 AP600 Plant Total Wall and Liquid Surface Condensate Flow Rate for Different Water Levels and a Mixing Depth of 3 Feet

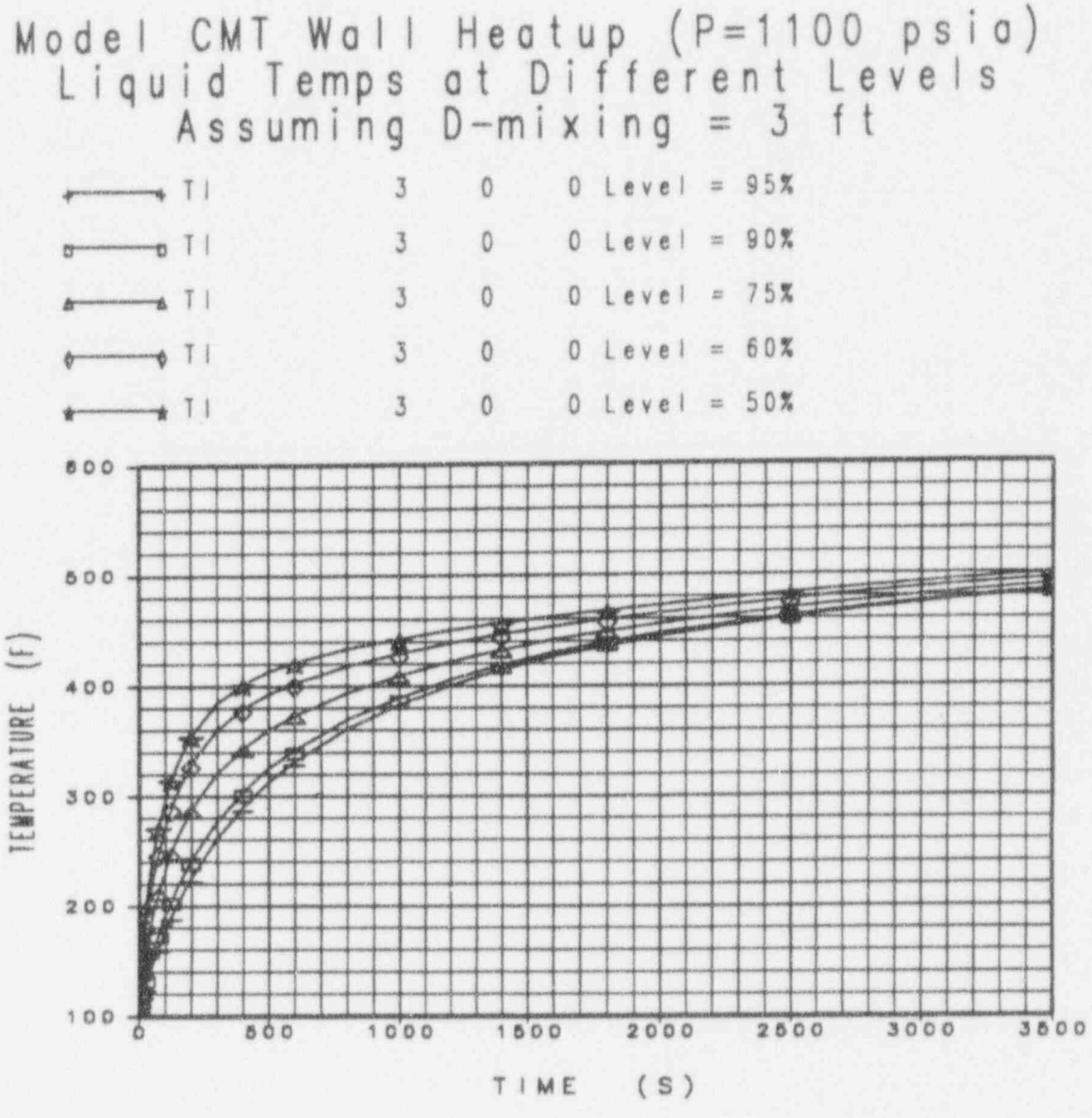

Figure 3-17 CMT Model Calculated Water Temperatures for Different Water Levels with a Mixing Depth of 3 Feet

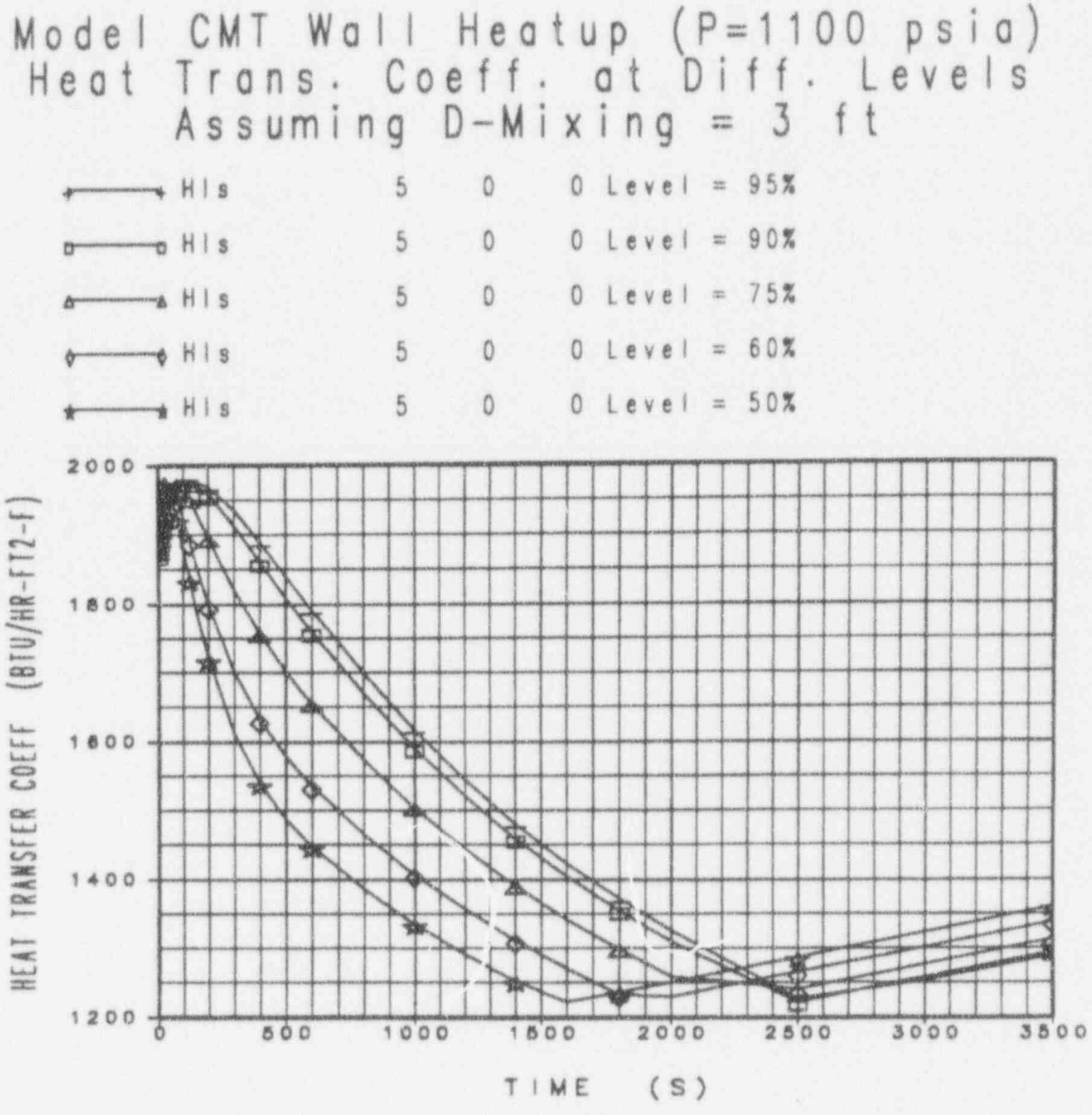

Figure 3-18 CMT Model Calculated Water Surface Condensation Heat Transfer Coefficient at Different Water Levels and a Mixing Depth of 3 Feet

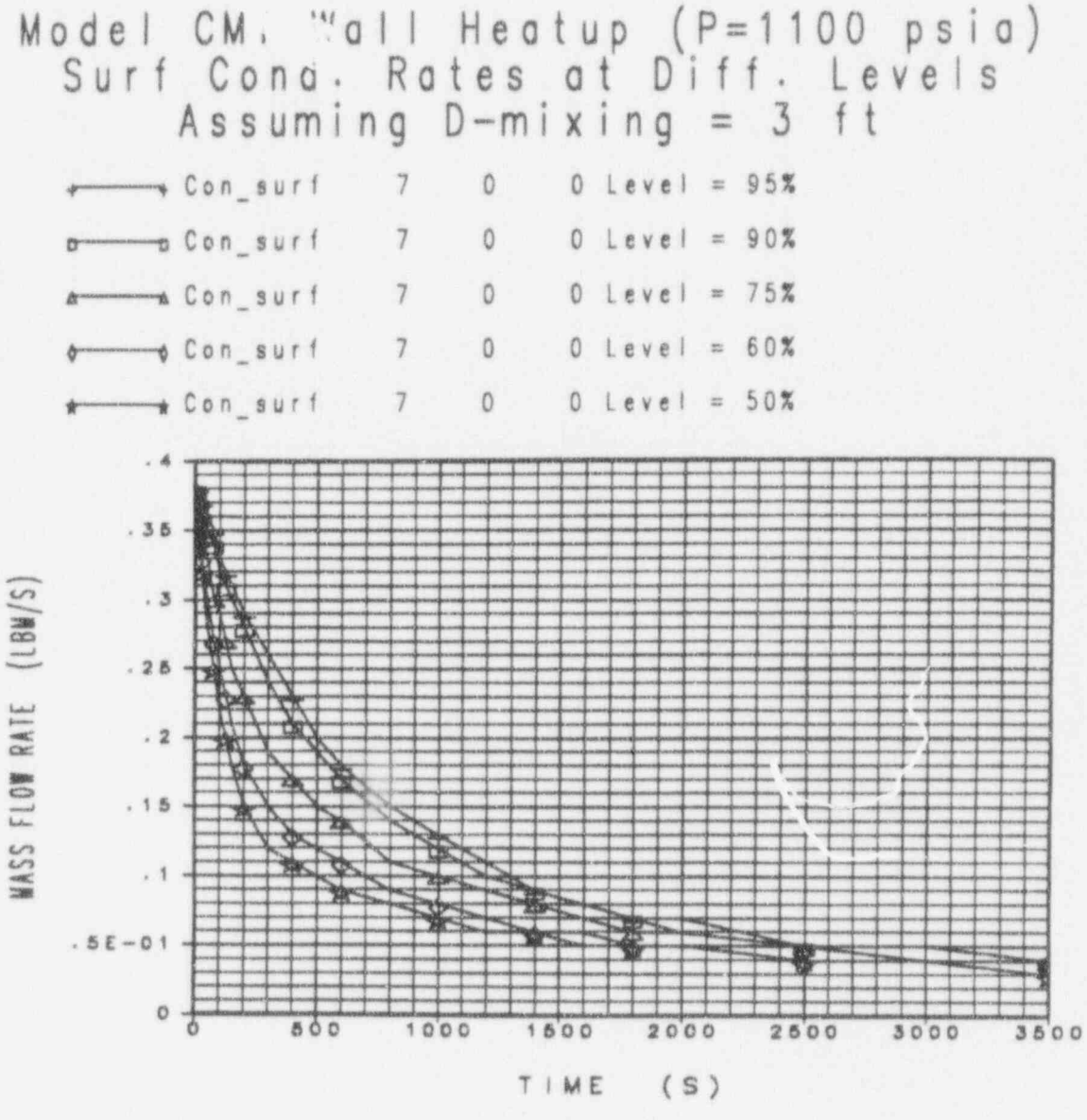

Figure 3-19 CMT Model Surface Condensate Flow Rate for Different Water Levels with a Mixing Depth of 3 Feet

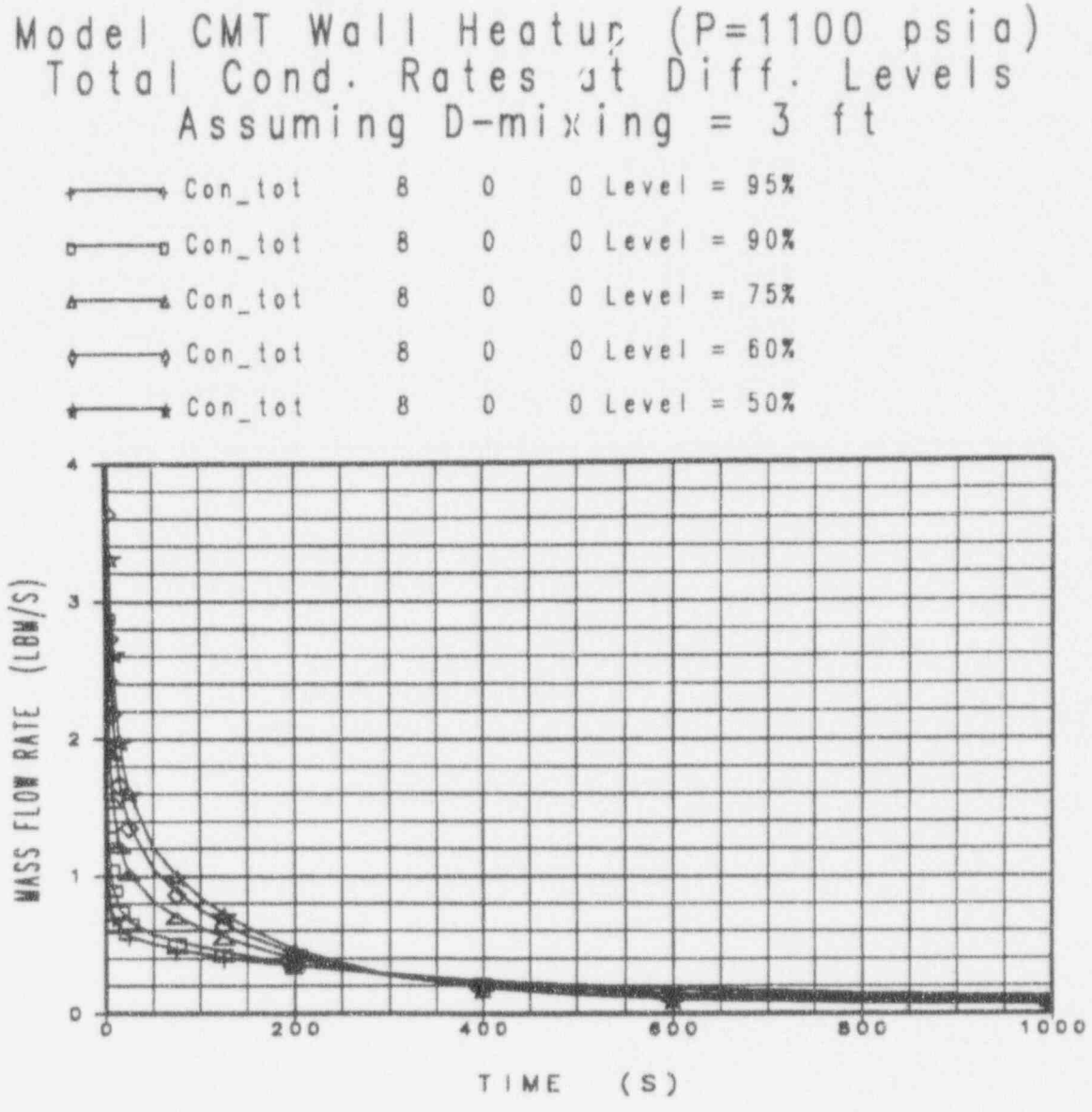

Figure 3-20 Total CMT Model Wall and Liquid Surface Condensate Flow Rate for Different Water Levels at a Mixing Depth of 3 Feet

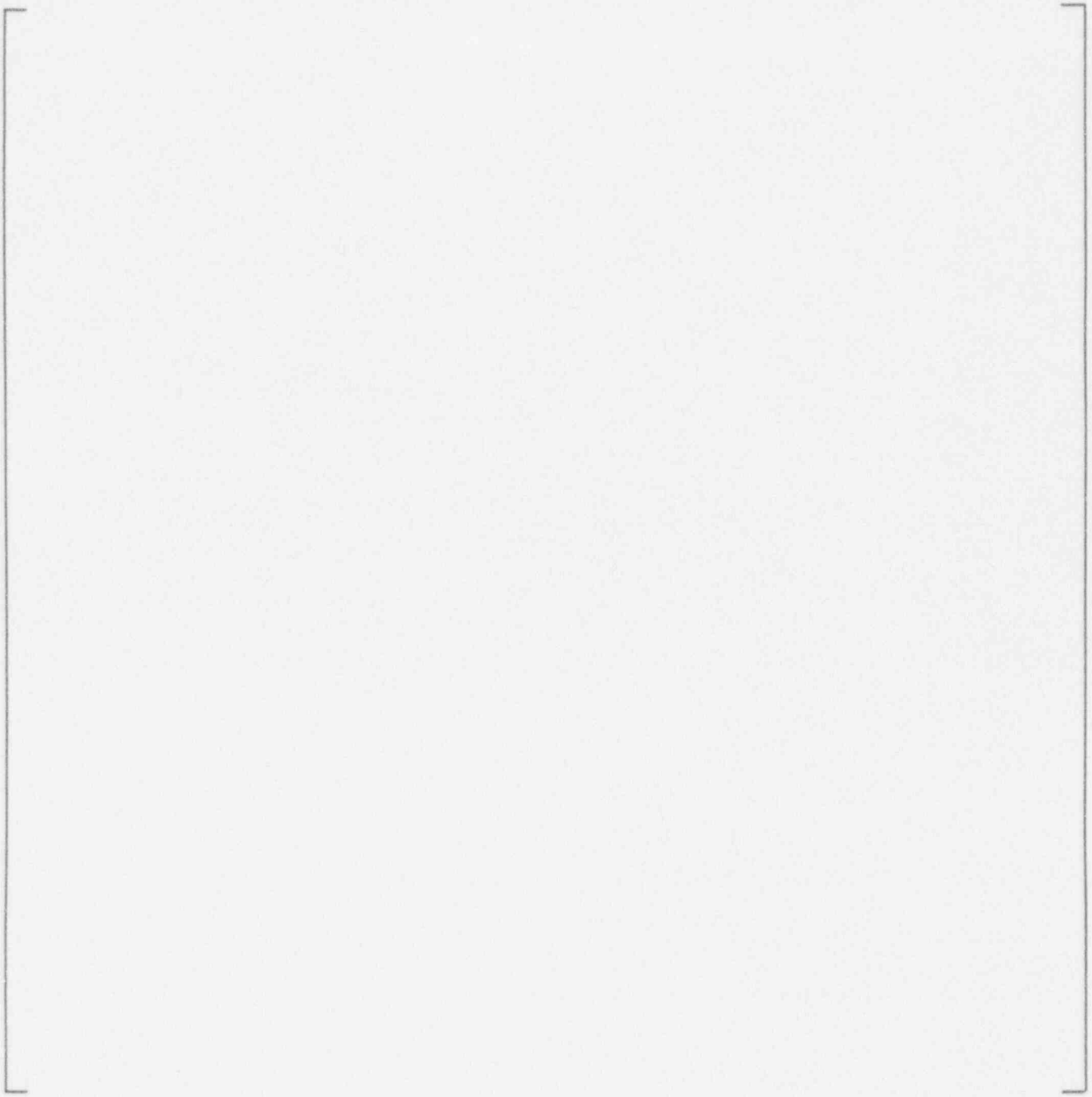

a,c

Figure 3-21 Ratio of the CMT Model to AP600 CMT Plant Wall Condensate Mass Flux for Different Water Levels and a Mixing Depth of 3 Feet

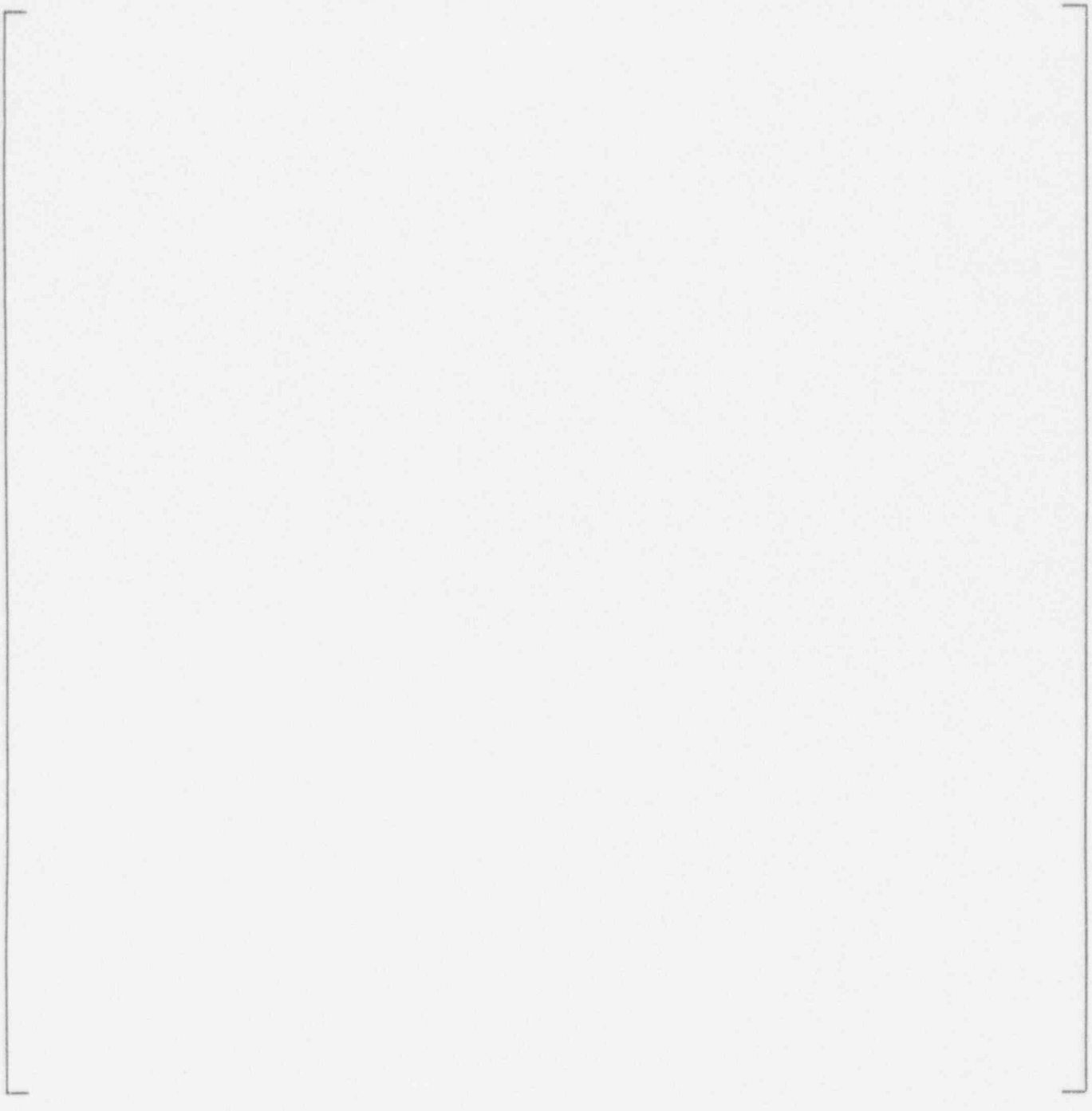

a,c

Figure 3-22 Ratio of the CMT Model to AP600 CMT Plant Surface Condensate Mass Flux Rates for Different Water Levels and a Mixing Depth of 3 Feet

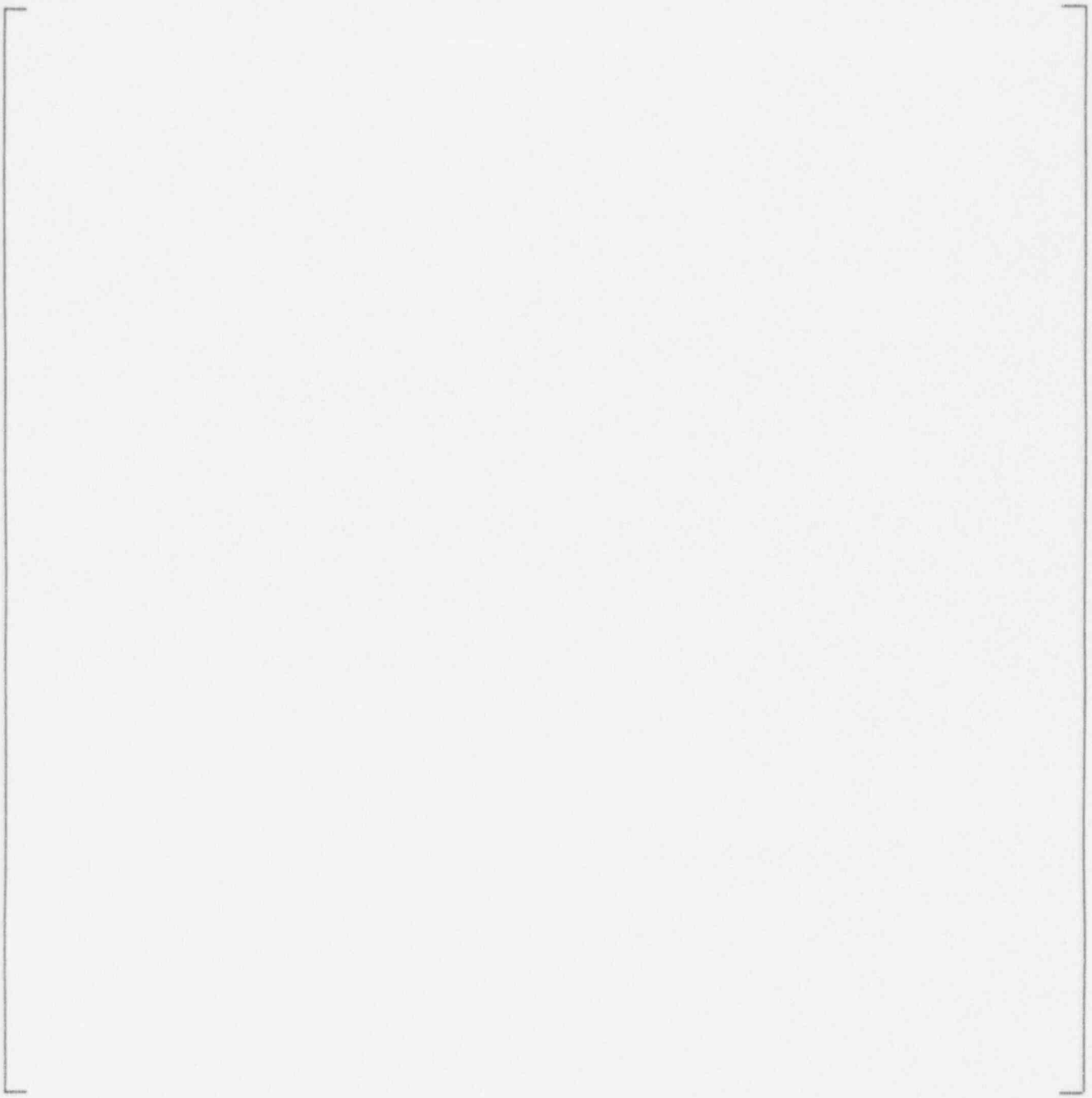

a,c

Figure 3-23 Ratio of the CMT Model to AP600 CMT Plant Total Condensate Mass Flux Rates for Different Water Levels and a Mixing Depth of 3 Feet

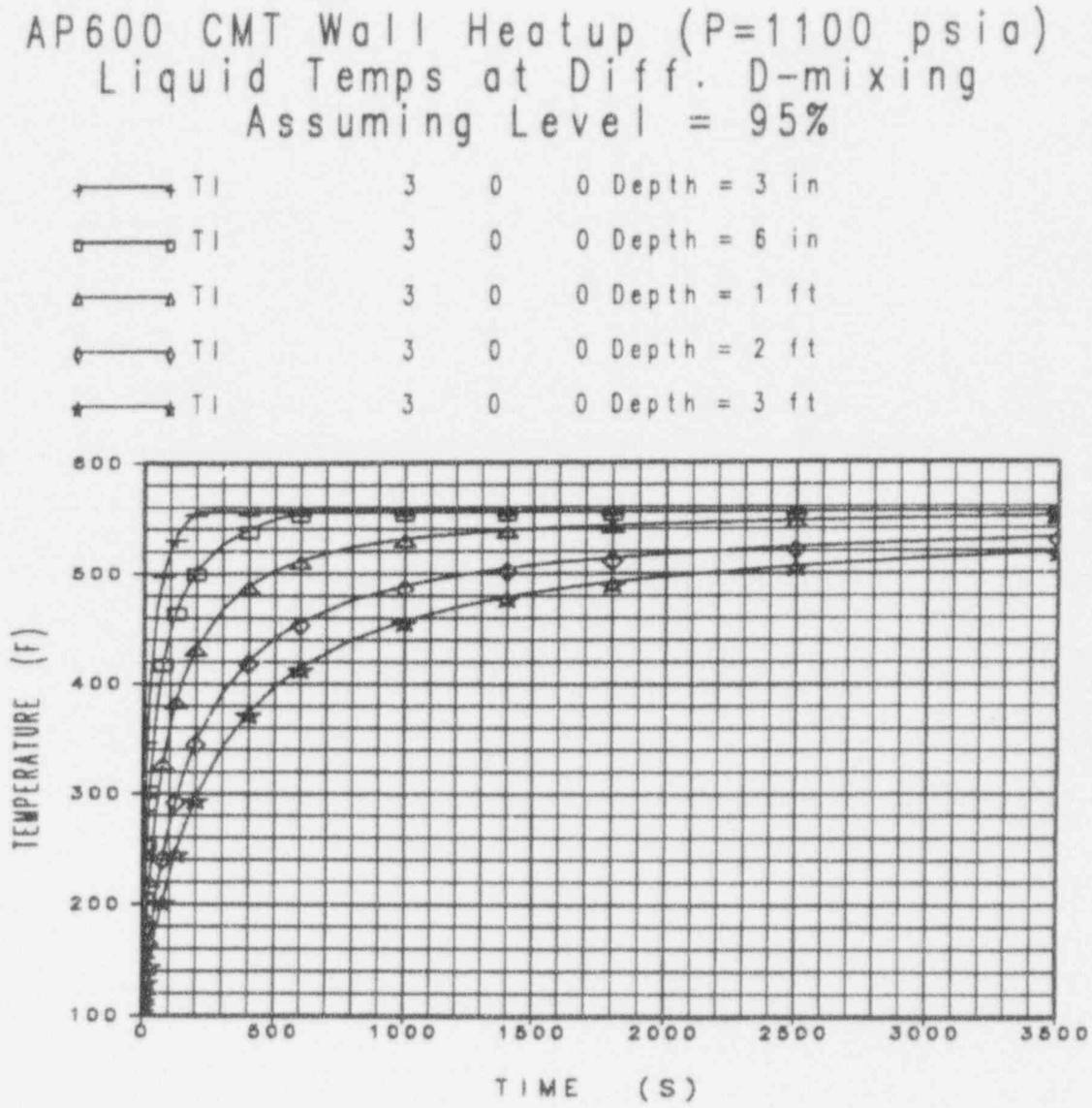

Figure 3-24 AP600 Plant CMT Liquid Temperatures for Different Mixing Depth at 95% Water Level

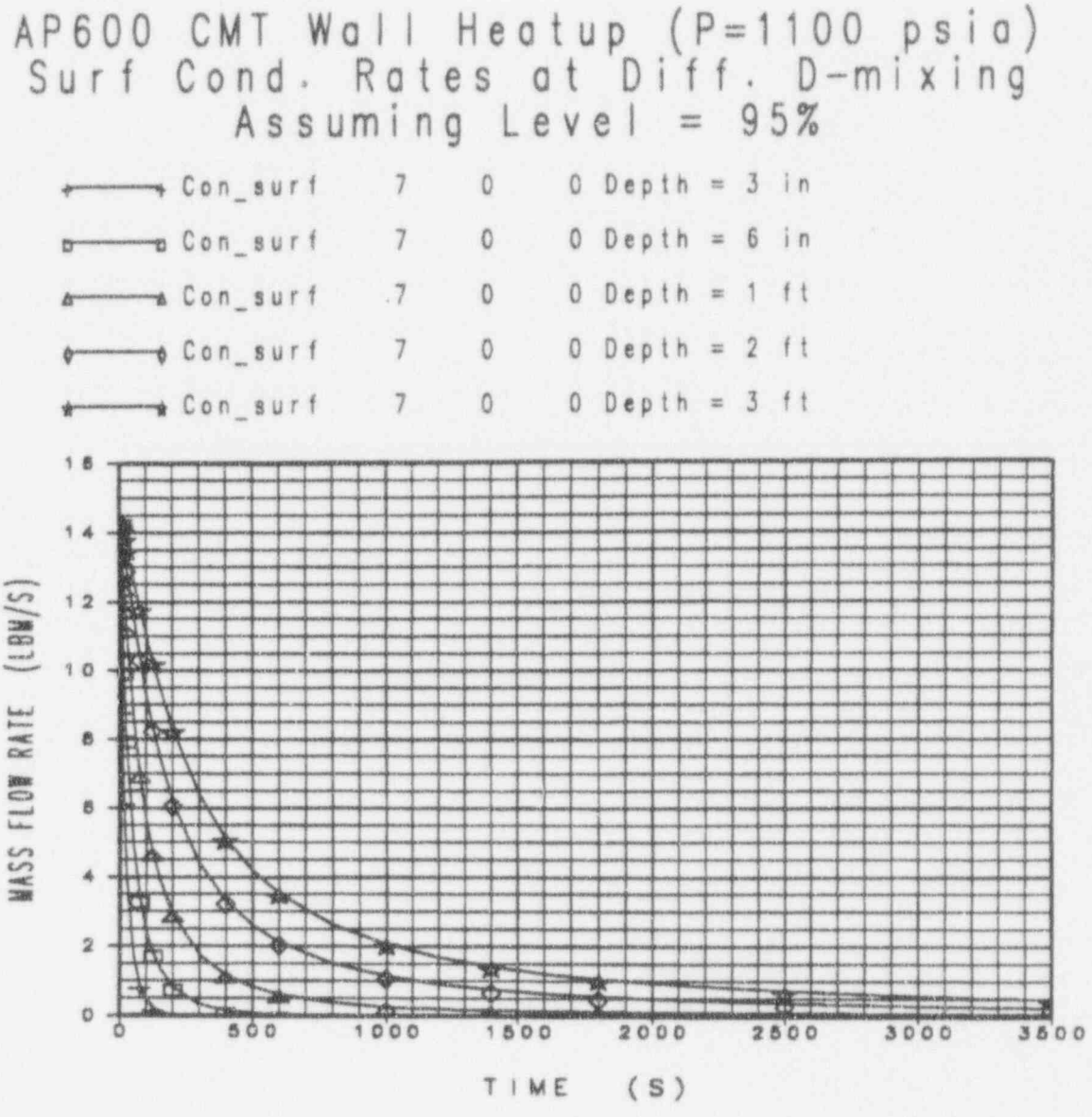

Figure 3-25 Calculated AP600 CMT Plant Water Surface Condensate Flow Rates for Different Mixing Depths at a Water Level of 95%

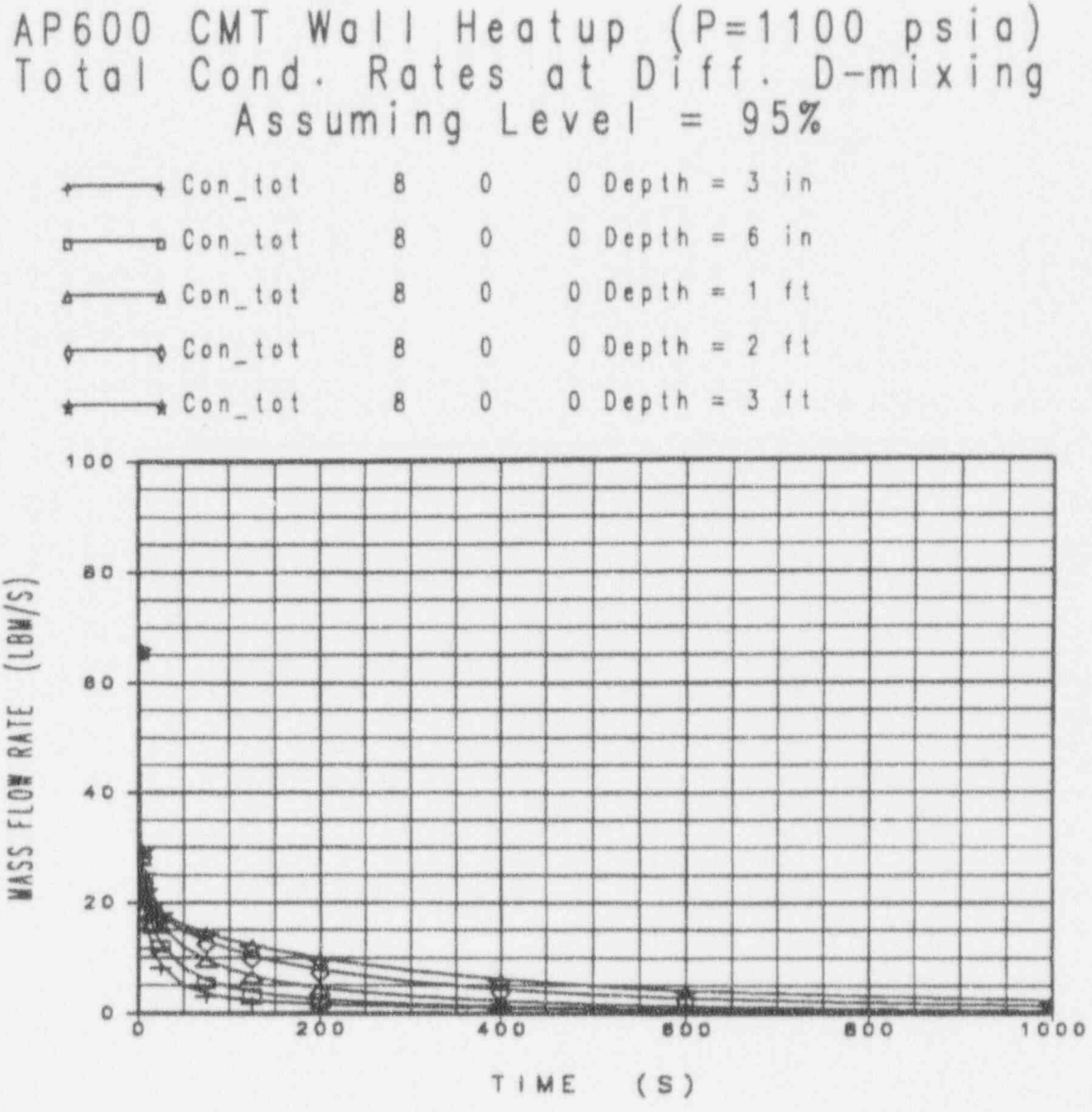

Figure 3-26 Calculated Total Plant CMT Condensation Flow Rates for Different Mixing Depths at a 95% Water Level

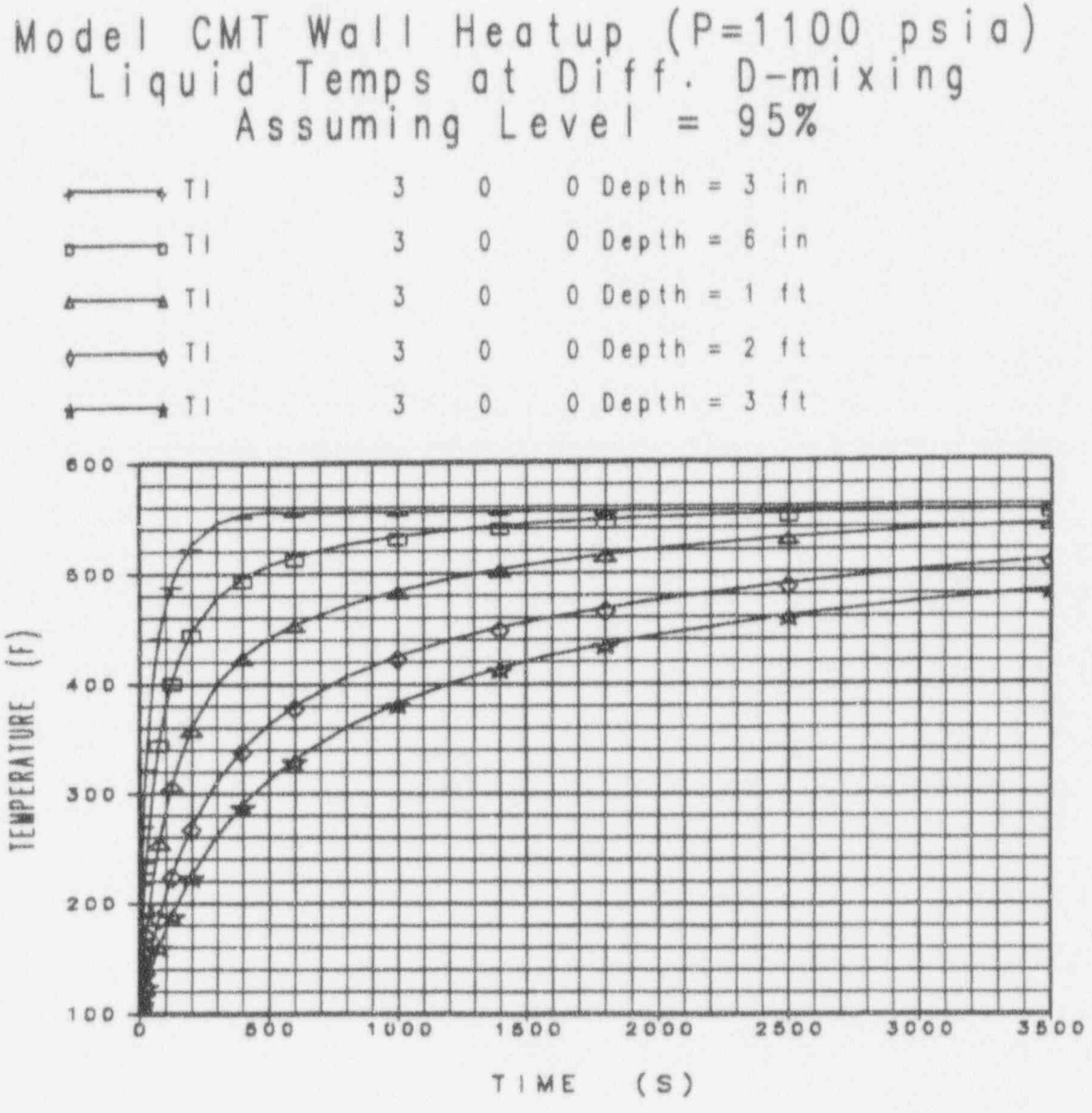

Figure 3-27 CMT Model Calculated Liquid Temperatures for Different Mixing Depths for 95% CMT Water Level

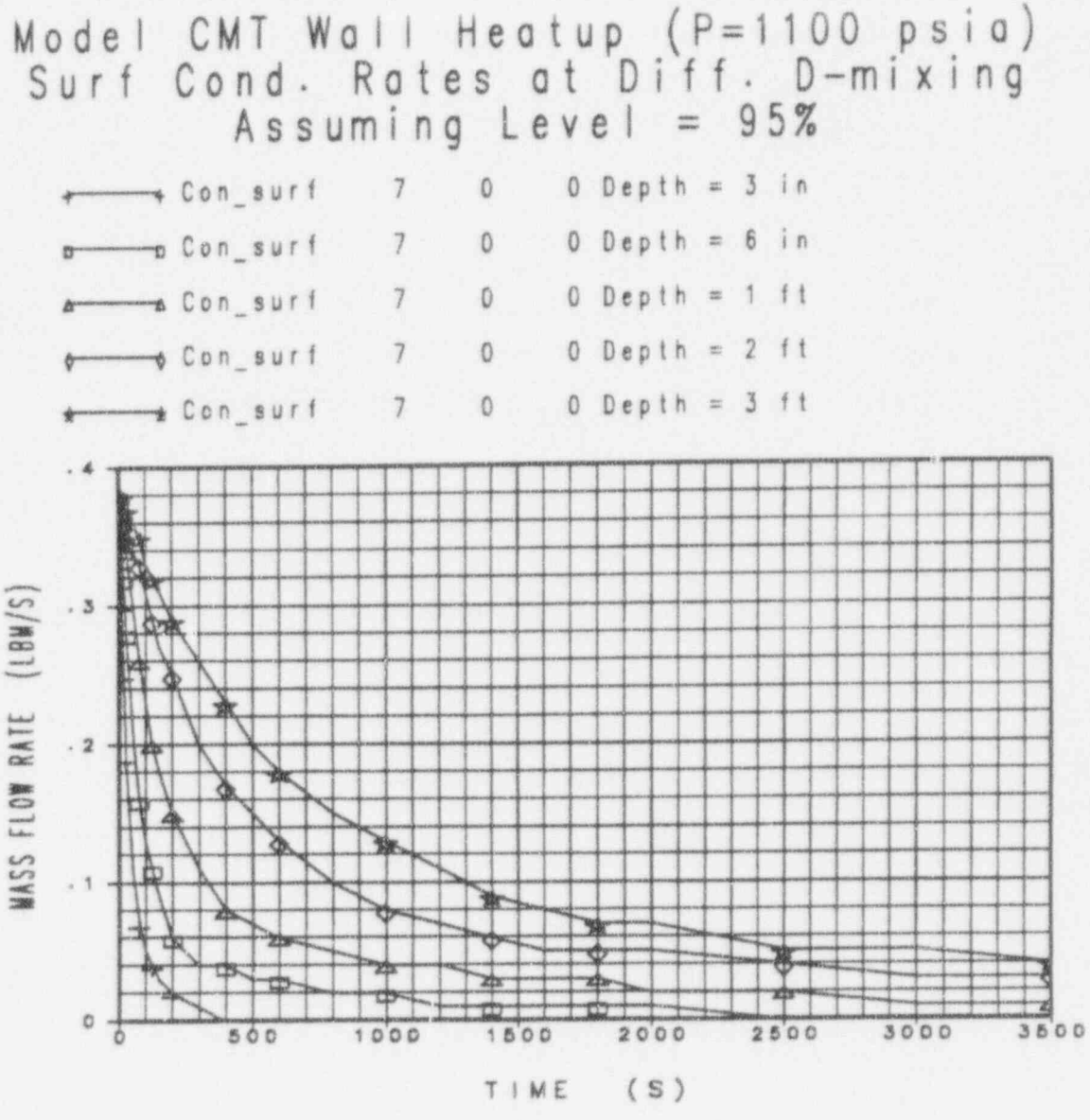

Figure 3-28 Calculated CMT Model Surface Condensation Rates for Different Mixing Depths with a CMT Level of 95%

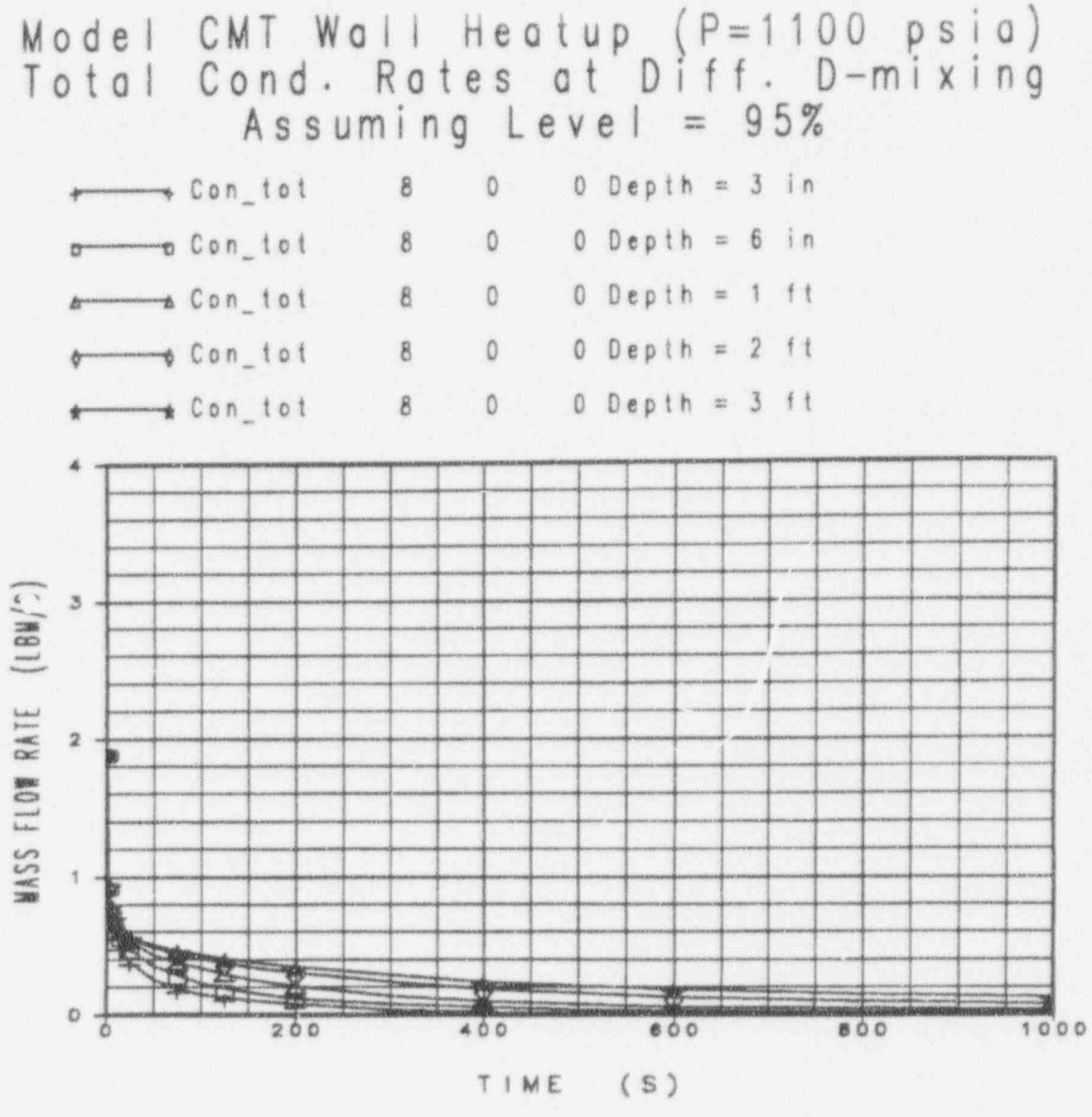

Figure 3-29 Calculated CMT Model Total Condensate Flow Rates for Different Mixing Depths at a CMT Level of 95%

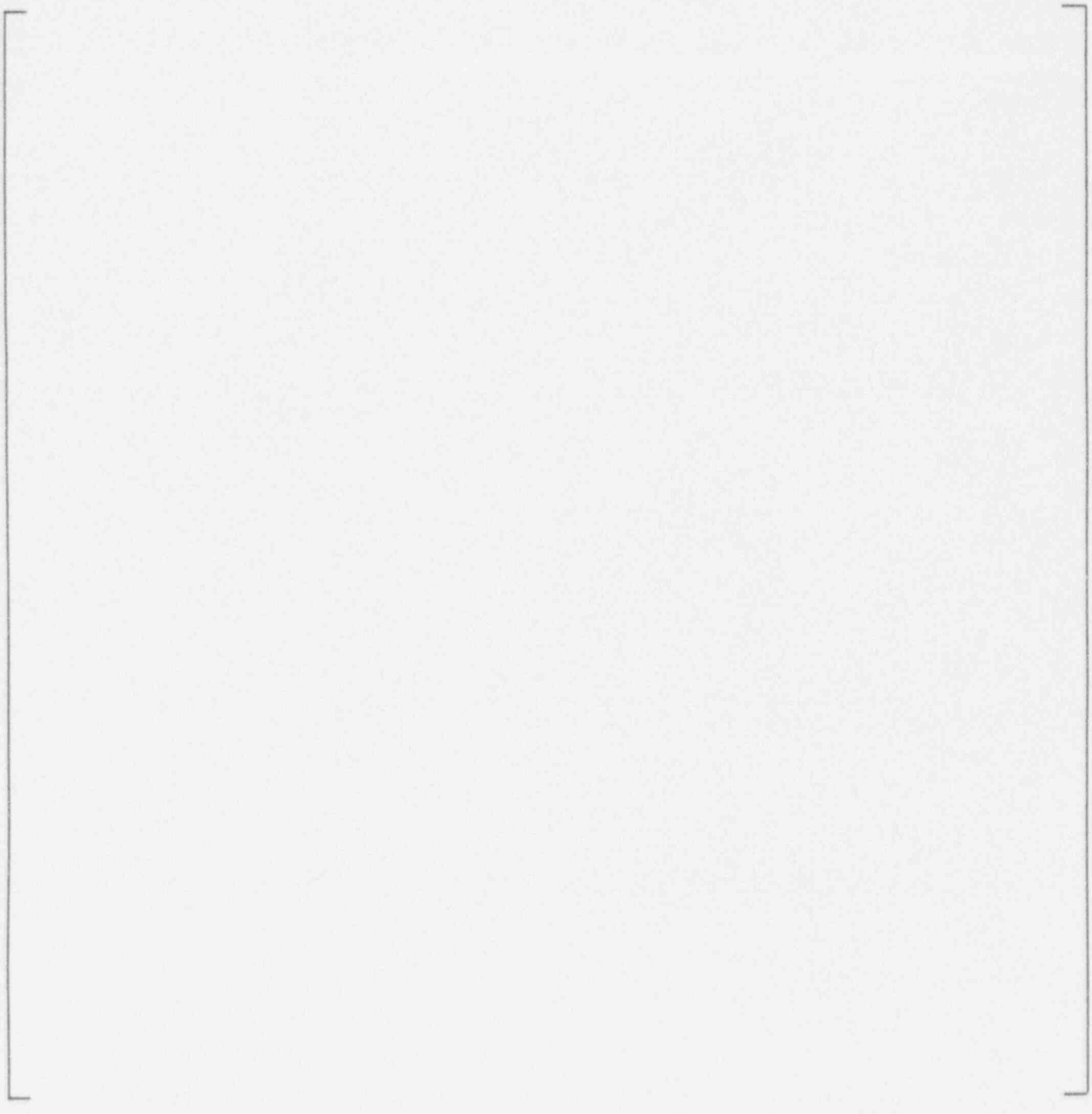

Figure 3-30 Ratio of the Calculated CMT Model to Plant Condensate Flow Rates for Different Assumed Mixing Depths at a CMT Water Level of 95%

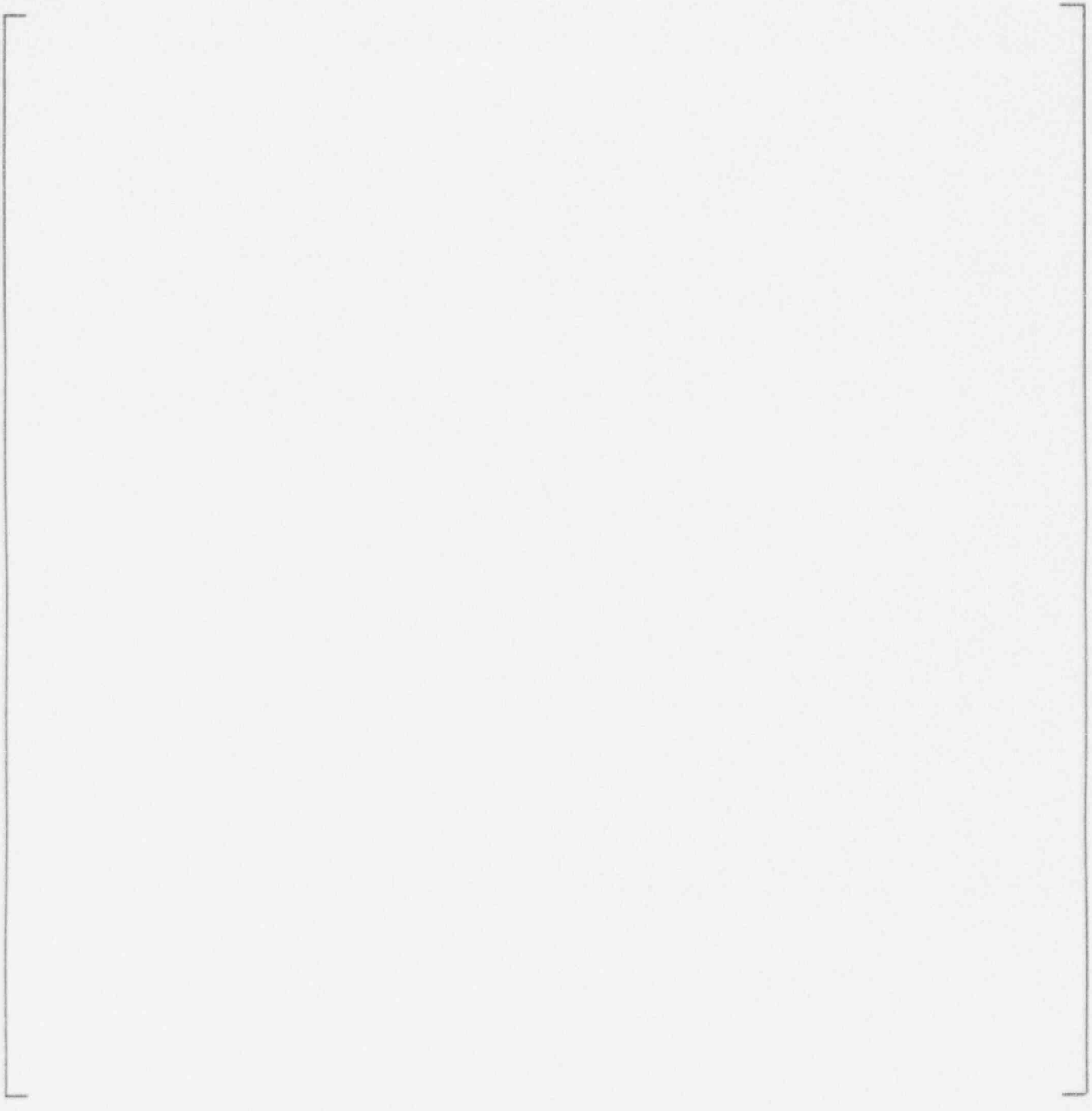

a,c

Figure 3-31 Ratio of the Total Calculated CMT Model to Plant Condensate Flow Rates for Different Assumed Mixing Depths With a CMT Water Level of 95%

[a,c]

Figure 3-32 Calculated Wall Surface Condensation Π Group for the Plant CMT for a 3-foot Mixing Depth and Different CMT Levels

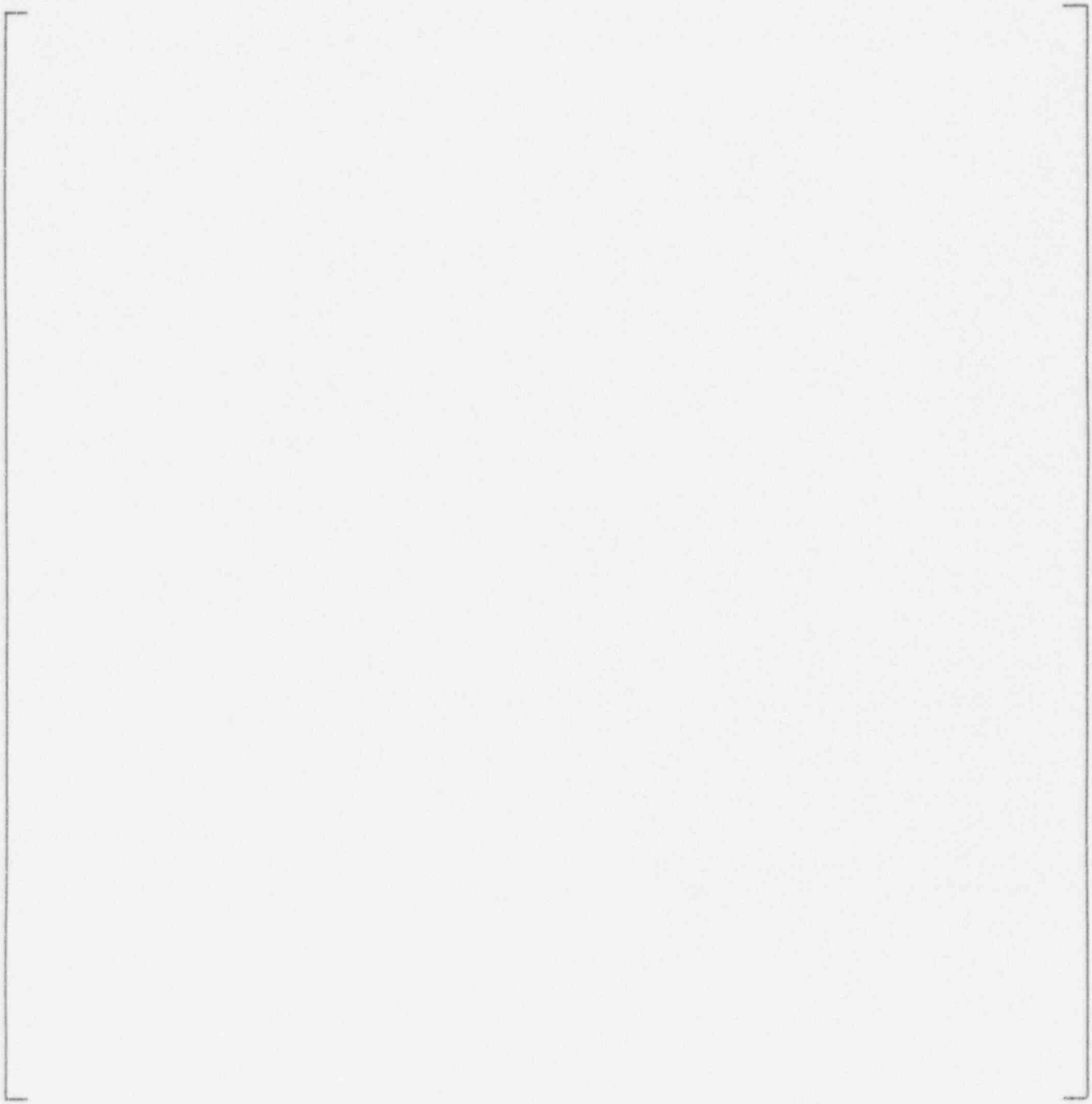

Figure 3-33 Calculated Wall Surface Condensation Π Group for the Test CMT for a 3-foot Mixing Depth and Different CMT Levels

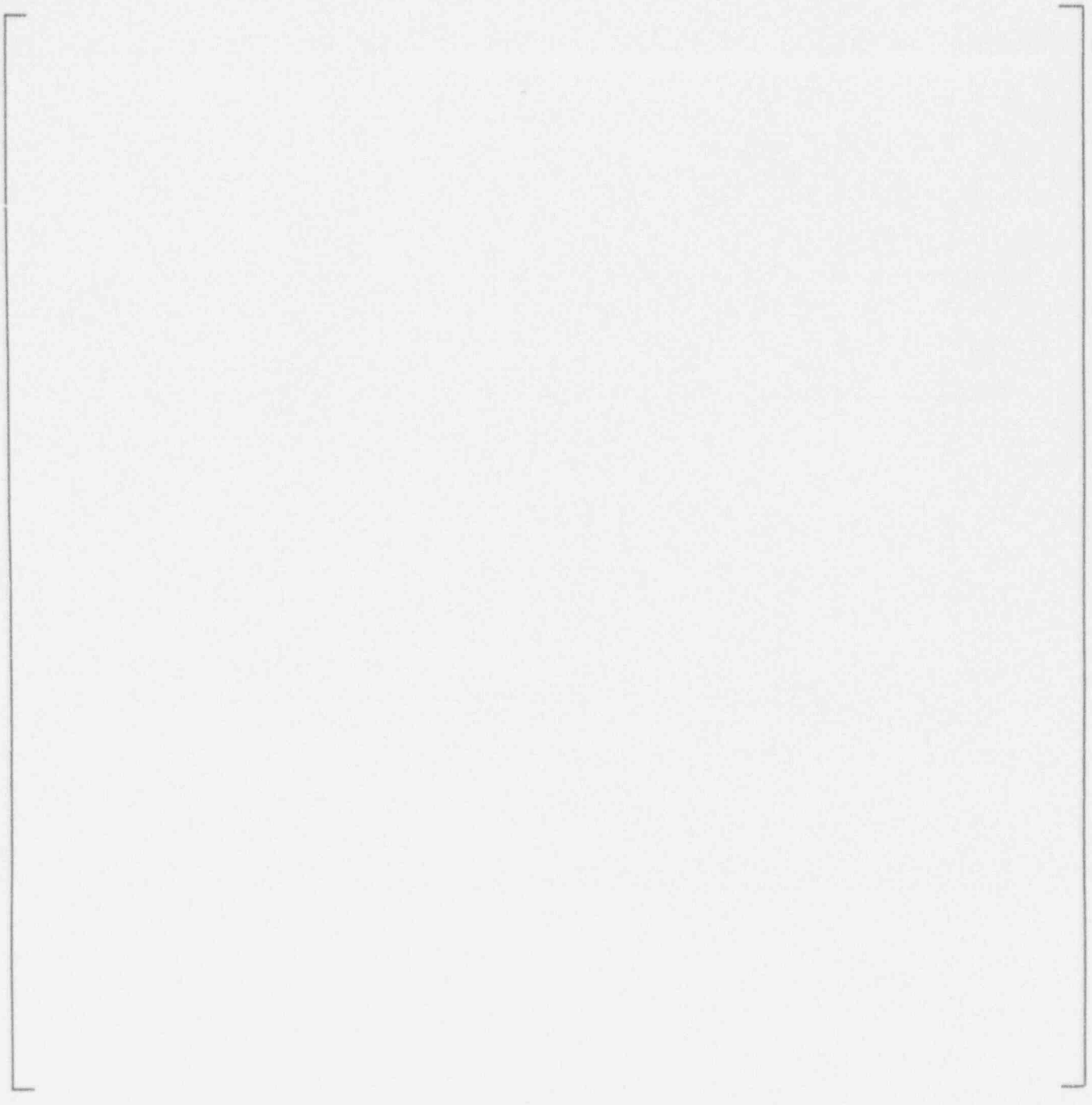

a,c

Figure 3-34 Calculated Π Group Ratios for Wall Condensation for a 3-foot Mixing Depth and Different CMT Levels

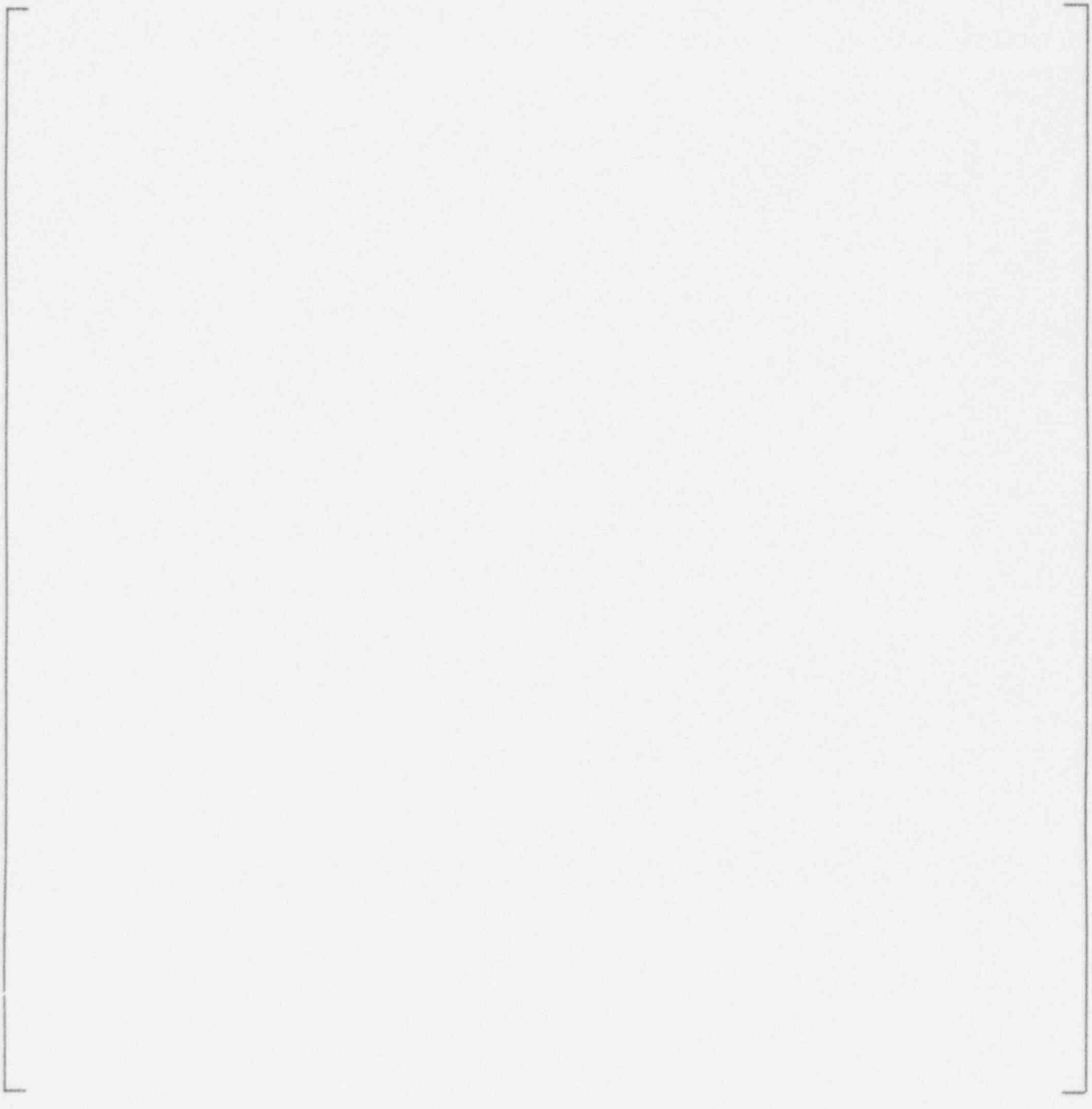

a,c

Figure 3-35 The Water Surface Condensation Π Group for the AP600 Plant CMT at a CMT Level of 90% and Different Mixing Depths

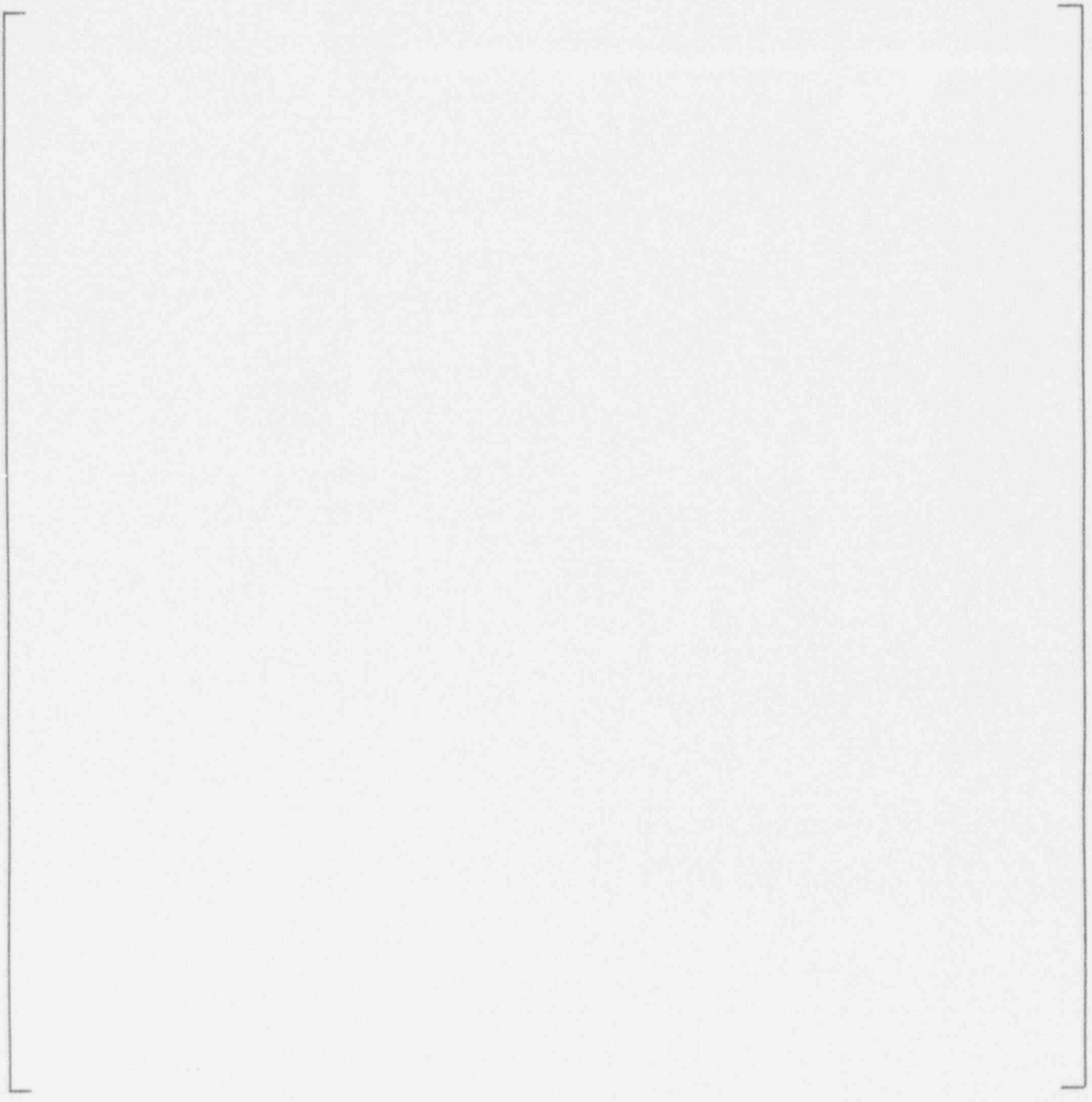

a,c

Figure 3-36 The Water Surface Condensation Π Group for the Test CMT at a CMT Level of 90% for Different Mixing Depths

[a,c]

Figure 3-37 Water Surface Condensation Π Group for the AP600 CMT at a CMT Level of 90% for Different Mixing Depths

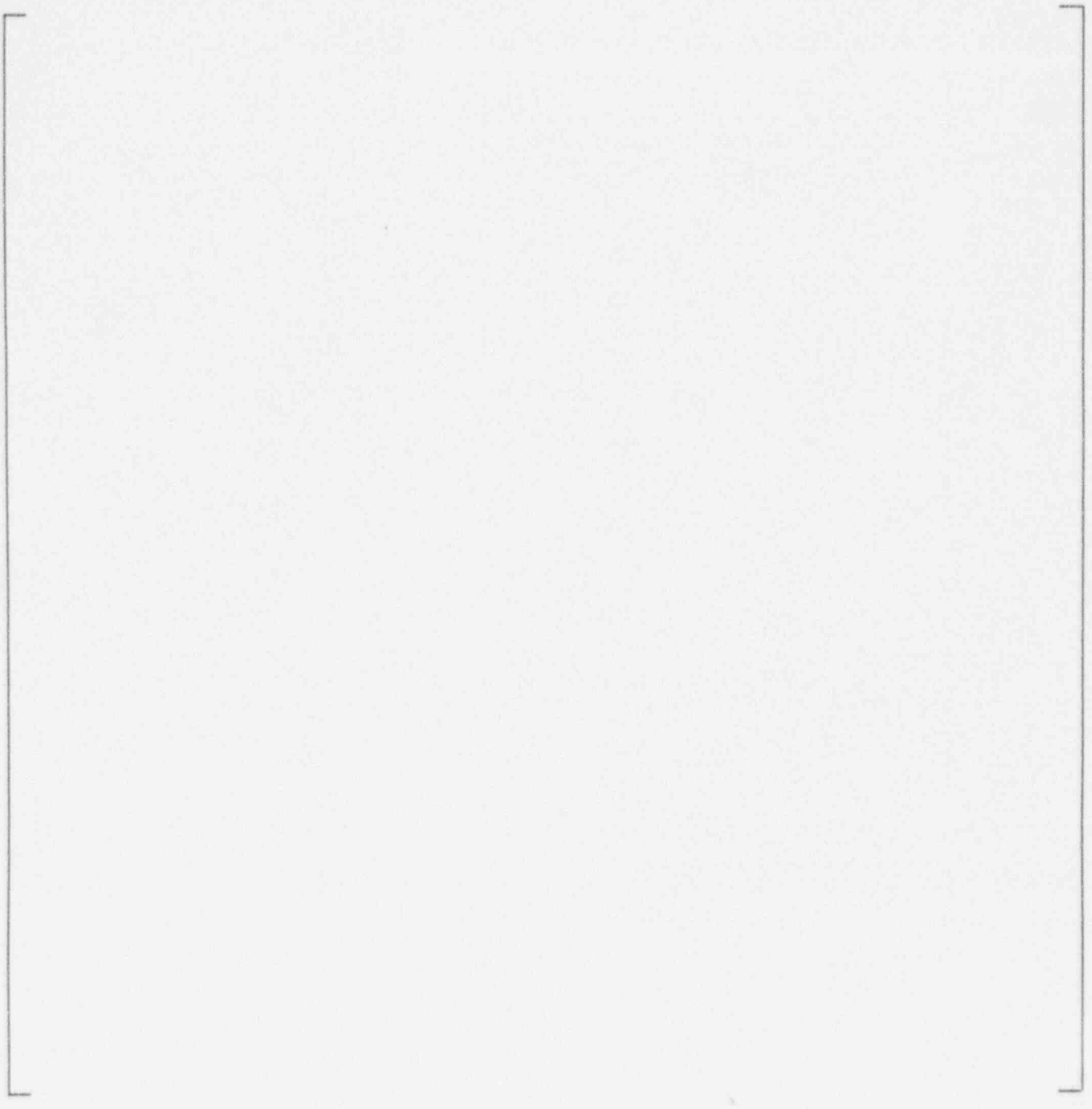

a,c

Figure 3-38 Calculated Wall Condensation Π Group for the AP600 Plant at a CMT Level of 95% for Different Mixing Depths

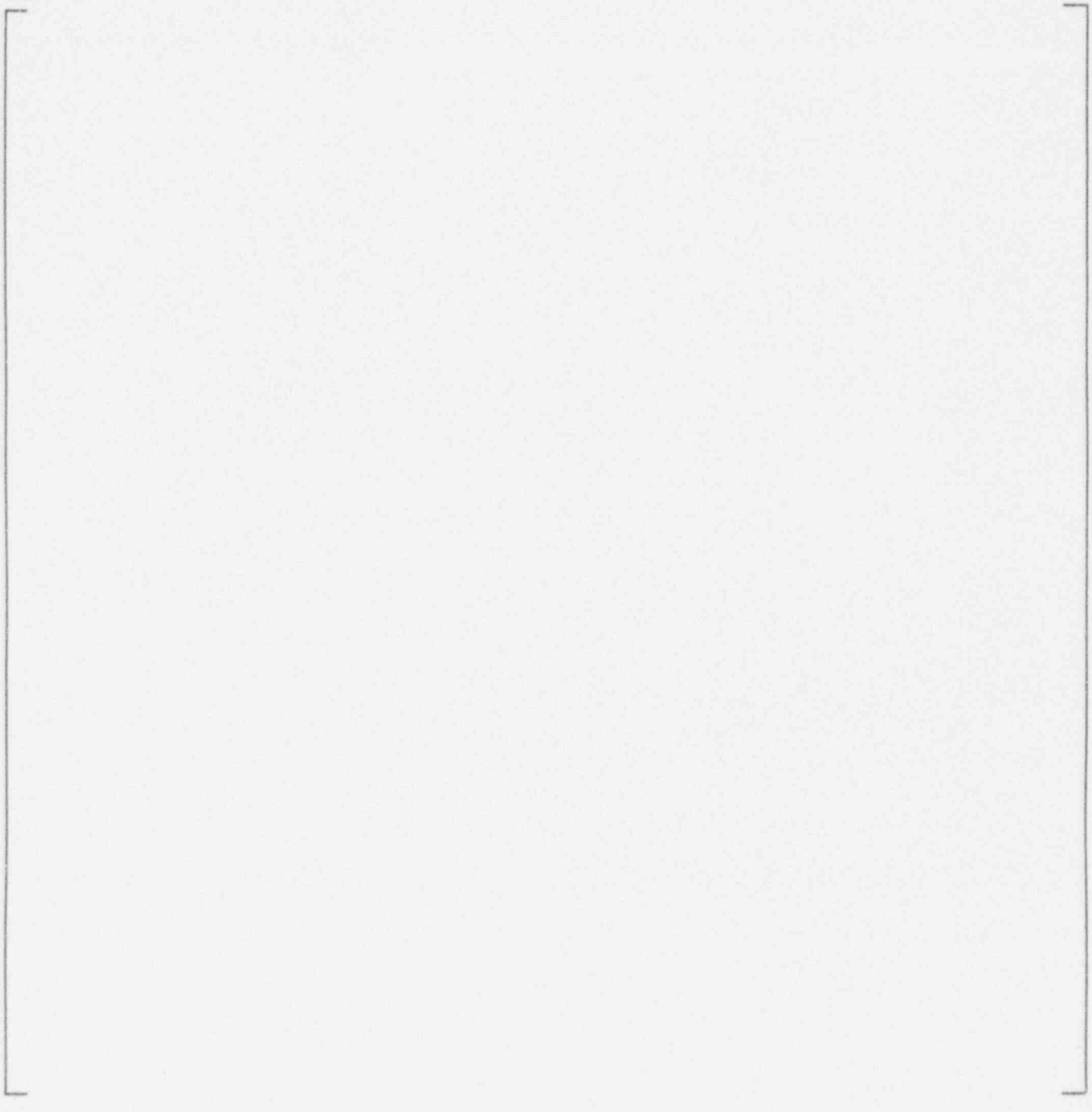

a,c

Figure 3-39 Calculated Wall Condensation Π Group for the CMT Test at a CMT Level of 95% for Different Mixing Depths

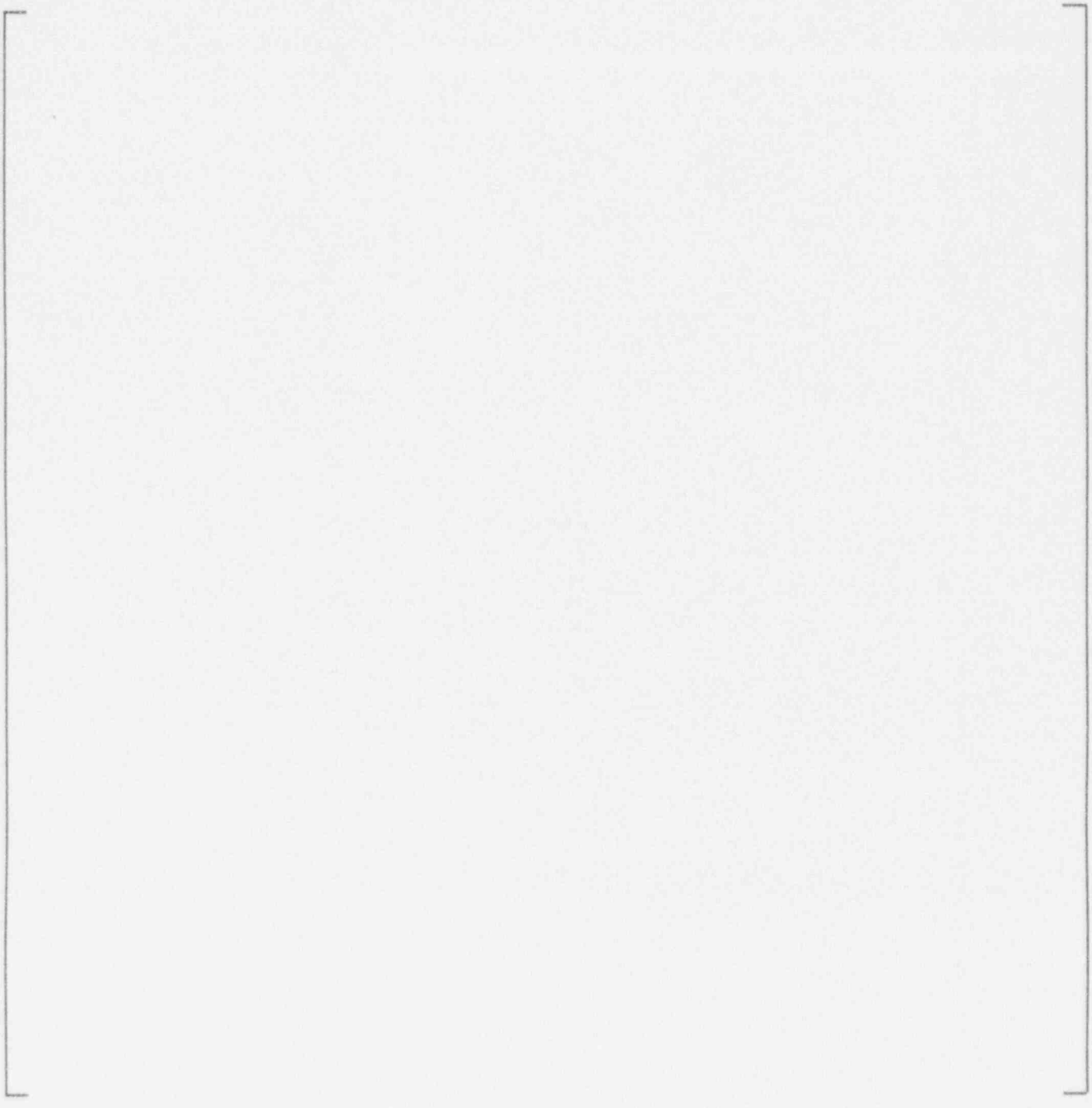

a,c

Figure 3-40 Calculated Wall Condensation Π Group Ratio at a CMT Level of 95% for Different Mixing Depths

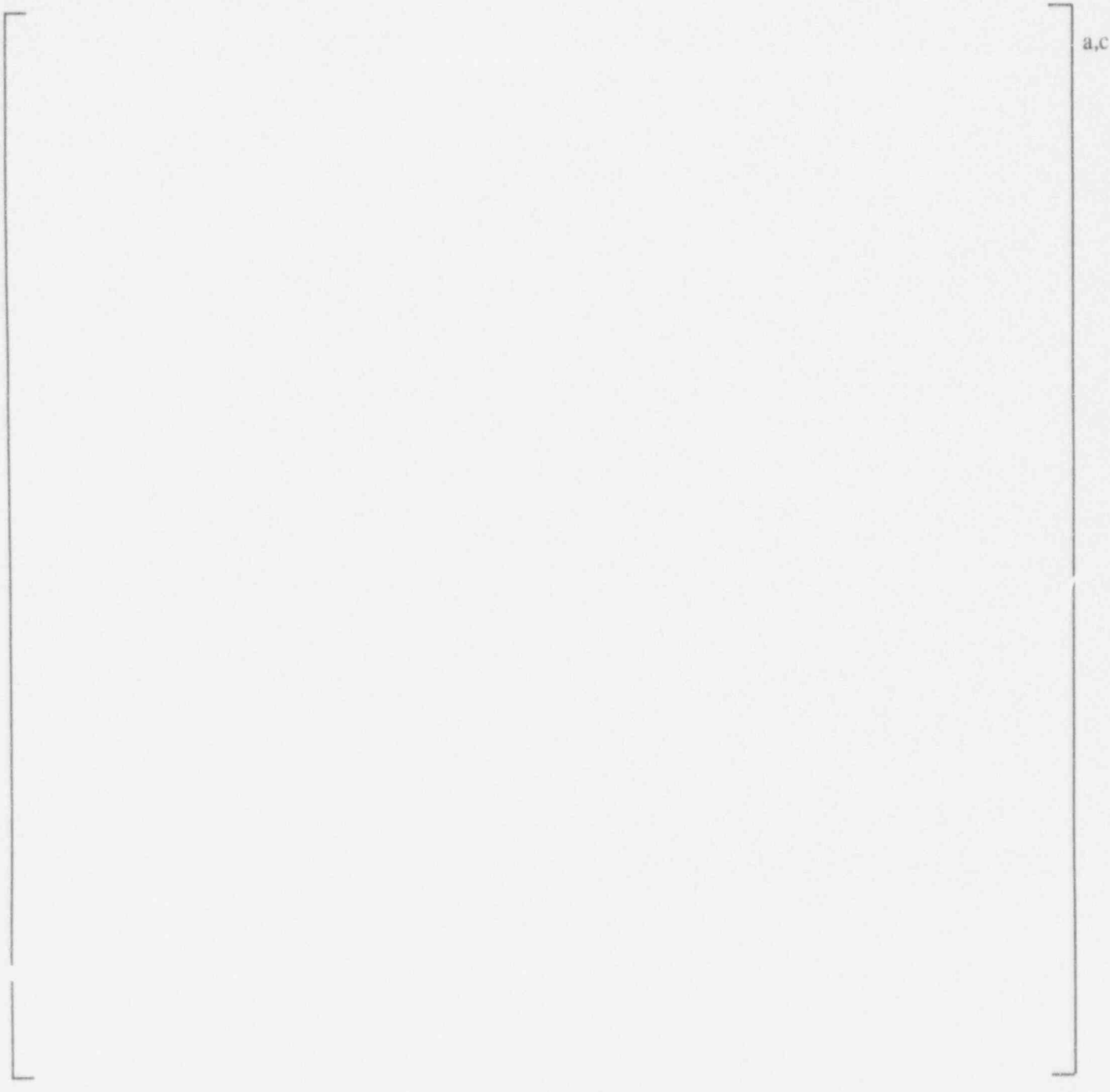

Figure 3-41 Calculated Surface Condensation Π Group for the AP600 Plant at a CMT Level of 95% for Different Mixing Depths

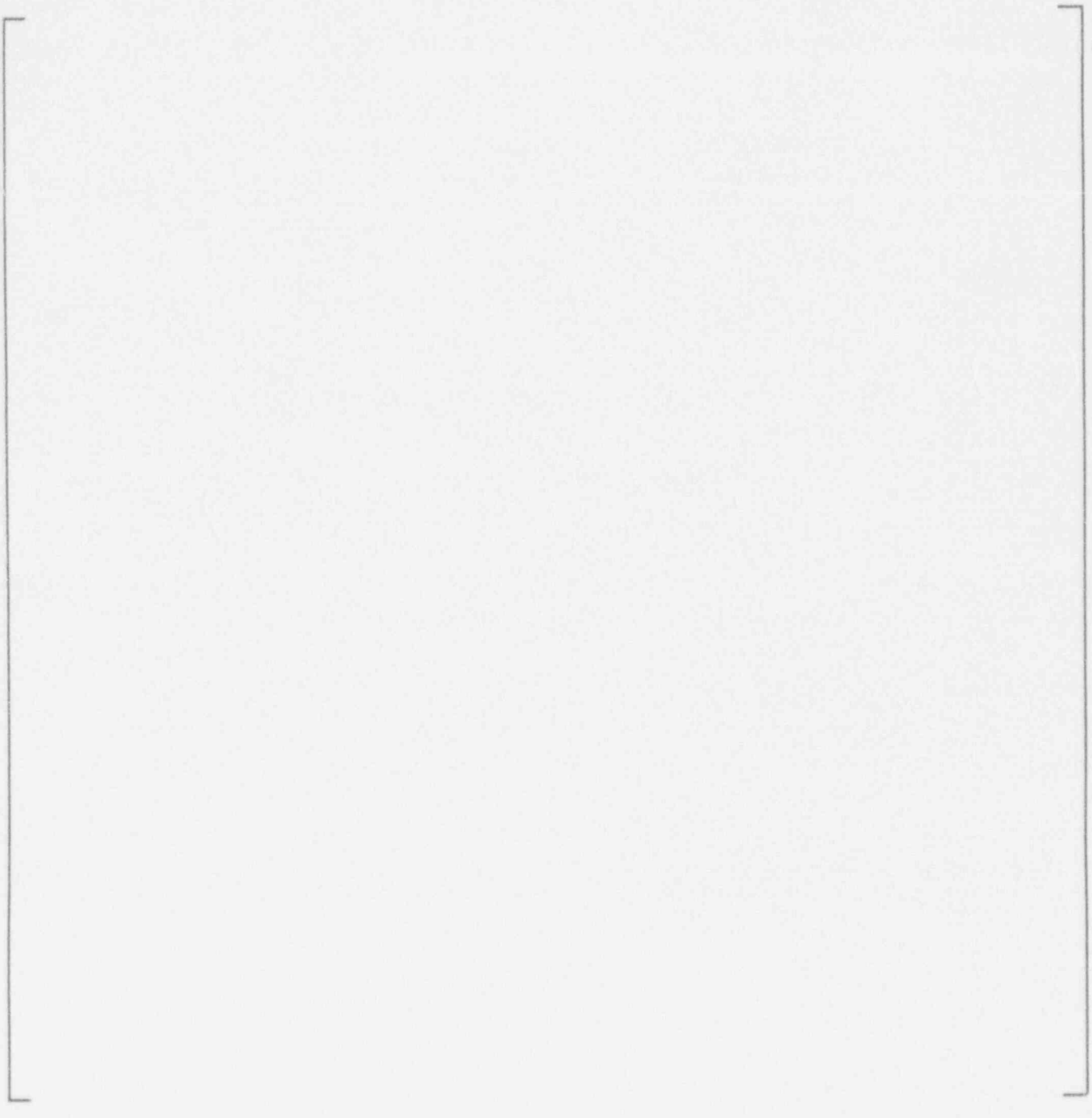

a,c

Figure 3-42 Calculated Surface Condensation for the CMT Test at a CMT Level of 95% for Different Mixing Depths

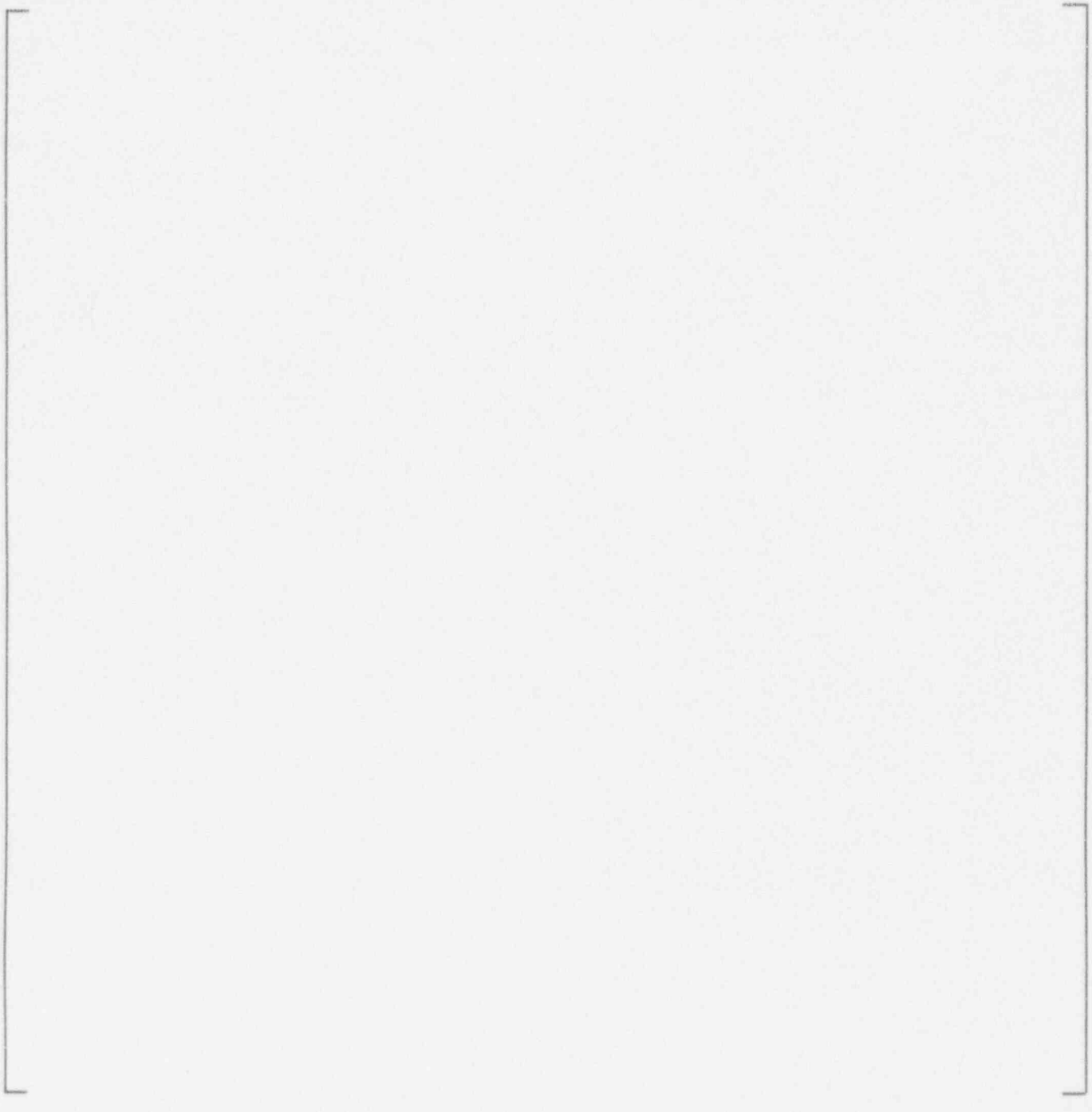

a,c

Figure 3-43 Calculated Surface Condensation Π Ratio for CMT Level of 95% and Different Mixing Depths

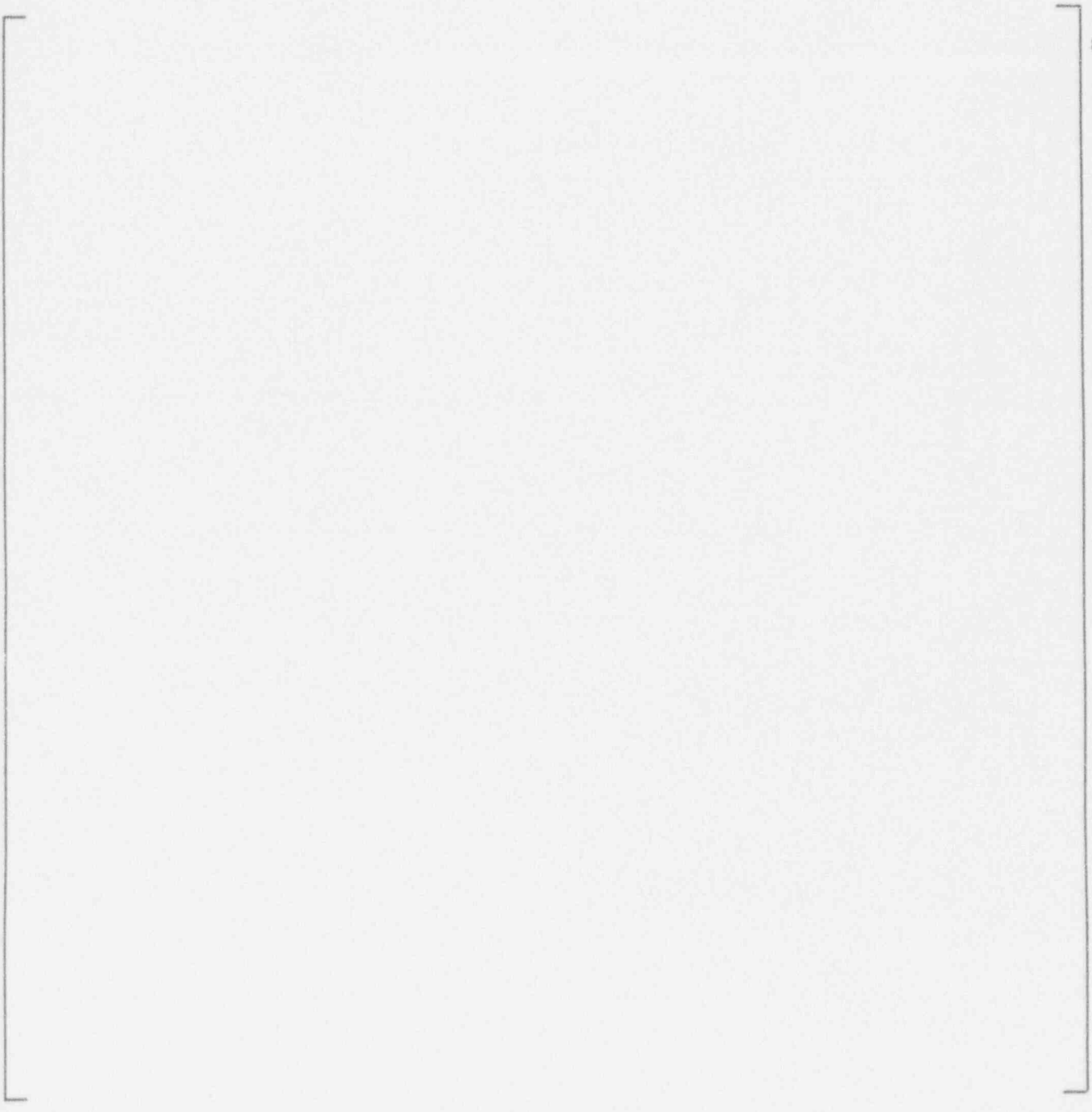

a,c

Figure 3-44 Calculated Ratio of the Inlet Jet Velocities at a CMT Level of 95% for Different Mixing Depths

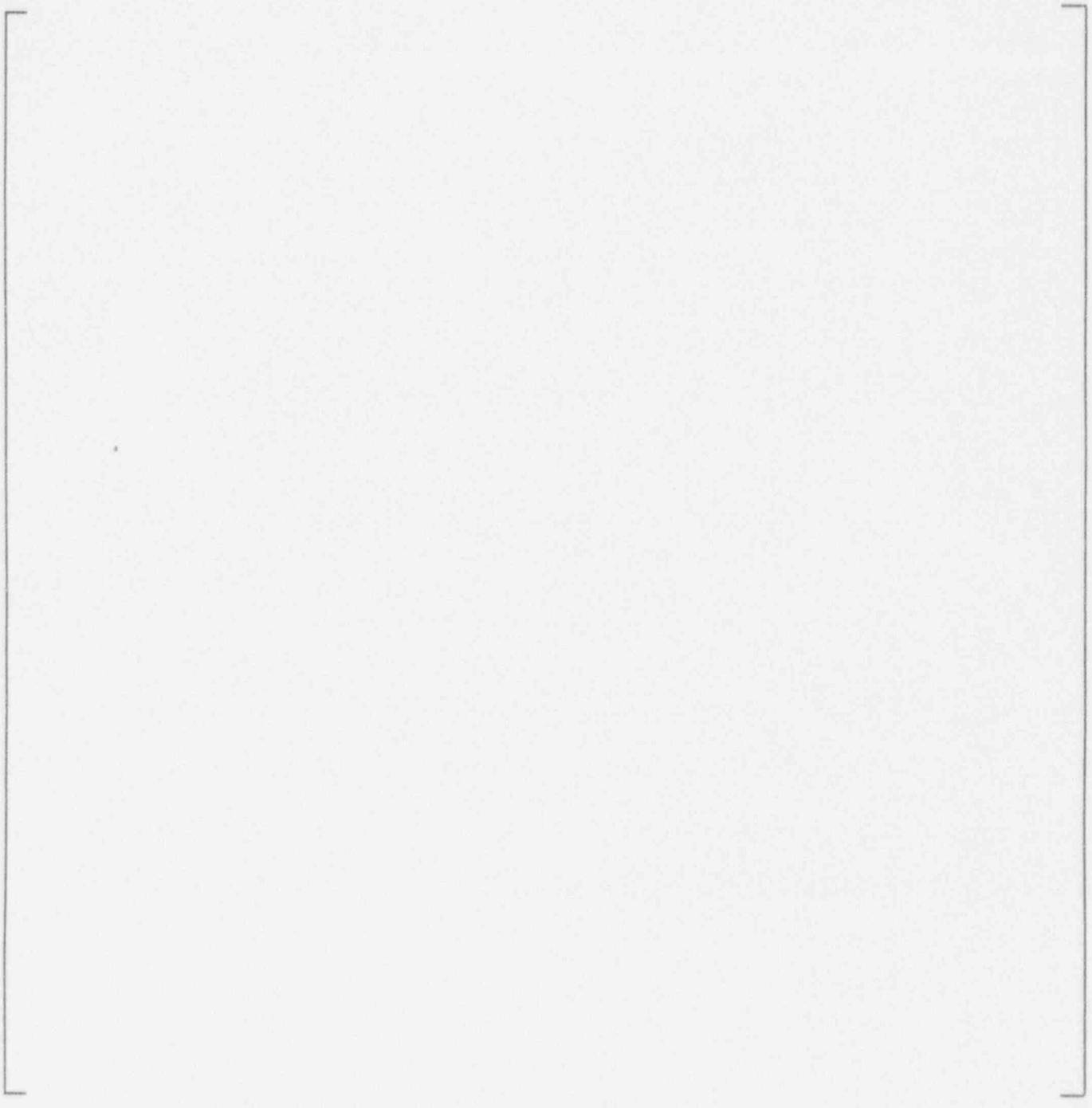

a,c

Figure 3-45 Calculated Ratio of Wave Heights for a CMT Level of 95% for Different Mixing Depths

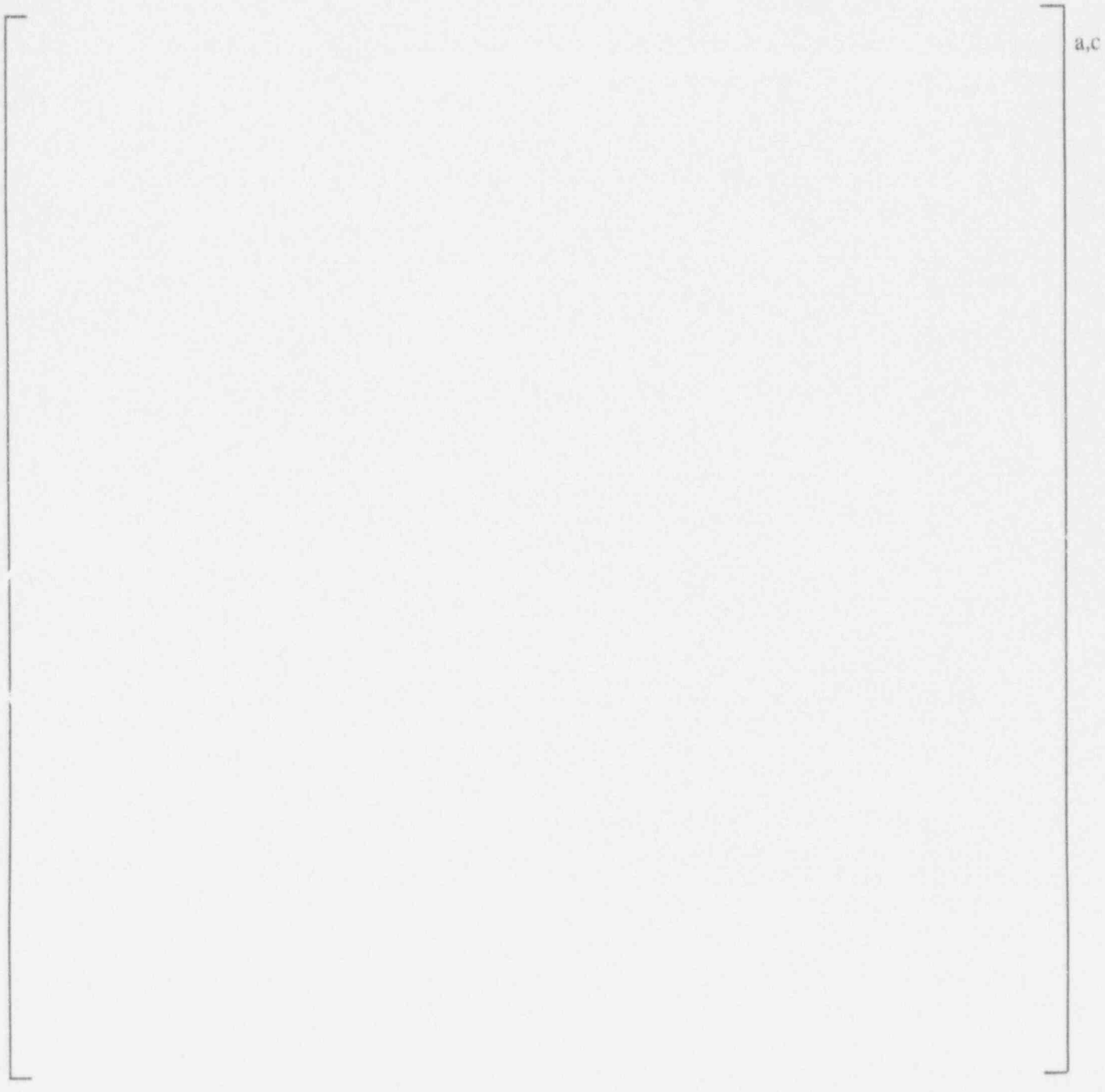

Figure 3-46 Ratio of Wave Velocities for a CMT Level of 95% and Different Mixing Depths

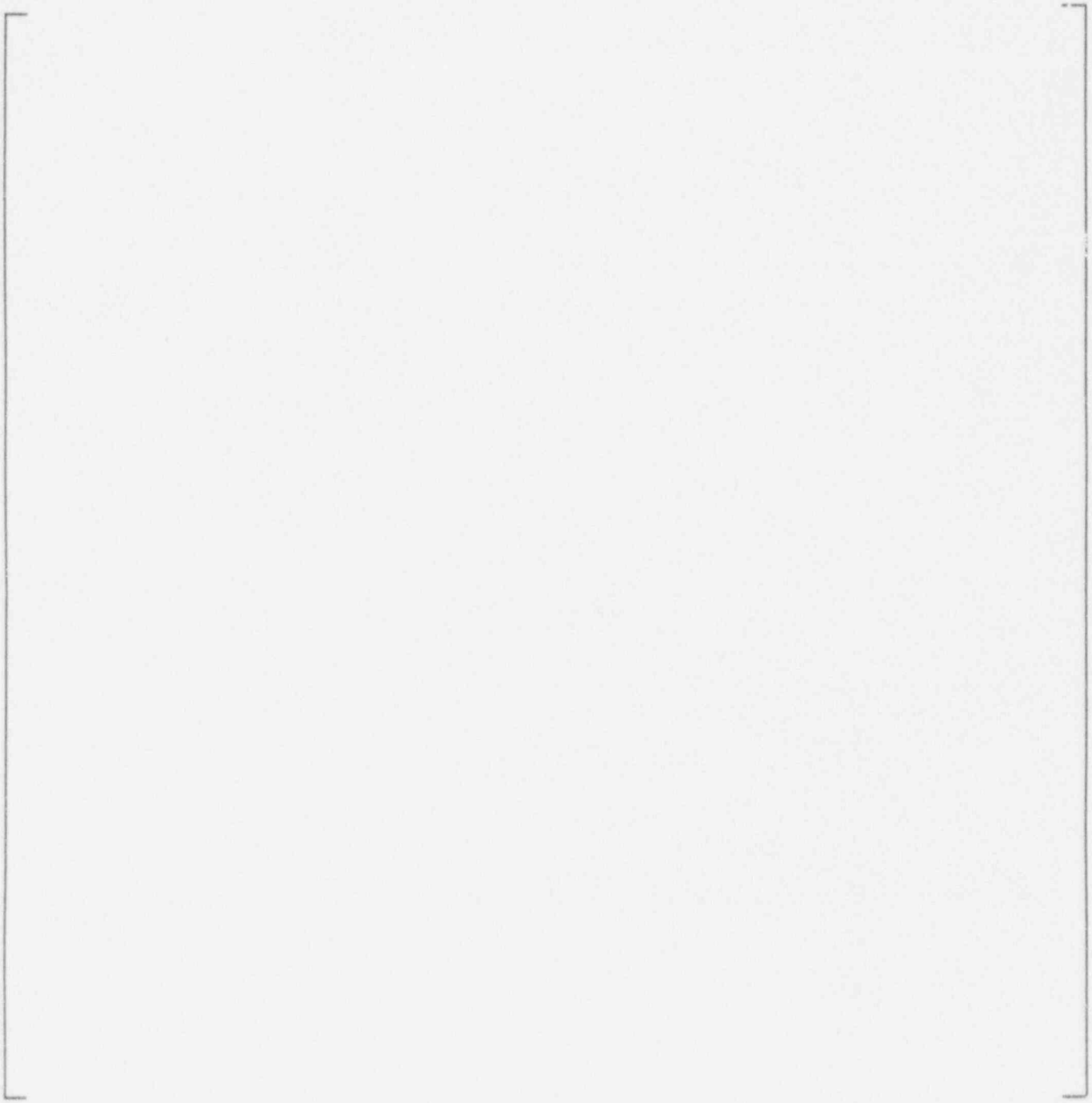

a,c

Figure 3-47 Calculated Ratio of the Time Constants for a CMT Level 95% and Different Mixing Depths

4.0 PROPOSED CMT TEST MATRIX

4.1 INTRODUCTION

The proposed CMT test matrix is examined to insure that the tests will obtain data on the key thermal-hydraulic parameters for the CMT that have been identified in the PIRT, Table 1-1.

4.2 TEST MATRIX

The cold and hot pre-operational tests will characterize the test facility and provide basic data that can be used to help model and interpret the test matrix. One cold pre-operational test will characterize the loop resistance such that the recirculation flow can be calculated. Other cold pre-operational tests will characterize the draindown rate of the facility and the volumes in the test facility.

[

]^{a,c}

There will also be CMT draindown experiments used to calibrate the drain line resistances and draindown rate for different tank levels. The hot pre-operational tests will also examine the effects of the [

]^{a,c}

The proposed test matrix is shown in Table 4-1 and is structured to increase the complexibility with each test series until, at the end of the matrix, the CMT will be operated in a systems manner. Each test series will now be discussed and related to the key phenomena identified in Table 1-1. Table 4-2 shows the CMT PIRT from Section 1 and identifies which matrix tests address the key thermal-hydraulic phenomena identified on this PIRT.

[a,c]

[ ] a,c

As Table 4-2 indicates, there are several tests that capture the key CMT thermal-hydraulic phenomena identified in the initial PIRT in Section 1. Therefore, the tests, as currently planned, will provide the necessary data identified in the PIRT needed for computer code model development and validation.

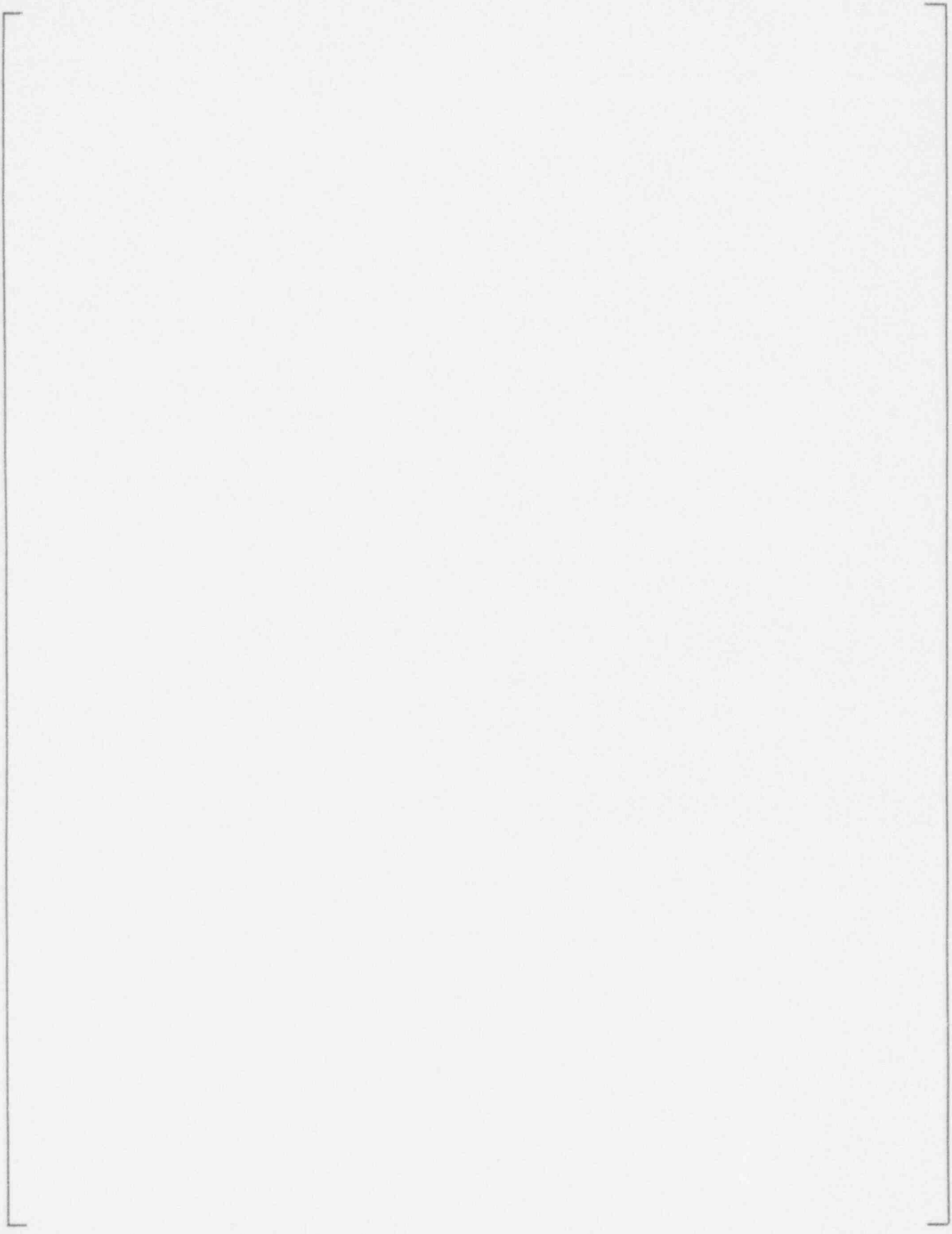

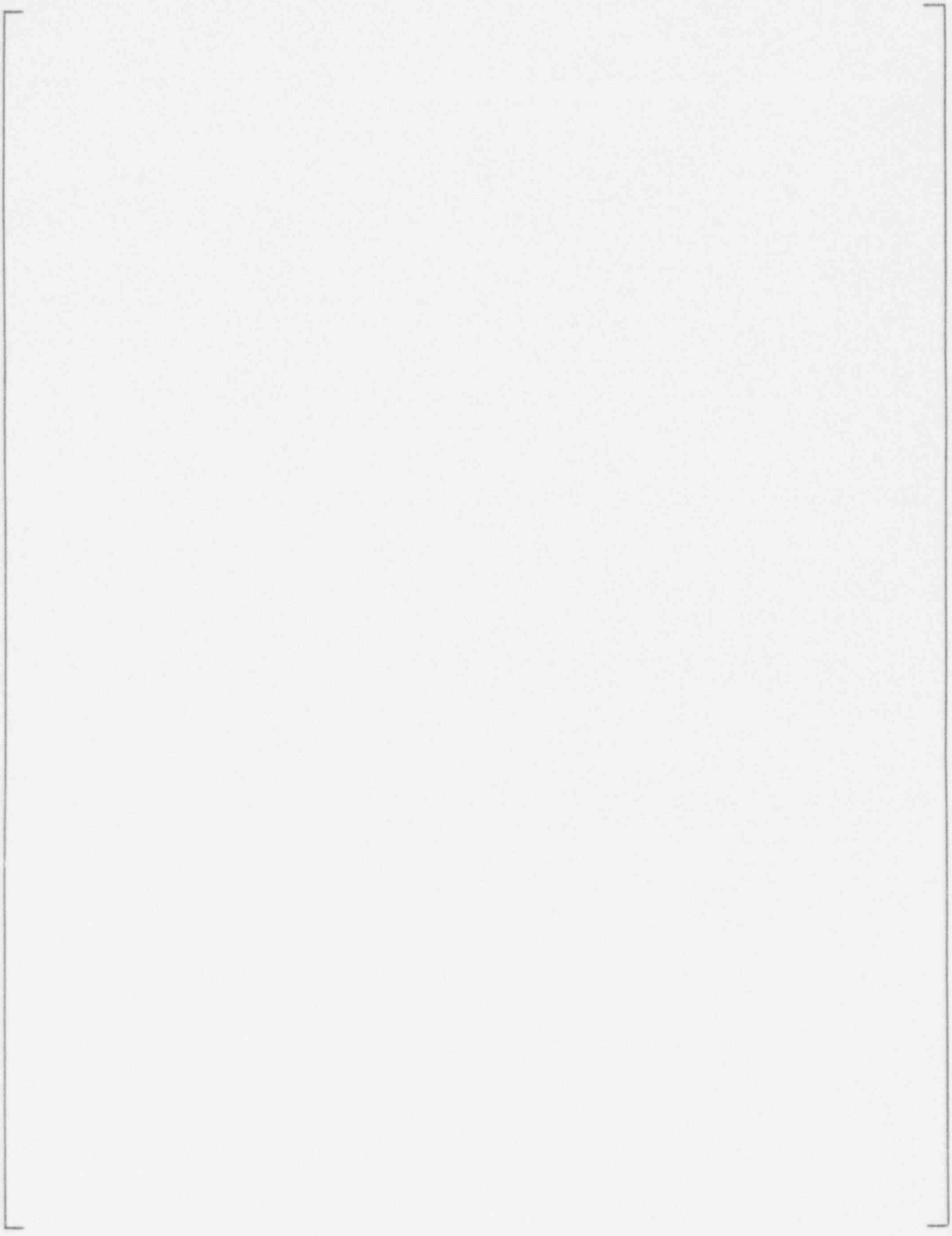

a,c

5.0 CONCLUSIONS

The scaling of the AP600 CMT test facility has been assessed relative to the AP600 Plant CMT and the PIRT. The PIRT identifies the key thermal-hydraulic data needed to develop and/or verify the CMT model. The scaling analysis methodology used for the AP600 Low Pressure Integral Systems effects test at Oregon State University, developed by Dr. J. Reyes (1993), was adapted and applied to the CMT component. The dimensionless parameters were developed and were compared for the test CMT and the plant CMT over a range of pressures at which the CMT would operate. Both the recirculation and draining modes were examined and the test CMT was compared to the plant CMT.

[

]^{a,c} One effect that was observed is that head geometry differences between the test and plant can make some differences, since the recirculation phase is a volume replacement calculation with hot liquid replacing the cold liquid in the tank. The CMT test facility does have distortion in the recirculation mode relative to the plant CMT; the test steam/water reservoir will develop a layer of cold water as the test recirculates, which acts to decrease the driving head in the test faster than in the plant, where there is no reservoir effect. However, these effects are small, and it is believed that the recirculation mode can be adequately modelled in the test.

The governing equations were also developed for the draindown mode of the plant and test CMT, and the dimensionless Π parameters that govern the wall and liquid surface condensation were assessed.

[

]^{a,c}

[

]^{a,c}

[

]^{a,c} Therefore, the AP600 CMT test will provide valid data for development and verification of the CMT computer model.

6.0 REFERENCES

1. Bankoff, S. G., Kim, H. J., Tankin R. S. and M. C. Yuen, "Counter-Current Steam-Water Flow in a Flat Plate," NUREG-CR-2783, 1982.

2. Bennett, C. O., and J. E. Meyer, Momentum, Heat, and Mass Transfer, 1960 McGraw-Hill, New York, New York.

3. Belyayev, V. V. and B. V. Dyadyakin, "Condensation of Steam in a Bubbling Pool into Which it is Injected from Non-Submerged Nozzles," Fluid Mechanics, Soviet Research, Vol. 18, No. 3, May-June 1989.

4. Bird, R. B., Steward W. E. and E. N. Lightfoot, Transport Phenomena, 1960, John Wiley and Sons, New York, New York.

5. Colburn, A. P., "The Calculation of Condensation Where a Portion of the Condensate Layer is in Turbulent Flow," Trans Am. Inst. Chem. Engrs., Vol. 30, pg 187, 1933.

6. Conway, L. E., "AP600 Core Makeup Tank Test Specification," WCAP 13345, Revision 1, Westinghouse report issued to the NRC and DOE, January, 1994.

7. Dittus, F. W. and L. M. K. Boelter, University of California, Pubs, Engr. Vol 2, pg 443, 1930.

8. Eckert, E. R. G., and T. W. Jackson, Natl. Advisory Aeronaut. Report 1015, (1951).

9. Fisher, J. E., Boncher, T. J., and J. M. Cozznol, "Evaluation of Westinghouse CMT Test Facility and Test Matrix for Relap 5/Mod 3 Code Assessment," Letter Report transmitted from J. M. Cozznol to Dr. F. Odar U.S. NRC, May 28, 1993.

10. Grigull, U., Forsch. Ing. Wes. Vol 13, pg 49-57, (1942); Z. Ver Deutch Ingr. Vol 86, pg 444-445, 1942.

11. Kreith, F, Principles of Heat Transfer, 1962, International Textbook Company, Scranton, Pennsylvania.

12. Lamb, H, Hydrodynamics, 1932, Dover Publications, New York, New York.

13. Nusselt, W., "Die Oberflächenkcondensatiin des Wasserdampfes," Z. Ver. Deutsch, Ing. Vol 80, pg 541, 569, 1916.

14. Prandtl, L., and O. G. Tietjens, Fundamentals of Hydro- and Aeromechanics, 1934, Dover Publications, Inc., New York, New York.

15. Reyes, J., "Scaling Analysis for the OSU AP600 Integral System and Long Term Cooling Test Facility," OSU-NE-9204, July 1993.

16. Yonomoto, T., Kukita, Y. and Anoda, Y, "Passive Injection Experiment at the ROSA-V Large Scale Test Facility," to be presented at the 1993 National Heat Transfer Conference, Atlanta, Georgia, August 8-11, 1993.

17. Yonomoto, T. and Kukita, Y., "RELAP5 Analysis of a Gravity-Driven Injection Experiment at ROSA-V Large Scale Test Facility," submitted for presentation at the 1993 ASME Winter Annual Meeting, paper 93-WA/HT-74, New Orleans, Louisiana, Nov. 28 - Dec. 3, 1993.

7.0 NOMENCLATURE

7.1 NOMENCLATURE FOR SECTION 2.0

A_{BL}	area balance line
a_c	cross section flow area of CMT
A_{CL}	area cold leg
A_{DVI}	area DVI line
A_{N_p}, A_{N_m}	CMT nozzle area for prototype (p) and model (m)
A_S	heat transfer surface area
β_T	coefficient of volume expansion
$C_{p\ell}$	liquid specific heat at constant pressure
$C_{v\ell}$	liquid specific heat at constant volume
C_{vs}	solid specific heat
D	Diameter of Piping (CL, DVI, CLBL)
D_h	hydraulic diameter of the heated subchannel ($d_h = 4a_{SC}/\xi$)
d_{N_p}, d_{N_m}	CMT nozzle diameter for prototype (p) and test (m)
f	Darcy friction factor
g	gravitational acceleration
gc	Newton's law conversion factor
H_S	average convective heat transfer coefficient over the heated length
K	loss coefficient
K_{CKV}	CMT discharge line check valve loss coefficients
K_{CL_N}	cold leg nozzle loss coefficient
K_{CMT_N}	CMT inlet nozzle loss coefficient
$K_{CMT_{EX}}$	CMT outlet nozzle loss coefficient
K_{DVI_N}	DVI nozzle loss coefficients
k_ℓ	liquid thermal conductivity
k_S	solid thermal conductivity
K_T	cold leg-to-cold leg balance line Tee
ℓ	heated length of the CMT
L	height of driving head for CMT flow

L_f	frictional lengths in cold leg, balance line and DVI line
Q_ℓ	volumetric flow rate
qs	heat loss
ρ_ℓ	liquid density
S	Scale factor
t_p, t_m	time for prototype (p) and model (m)
ΔT	axial fluid temperature difference across the length of the core
T_ℓ	liquid temperature
T_S	surface temperature
T_S-T_ℓ	average temperature difference over the heated length
U_ℓ	liquid velocity
U_{CL}, U_{BL}, U_{DVI}	average liquid velocities in cold leg, balance line and DVI line
x	distance in solid structure
Z	thickness of the hot liquid layer inside the CMT

7.2 NOMENCLATURE FOR SECTION 3.0

α	CMT wall diffusivity
a_{sa}	CMT outside surface area
a_{si}	CMT inside surface area
A_{tank}	CMT tank cross section area
a_{ws}	CMT metal wall surfaces exposed to steam
Ax	rod solid structure cross section area
Cp_ℓ	liquid specific heat at constant pressure
δ	conduction depth ($\delta = A_x/\xi$)
e_ℓ	is the average liquid energy per unit mass
H_{LF}	condensation of steam on metal surfaces
H_{LS}	condensation of steam on CMT liquid surface
H_{sa}	CMT outside convective heat transfer coefficient to ambient
H_{st}	CMT inside convective heat transfer coefficient
k_s	CMT wall thermal conductivity
$L_\ell(t)$	level in CMT tank
ρ_ℓ	is the density of the liquid inside the control volume
$\Delta[PQ]$	is the net rate of fluid mass entering or leaving the control volume
q_{LS}	condensation on the CMT water surface
q_t	is the heat loss to the ambient
q_{WS}	condensation on the CMT walls
R_i	inside radius of the CMT
R_O	outside radius of the CMT
T_d	condensate interface temperature
T_s	structure temperature
T_{sat}	saturation temperature
T_{WS}	inner CMT wall temperature with a condensate film
V_ℓ	is the volume of liquid inside the control volume
V_t	CMT tank volume
W_t	is the shaft work done by the liquid
ξ	wetted perimeter of the heated subchannel